SOME APPLICATIONS
OF
OPTICAL FIBRE SENSOR

by

POON Wing-Chak

A Master Thesis

submitted in partial fulfillment of the requirements

for the award of

Master of Philosophy

in

Department of Electronic Engineering

The Chinese University of Hong Kong

Nov, 1989

Content

Content

ACKNOWLEDGEMENT

I would like to thank my supervisor, Dr. P.S. Chung, for his kind guidance and encouragement throughout the course of the project.

Sincere thanks is also sent to Mr. C.K. Wong for his technical support and photograph preparation.

Special thanks is also sent to Mr. W.Y. Hung and Mr. H.P. Chan for their valuable discussion throughout the project.

Finally, I would like to thank all the staff in the Department of Electronic Engineering, The Chinese University of Hong Kong.

ABSTRACT

There is no doubt that optical communication is becoming a majority in communications market, especially in long-haul telecommunication and local area network. Optical sensors are also rushing into the market of sensors. Due to the advantage of optical fibre on sensitivity, intrinsically safe, intrinsic freedom from electromagnetic interference and low cost, optical communication and optical sensors will become more and more popular.

Intensity sensors for measuring weight and displacement are demonstrated. Theoretical calculation is developed to analyze the characteristics of the sensors.

A modal sensor is proposed. It senses the environmental change by detecting the phase between the lightwaves in the cladding and in the core. The principle was demonstrated in the experiment. The phase change rate of the experimental setup was 39.6 rad/kg.

Polarization-division-multiplex is proposed to double the information capacity of an optical fibre. Two channels are multiplexed into a fibre. One of the channels is carried by the major axis while another channel is carried by the minor axis. The signal-to-noise ratio in audio channel was 9.5 dB, while the signal-to-noise ratio in the video channel was 12 dB.

Integration of optical sensing technique and optical communication system had been demonstrated in an experiment. Encouraging result is obtained in the experiments.

CHAPTER 1
REVIEW ON OPTICAL COMMUNICATION AND OPTICAL SENSING

1.1 Introduction

Using light as a medium for transmission of information is, of course, not a new technique. Visual methods of communicating are widely used in the animal kingdom, obvious examples being courtship displays and warnings of aggressive intent, and from the time of the most primitive human civilizations man has employed artificial optical techniques to send information over long distances. For example, smoke or reflected sunlight is used for signaling at daytime, while fire beacons are used at night time.

Measurement using light began in the ancient history. Far behind Chau Dynasty in China, the Chinese had used 'Disc of the Sun' for measuring time. It only began to be replaced by other timing machines at several centuries before. The optical lever (e.g. mirror galvanometer) has been around for over a century. Remote chemical analysis using light (e.g. Fraunhofer lines) was discovered a considerable time ago.

In all these systems, the eye did the optical detection, and the light was transmitted through air. Air can, of course, have a remarkably low loss. But it fluctuates continually in its transmission characteristics. The human eye has many excellent features as a very complex high-resolution but slow optical detector. Hands were sometimes used as the modulator. The human hand leaves much to be desired as an optical modulator. While a complex and extensive electronic industry developed in the background, optical systems remained in this basic form for a considerable time. The change came in 1966 when Kao and Hockham published a paper demonstrating that light may be guided with low loss in thin, flexible glass fibre guides [1.1]. This opened up new vistas. It became feasible to consider guided light over many kilometers, thereby eliminating the uncertainties of atmospheric transmission. Fifteen years later, the industry became established, and lightwave

communication became one of the important cornerstones of the telecommunications industry.

Meanwhile, in the mid 1970 it was realized that the fibre itself may form the basis of a new direct transduction principle, interfacing the field to be measured with the light guided within a fibre without any intervening stages [1.2-1.4]. The concept of the all-fibre sensor has since then become reality in numerous laboratories throughout the world.

There are many advantages of optical communication links in comparison with traditional electrical communication systems. Optical fibre communication has low attenuation, low dispersion, high bandwidth, high channel capacity, immunity to electromagnetic interference and insensitive to thermal, mechanical and chemical change. Optical fibre cables have advantages of light in weight, small in size and cheap in price.

There are many attractive features of optical fibre in sensing, including immunity to electromagnetic interference, low thermal and mechanical inertia for the sensing material and the use of chemically inert materials for the sensing head. In addition, the sensor consumes zero electrical power and mostly zero mechanical power, and, particularly in future installations, there is a considerable potential for a flexible system format, possibly incorporating signal processing into the basic sensor. This will give a much shorter processing time than traditional techniques.

The following chapters will introduce different sensing techniques and communication systems. After presenting optical fibre sensors for measuring distance, weight and tension, Polarization-Division-Multiplexing technique in optical communication will be introduced. Finally, a general conclusion and discussion will be given, after integration of optical fibre sensing system and optical communication system are introduced.

1.2 REVIEW ON OPTICAL COMMUNICATION

1.2.1 Introduction

Many examples of using light as the medium for transmitting information can be found in history. At the earlier stage, a single item of information was transmitted by means of a pre-arranged signal. Although many sophisticated methods of signaling had been proposed, only the use of beacons seems to have continued over the intervening centuries. It had been interrupted at the end of eighteenth century due to the development of semaphore. At that time, this was overtaken by the electric telegraph on land. However, signaling flags and shuttered signaling lamps are still used at sea. Later on, such techniques were largely replaced by the telephone and by the wireless telegraphy. The form of transmitting information had a major change at this time due to different transmission techniques. These early transmission systems using light as medium were all, now called, digital systems. Later systems, such as telephones, radios, etc., are analogue information transmission, which represents analogue information by continuous time-varying electrical waveforms in transmission of information.

At the end of twentieth century, telecommunication again partly reverted from analogue to digital with the successful development in semiconductor and multiplexing technologies. At the same time, electrical waveforms (low frequency carrier) is going to be partly replaced by the optical frequency (high frequency carrier). Information is transmitted as a sequential stream of light pulses guided along silica optical fibres.

1.2.2 Guiding Material of Optical Transmission

Optical Communication had only been justified after a low loss light guiding material had been developed. For light transmission, a highly transparent material must be used. The attenuation of light over the used wavelength range must be kept as low as possible.

At 1966, Kao and Hockham [1.1] firstly proposed that silica optical fibre was the most suitable material for optical communications. This form of waveguide had a larger information capacity and possible advantages in basic material cost. At that time the best glass available gave a minimum attenuation of about 1000 dB/km at visible wavelengths while atmospheric attenuation on a clear day might be a few dB/km. By seeking ways to eliminate the absorbing impurities from the glass fibre, glass manufacturers led by Corning in the U.S.A. succeeded in reducing the attenuation in a glass fibre to 20 dB/km by 1970 and to 2 dB/km by 1975. Japanese workers succeeded in reducing the attenuation to 0.5 dB/km in 1976 and 0.2 dB/km in 1979 with using 1.55μm light source. Light-wave telecommunication systems using glass fibre guides are now being manufactured and installed routinely [1.5-1.7].

The three processes - vapor-phase oxidation (OVPO), modified chemical vapor deposition (MCVD), vapor-phase axial deposition (VAD) [1.8] - for making the fibres are used commercially. The price for an armoured optical fibre cable is now less than USD10/m. Splicing and making demountable connectors are available in commercial market at a cheap price. The progress has been so rapid that single-mode fibre and multimode fibre communication have been developed and installed in the field for commercial use. Meanwhile, research work is readily forging ahead to broaden areas of application of single-mode fibres, multimode fibres and special fibres.

1.2.3 Review of Optical Light Source

The reliability of the optical source was a cause of the greatest uncertainty during the initial development period of optical fibre communication systems. Before optical fibre communication systems were properly operated, many requirements of laser sources must be fulfilled. They must have a long operating life, stable characteristic, ability to operate at room temperature, high mean-time-between-failure (MTBF), a low threshold current, a high radiance, a high modulation bandwidth, a narrow spectral width, linear intensity/current characteristic, small emissive area, and output power stability in both short-term and long-term. And also, they must be small, light, cheap and able to be mass produced.

Semiconductor lasers were first fabricated in 1962 using GaAs in the form of diffused p-n homojunctions. The threshold current density of these early devices was about 300 - 500 A/mm^2 at room temperature and about 5 - 10 A/mm^2 at nitrogen temperature, 77K.

Techniques of forming GaAlAs/GaAs heterojunctions [1.9,1.10] on GaAs substrates was developed in late 60's. For a typical single-heterojunction, the room-temperature threshold current density was reduced to about $100A/mm^2$. The ability to make double heterostructures soon followed. Their improved confinement caused a further reduction of threshold current density to as low as $50A/mm^2$. Heterojunctions have the advantages of high injection efficiency, confinement of the minority carriers, improvement of ohmic contacts, transparency of the wide band gap material and optical guidance. They become the basic structure of today's laser sources [1.11].

The semiconductor light sources of interest in optical communications can be divided into two groups: AlGaAs devices for the 0.8-0.9μm wavelength region, and long-wavelength devices (mostly InGaAsP) for the 1.1 - 1.7 μm wavelength region [1.12-1.14]. Mostly for historical reasons, the state of art in AlGaAs devices is well ahead of the state of the art in InGaAsP devices. For short optical data links [1.15] (intra-urban, local computer networks, etc.) AlGaAs

sources are the solution [1.18-1.24]. Furthermore, for the 0.8 - 0.9 μm region, inexpensive high-quality photodetectors are readily available on a commercial basis (less than USD2000 for one set of transmitter and receiver), which is not the case for the 1.1 - 1.7 μm region. InGaAsP devices are extremely attractive for long-distance optical communications (interurban, submarine, etc.) in the low-loss low-signal-dispersion regions of silica-based fibres (1.1 - 1.35 μm and 1.5 - 1.7 μm).

At first look LED's appear much less attractive for fiber optical communications than lasers, due to their relatively wide spectra, and much poorer coupling efficiencies to low NA fibers (at least 10-dB difference). However, an LED has better linearity, less sensitivity to gradual degradation, and smaller temperature dependence of the emitted power than a diode laser.

By comparison to LED's, laser diodes offer the advantages of narrow emission spectra of less than 2 nm (30 nm for AlGaAs and 100 nm for InGaAsP LED's), larger modulation bandwidths of more than 2 GHz [1.9] (100 MHz or 200 MHz for LED's [1.25-1.29]), and greater coupling efficiency of about 50% [1.9] to low NA optical fibres (2 - 10 % for LED's [1.25]).

Intensive research for the realization of LED's and lasers in the long-wavelength region 1.0 - 1.7 μm [1.30-1.36] is triggered by the advantage of the fibre windows at 1.3 μm and 1.5 μm. The materials mostly studied for this purpose are ternary and quaternary compounds involving the group III elements in In, Ga, Al, and group V elements P, As, Sb.

The He-Ne laser is a typical example of atomic lasers. There is a mixture of about ten parts of helium to one part of neon in the active medium of the He-Ne laser. The power output from He-Ne laser is rather small; however, the radiation is extremely useful in a wide range of applications because it is highly collimated, coherent and has an extremely narrow linewidth.

1.2.4 Review of Photodetector

At the receiving end of an optical transmission line, the photodetector should have high sensitivity and fast response time to allow long-distance transmission of information at high data rates.

For the 0.8 - 0.9 μm region, silicon photodiodes, both p-i-n and avalanche, have sufficiently high sensitivity and fast response [1.37-1.39]. The quantum efficiency of commercially available Si p-i-n diodes is typically 85%, in this wavelength range, from dc close to 1 Gbit/s. Dark currents are sufficiently low as to introduce negligible system noise [1.37]. However, in an actual receiver the effects of the amplifier and circuit noise can amount to loss in sensitivity, and thus should be taken into account.

Various high-sensitivity optical receivers have been developed for the 1.0 - 1.4 μm range [1.40,1.41]. Germanium is sensitive to wavelengths below 1.8 μm and has a broad-band quantum efficiency of about 40 percent, but has an inherently high multiplication noise level [1.40]. Therefore, direct-bandgap III-V materials are being investigated for use in this wavelength region [1.41]. The III-V alloy semiconductors are superior to germanium because their bandgap can be tailored to the desired wavelength, resulting in lower dark currents. Also, the III-V alloys can be fabricated in heterojunction structures that enhance high-speed operation. Ternary alloys such as InGaAs [1.42] or GaAlSb [1.43,1.44] (deposited on GaSb substrates) have also been used to fabricate photodiodes that are sensitive to light in the 1.0 - 1.4 μm range. However, defects due to lattice mismatch, which accompany the growth of these alloy systems, are thought to cause increased dark current and microplasma sites, which ultimately limit avalanche performance [1.45]. Thus lattice-matched alloys appear to offer the best chance for obtaining high performance avalanche photodiodes. Two III-V alloys systems that can be lattice-matched over the 1.0 - 1.7 μm wavelength region are GaAlAsSb grown on GaSb [1.41] and InGaAsP grown on InP. The GaAlAsSb heterojunction avalanche diodes [1.41] have shown the best high-speed (subnanosecond) performance. The InP-based ternary and quaternary

systems have shown slow pulse fall times (1 - 5 ns) because the p-n junction has been located a few micrometers away from the heterojunction [1.46].

The GaAlAsSb APD has a quantum efficiency in excess of 90 percent and a dark current in the range of 10 - 40 nA at 20 V reverse bias. The GaAlAsSb APD/GaAs FET hybrid integrated optical receiver [1.41] has a sensitivity 10 - 20 times better than the Ge APD with the same preamplifier over a 100 MHz bandwidth. The best performance was achieved with moderate gains (10 - 30). APD dark currents ≃ 1 nA are adequate to achieve near maximum performance.

A number of lattice-matched InGaAsP/InP heterojunction geometries have been evaluated as photodetectors for light in the wavelength range from 1.0 - 1.7 μm [1.46]. Avalanche gains as high as 15 with 83 percent quantum efficiencies and 150 ps rise times have been obtained [1.46]. It has been reported [1.47] that a pronounced reduction in leakage current (to ≃ 10^{-6} A/cm^2) occurs after diffusing the p-n junction away from the top InP/InGaAsP heterojunction. Other workers [1.48] also report low leakage currents up to 70 percent of the breakdown voltage, and suggest that the leakage is surface dominated. An InGaAs avalanche detector has recently been reported [1.49]. An avalanche gain as high as 50 was reported.

The noise characteristics of quaternary avalanche photodiodes are far from matching the performance of silicon APD. Unless dramatic improvements in noise and gain uniformity are achieved for quaternary APD's, the detectors to be used for the 1.1 - 1.7 μm region might well be either optimized APD's [1.50], or a combinations of quaternary or ternary p-i-n detectors and low-noise amplifiers [1.51]. Already these have been reports of InGaAsP [1.52] and InGaAs [1.53] low-dark current p-i-n detectors with photoresponse to 1.26 and 1.7 μm, respectively.

1.2.5 Review of Optical Communication Technique

Following the first thoughts of using fibers for telecommunications [1.1,1.54,1.55], the first engineered fiber systems began to emerge in about 1980. They operated at a wavelength of 850-900 nm, with repeater spacings of 5-10 km and bit rates in the range 8-140 Mbit/s in Europe (8-90 Mbit/s in the United States, 6-100 Mbit/s in Japan). A changeover was hastened by the realization that fiber properties were better at 1300 or 1500 nm wavelength. The smaller material dispersion and much lower fiber attenuation (0.2-1 dB/km versus 2-5 dB/km at 850-900 nm) offered the promise of greater system simplicity coupled with higher transmission performance [1.56].

Before the first graded-index systems had entered service, a rapid shift of research interest took place back to single-mode fiber and systems. The early experiments have led to a second generation of fiber systems entering production, operating at 1300-nm wavelength and at bit rates in the range 100-600 Mbit/s with typical repeater spacings of 25-30 km, a major advance on the graded-index technology which was largely restricted to bit rates below 100 Mbit/s and repeater spacings under 10 km.

The attenuation of a typical single-mode [2.66] fiber is even lower at 1500 nm and approaches 0.2 dB/km [1.57-1.59]. This is immediately attractive to a system designer with an interest in pushing repeater separation. However, the dispersion has crept up to nearly 20 ps/nm km. Studies aimed at exploiting this lower attenuation window have taken two directions. The first has been to develop narrow spectral linewidth lasers, the second to optimize the fiber design to reduce the dispersion.

Noting that the source linewidth must be smaller than the modulation bandwidth, a 1-GHz spectrum width centered at 1500-nm corresponds to a linewidth of 0.0075nm. Narrow linewidth lasers have been used for a wide variety of transmission experiments spanning rates to many gigabits per second [1.60] and repeater spacings to

beyond 200 km [1.61] and were used for the first 100-km transmission experiment [1.62].

In direct detection systems, the various receivers available all fall far short of the quantum limit for detection, typically by 15 dB (optical). The recent demonstration of coherent detection schemes employing optical heterodyne [1.63] and homodyne [1.64] receivers with optical laser local oscillators has made clear that this gap can be closed. At the same time, it becomes possible that the use of modulation formats other than ASK, such as PSK and FSK. Moreover, because these systems employ very narrow spectral linewidth sources, they truly occupy only that cause of the selectivity of the receivers, could thus access the optical spectrum space in the fiber in the same manner as a radio receiver. The implication of this is staggering. The 1500-nm transmission window of the fiber is some 25000 Ghz in extent!

Most noticeable is the fact that the bit rates transmitted have advanced less than the repeater spacings achieved, the former by a factor of two to five, the latter by ten to twenty. Indeed, for many years, there has been no increase in the maximum time division multiplex (TDM) bit rates transmitted over a fiber link until the very recent report of a 4-Gbit/s transmission by AT & T Bell Laboratories [1.60]. Neither electronic components nor test gear are readily available for operation at bit rates much above 2 Gbit/s. This is in stark contrast to the optical transmission components which already have the capability to go to far higher rates. With optical modulator, excess of 20 GHz in modulation can be obtained [1.65].

Looking at the various markets for long haul fiber systems, there are two distinct groupings, the inland and the undersea. In the case of the inland systems, running between major centers of population, it will generally be the case that once the repeater separation has been increased to a distance of 30-60 km, the economic savings from further increase will be small. All equipment would be housed in readily accessible locations for servicing purposes and

would be a small part of the system cost. The pressure seems most likely to be to transmit higher bit rates over existing cables, particularly once it is widely understood the extent to which this should be possible. Upgrading could go in two directions, higher levels of TDM (greater bit rate) or wavelength division multiplexing [1.66,1.67].

In the undersea market, a different set of constraints applies. The pressure for higher bit rates is less than the pressure to reduce the cost of existing exceedingly complex designs. Increasing the repeater spacing has an immediate payoff, in that it reduces the number of undersea regenerators so reducing the power feed, servicing, and reliability problems. However, an even greater prize can be won if the system can be made repeaterless. For a North Atlantic system, island hopping would allow repeaterless operation (land based repeaters only) if a repeater spacing of about 450 km could be achieved.

Consideration of the potential power budget available to a silica-based fiber system suggests that this is certainly within the limits set by physics but implies exceedingly tight engineering margins. Of more immediate significance are the reports already of repeaterless operation over 230 km [1.61]. The most likely avenues for system development in the long haul systems market for the next few years is the present divergence of interest between inland and submarine [1.68-1.72].

Other applications of fibre in LAN are under active study. This has led to LED sources and graded-index or large core step-index fiber being considered. The implications of using single-mode fiber in the local loop is also seriously examined.

Connector and component costs tend to be higher. However, on the positive side is an almost infinite growth capability, a commonalty of component technology with the rapidly growing long-haul market and the potential for a highly innovative approach to the design of the local loop topology.

Examining the potential of 1500-nm single-mode fiber in LAN contest, the transmission medium within the distances of interest (a few kilometers) can be considered to have zero attenuation and infinite bandwidth from an engineering point of view. The design constraints are thus quite different to those applying in a long-lines environment. Now the whole power budget can be assigned to losses in passive components such as connectors, wavelength multiplexers, or power dividers and the potential exists for a large degree of fan-out, comparable to a coaxial tree network. Linking of telecommunications and CATV services, with major regulatory and social implications in addition to the technical ones by optical fibre is going to be the only solution.

1.3 REVIEW ON OPTICAL SENSING

1.3.1 Introduction

In ancient history, the optical sensing device was only some primitive setups. The human eye was employed to be the optical detector. The sunlight was the light source of the optical sensing systems. As there was a great success in lightwave technology at these ten years, optical fibre sensors will be a major type of sensors in the market of instrumentation.

There are many ways in which guided light may be modulated by an environmental parameter. A general optical fibre sensor can be defined as a constant light source launching into an optical fibre to a region in which the light is modulated by the measured parameter and then returned, detected and demodulated by the detector.

There are two basic classes in fiber sensors. The first class of sensors is one in which the fibres serve as a light source and light collector and the modulation process takes place externally from the fibre. The second class of sensors is one in which the measurand interacts directly with the light in the fibre. Phase, polarization and intensity may all be modulated within the fibre, using appropriately designed fibre and cable [1.73-1.80]. The last of these is probably the most common.

The advantages of the second class of sensors stem from the fact that there is no optical interfaces at the modulator head. The disadvantages stem from the fact that, in general, if the fibre within the modulator head is capable of imposing modulation of the light passing within it, so too are the feed and return fibres. In some of these sensors, this lead sensitivity problem does not arise. A number of solutions to the lead sensitivity problem are emerging. This will open up the potential for highly sensitive optical fibre remote sensors with the capability of multiplexing several of these on to one fibre link.

1.3.2 Various Sensing Technique

Regardless of whether it is modulating externally or internally, the type of lightwave modulation can be classified into intensity modulation, phase modulation, frequency modulation, wavelength distribution modulation and polarization modulation.

The intensity of light can be modulated externally by mechanical movement of reflectors or transmitters, or internally by changing of refractive index or microbending. The response of the externally modulated intensity sensor with a moving reflector modulator or a moving transmitter can be easily calculated by the principle in optics.

The total phase of the light path along an optical fibre depends on the physical length, the refractive index and the index profile, and the geometrical transverse dimensions of the optical fibre. The phase of the light may be modulated by changing these parameters through changing environmental parameters. Phase modulation of light as a highly sensitive monitor of environmental changes has been increasingly exploited over the past hundred years. The principal attraction of optical phase modulation is its intrinsically high sensitivity to environmental modulation, so that very high resolution measurements are feasible.

1.3.3 Phase Detection Technique

There are many optical systems which utilize the phase modulation of light as the means for transmitting information. In coherent communications, one of the modulation technique is the Phase Shift Key (PSK). It carries the information by modulating the phase of the light. In optical sensing device, phase sensors are going to be more and more popular. It also use the phase to carry the information of the measurand. The detection of optical phase modulation is usually performed via interferometric techniques. This technique has been employed since early development in optics. In a Mach Zehnder interferometer, a portion of the light to be modulated is taken from the main beam by a beam splitter or a coupler as a reference and later combined with the modulated beam by another beam splitter or coupler. The resultant fields added by the two light beams is detected by a photodetector. The interference phenomenon then converts the difference in phase between the beams to an intensity variation, and hence converts to electrical variation by the photodetector.

1.3.4 Current Status of Optical Fibre Sensors

After about ten years of development, optical fibre sensors are no longer brash upstarts, new comers in the neighbourhood. Through alternation of light by external stimuli, these sensors can now detect virtually any stimulus that other sensors can - from pressure and magnetism to acidity and acceleration - and often more sensitively and accurately, over a wider dynamic range [1.81].

Optical fibre sensors are more rugged and more resistant to corrosion than other sensors, immune to electromagnetic interference, and, of course, compatible with optical fibre telemetry. Several types of fibre sensors are in commercial production, others are being field-tested, and still others are in advanced development. Whereas developers used to concentrate on demonstrating the sensors' superior sensitivity, they now emphasize improved packaging, cost, and reliability - signs of a maturing technology. A sampling of developmental optical fibre sensors is tabulated in table 3.1 [1.82].

Optical fibre sensors are making their commercial appearances in measuring instruments and controls where such attributes as sensitivity, resistance to hostile environments, and compactness are essential [1.83,1.84]. Optical fibre sensors for measurements of temperature, pressure, acceleration, flow of liquids and gases, and the level of a liquid in a container are commercially available. Several machinery manufacturers, for example, offer fibre sensors as options in control systems [1.85,1.86].

Another important application is medical probes, where fibre sensors may be the technology of the future. They are small, compatible with living tissue, and require no electric wiring. Eventually invasive medical probes with fibre sensors may be as common place as endoscopes in clinics and laboratories.

The next big application is likely to be all-fibre control systems in which many various fibre sensors feed signals to a central computer over a fibre network [1.87]. In these 'passive' systems,

sensed parameter	sensor types	performance range	accuracy
temperature	A	300-2000°C	±1°C
	C	0-100°C	±0.001°C
	A	-50 to +150°C	±0.2°C
pressure	A	0-35MPa	±0.5%
position (displacement)	A	Rotary 0 to 40°	±0.04°
		Linear 0 to 15cm	±0.003cm
acceleration (vibration)	A	0.01 to 32g	±0.1%
	C	1µg to 10g	±1%
pH	A	6 to 8, 7 to 12	±0.02
flow	C	0.5 to 20m/s	±1%
	A	various ranges between 1µm/s to 100km/s	±1%
liquid level On-Off switch	A	determined by the number of sensors immersed in the liquid	±0.05mm
continuous measurement	A	several meters	±1mm
concentration of oil pollutants	A	15 to >1000ppm	±5%
sound pressure (hydrophone)	C	3-170dB with reference to 1µPa	N/A
magnetic field	C	0.1nT to 0.1mT	±1%
rotation rate (gyroscope)	B	1m deg/hr to 100 deg/hr	±0.1%

Table 3.1 Sampling of developmental optical fibre sensors. (A = light intensity modulation external to the fiber; B = phase modulation in one fiber; C = phase modulation in two fibers)

there will be no intervening conversion of light signals to electronic signals. Aircraft, ship, power plants, and manufacturing processes are prime candidates for all-fibre control systems.

Reference

1.1 C. K. Kao and G. A. Hockham: "Dielectric fibre surface waveguides for optical frequencies", Proc. IEE, 1966, 113, pp.1151-1158.

1.2 D. E. N. Davies and S. A. Kingsley: "The use of optical fibres as instrumentation transducers", CLEO, San Diego, May 1976, digest of technical papers, pp.24-25.

1.3 V. Vali and R. W. Shorthill: "Fibre ring interferometer", Appl. Opt., May 1976, 15, pp.1099-1100.

1.4 Roger Dettmer: "Guilding light - an interview with Prof. Charles Kao", IEE Review, May 1989, Vol.35, No.5, pp.160-161.

1.5 F. P. Kapron, D. B. Keck and R. D. Maurer: "Radiation losses in glass optical waveguides', Appl. Phys. Lett., vol.17, pp.423-425, Nov. 1970.

1.6 T. Li: "Optical fiber communication - The state of the art", IEEE Trans. Commun., vol.COM-26, pp.946-955, July 1978.

1.7 T. G. Giallorenzi: "Optical communications research and technology: Fiber optics", Proc. IEEE, vol.66, pp.744-780, July 1978.

1.8 Donald Keck: "Low cost manufacture for fibre optic cables", Comm. Int., June 1989, Vol.16, No.6, pp.67-70.

1.9 H. Kressel and J. K. Butler: "Semiconductors Lasers and Heterojunctions LEDs", New York, Acadamic Press, 1977.

1.10 H. C. Casey and M. B. Panish: "Heterostructure Lasers", New York, Acadamic Press, 1978.

1.11 Y. Nannichi: "Recent process in semiconductors lasers", Japan. J. Appl. Phys., vol.16, pp.2089-2108, Dec. 1977.

1.12 T. Kimura and K. Daikoku: "A proposal on optical fibre transmission systems in a low loss 1.0-1.4μm wavelength region", Opt. Quantum Electron., vol.9, no.1, pp.33-42, Jan. 1977.

1.13 J. Conradi, F. P. Kapron and J. C. Dyment: "Fiber-optical transmission between 0.8 and 1.4μm", IEEE Trans. Electron Devices, vol.ED-25, pp.180-193, Feb. 1978.

1.14 T. Miya, Y. Terunuma, T. Hosaka and T. Miyashita: "Ultimate low-loss single-mode fibre at 1.55μm", Electron. Lett., vol.15, pp.106-108, Feb. 15, 1979.

1.15 P. B. O'Connor, J. B. MacChesney and C. M. Melliar-Smith: "Large-core high-N.A. fibres for data-link applications", Electron. Lett., vol.13, no.7, pp.170-171, Mar. 1977.

1.16 K. Fujiwara, T. Fujiwara, K. Hori and M. Takusagawa: "The characteristics of $Ga_{1-x}Al_xAs$ double-heterostructure bonded with gold eutectic allay solder", Appl. Phys., vol.34, no.10, pp.668-670, May15, 1979.

1.17 M. Ettenberg: "A statistical study of the reliability of oxide-defined stripe CW lasers of (AlGa)As", J. Appl. Phys., vol.50, pp.1195-1203, Mar. 1979.

1.18 H. Imai, M. Morimoto, K. Hori and M. Takusagawa: "Long-lived high power GaAlAs DH laser diodes at 70°C", Tech. Dig. Topical Meeting on Opt. Fiber Commun. (Washington, DC), Paper ThB1, pp.90-91, Mar. 1979.

1.19 M. Ettenberg, H. Kressel and I. Ladany: " Long-term lifetime of CW (AlGa)As laser diodes at room temperature", Electron. Lett., vol.14, no.25, pp.815-816, Dec. 1978.

1.20 H. Kressel, M. Ettenberg and I. Landany: "Accelerated

temperature aging of $Al_xGa_{1-x}As$ heterojunction laser diode", Appl. Phys. Lett., vol.32, no.5, pp.305-308, Mar. 1978.

1.21 T. Yuasa, M. Ogawa, K. Endo and H. Yonezu: "Degradation of (AlGa)As DH lasers due to facet oxidation", Appl. Phys. Lett., vol.32, no.2, pp.119-121, Jan. 1978.

1.22 T. Furuse, T. Suzuki, S. Matsumoto, K. Nishida and Y. Nachi: "Insulating carbon coating on (AlGa)As DH laser facet", Appl. Phys. Lett., vol.33, no.4, pp.317-318, Aug. 1978.

1.23 H. Imai, M. Morimoto, H. Sudo, T. Fujiwara and M. Takusagawa: "Catastrophic degradation of GaAlAs DH laser diodes", Appl. Phys. Lett., vol.33, no.12, pp.1011-1013, Dec. 1978.

1.24 C. A. Wang, H. K. Choi and M. K. Connors: "Highly uniform GaAs/AlGaAs GRIN-SCH SQW diode lasers grown by organometallic vapor phase epitaxy", IEEE Photonics Technology Letters, vol.1, no.11, pp.351-353, Nov. 1989.

1.25 D. Botez and M. Ettenberg: "Comparison of surface- and edge-emitting LEDs for use in fiber-optical communications", IEEE Trans. Electron Devices, vol.ED-26, pp.1230-1238, Aug. 1979.

1.26 M. Ettenberg, H. Kressel and J. P. Wittke: "Very high radiation edge-emitting LEDs", IEEE J. Quantum Electron., vol.QE-12, pp.360-364, June 1976.

1.27 J. Heinen, W. Huber and W. Harth: "Light emitting diodes with a modulation bandwidth of more than 1GHz", Electron. Lett., vol.12, no.21, p.553, 1976.

1.28 R. C. Goodfellow and A. W. Mabbitt: "Wide bandwidth high-radiance gallium-arsenide light-emitting diodes for fibre-optic communication", Electron. Lett., vol.12, 2, pp.50-51, Jan. 1976.

1.29 K. Nawata, S. Machida and T. Ito: "An 800Mbit/s optical transmission experiment using a single-mode fiber", IEEE J. Quantum Electron., vol.QE-14, pp.98-103, Feb. 1978.

1.30 H. Namizaki, H. Kan, M. Ishii and A. Ito: "Current dependence of spontaneous lifetimes in GaAs-AlGaAs double heterostructure lasers", Appl. Phys. Lett., vol.24, pp.486-487, May 1974.

1.31 C. J. Nuese: "III-V alloys for optoelectronic applications", J. Electron. Mater., vol.6, no.3, pp.253-293, Mar. 1977.

1.32 K. Astani and T. Kumira: "Linearization of LED nonlinearity by predistortions", IEEE Trans. Electron Devices, vol.ED-25, no.12, pp.207-212, Feb. 1978.

1.33 I. Ladany: "The influence of stripe width on the threshold current of DH lasers", J. Appl. Phys., vol.48, no.5, pp.1935-1940, May 1977.

1.34 R. Lang: "Lateral transverse mode instability and its stabilization in stripe geometry injection lasers", IEEE J. Quantum Electron., vol.QE-15, pp.718-727, Aug. 1979.

1.35 M. D. Campos, C. J. Hwang, R. I. Bossi and J. E. Ripper: "Cavity competition in anomalous emission intensity in double-heterostructure DH lasers", IEEE J. Quantum Electron., vol.QE-13, pp.687-691, Aug. 1977.

1.36 K. Kobayashi, R. Lang, H. Yonezu, Y. Matsumoto, T. Shinohara, I. Sakuma, T. Suzuki and I. Hayashi: "Unstable horizontal transverse mode and their stabilization with a new stripe structure", IEEE J. Quantum Electron., vol.QE-13, pp.659-661, Aug. 1977.

1.37 H. Melchior: "Detectors for lightwave communication", Physics Today, vol.30, pp.32-39, Nov. 1977.

1.38 P. P. Webb, R. J. McIntyre and J. Conradi: "Properties of

avalanche photodiodes", RCA Rev., vol.35, no.2, pp.234-77, June 1974.

1.39 S. D. Personick: "Receiver design for digital fiber optic communication systems - Part I and Part II", Bell Syst. Tech. J., vol.52, pp.843-886, July-Aug. 1973.

1.40 H. Ando, H. Kanbe, T. Kimura, T. Yamaosa and T. Kaneda: "Characteristics of germanium avalanche photodiodes in the wavelength region of 1-1.6μm", IEEE J. Quantum Electron., vol.QE-14, pp.804-809, Nov. 1978.

1.41 L.R. Tomasetta, D. Low, R. C. Eden, I. Dehimy and K. Nakano: "High sensitivity optical receivers for 1.0-1.4μm fiber-optic systems", IEEE J. Quantum Electron., vol.QE-14, pp.800-804, Nov. 1978.

1.42 K. J. Bachmann and J. L. Shay: "An indium gallium arsenide detector for the 1.0-1.7μm wavelength range", Appl. Phys. Lett., vol.32, no.7, pp.446-448, Apr. 1, 1978.

1.43 H. D. Law, K. Nakano, L. R. Tomasetta and J. R. Harris: "Ionization coefficients of $Ga_{1-x}Al_xSb$ avalanche photodiodes", Appl. Phys. Lett., vol.33, no.11, pp.948-950, Dec. 1, 1978.

1.44 T. Sukegawa, T. Hiraguchi, A. Tanaka and M. Hagino: "Highly efficient P-GaSb-N-$Ga_{1-x}Al_xSb$ photodiodes", Appl. Phys. Lett., vol.32, no.6, pp.376-378, Mar. 15, 1978.

1.45 T. P. Lee, C. A. Burrus, Jr. and A. G. Dentai: "InGaAsP/InP photodiodes: Microplasma-limited avalanche multiplication at 1-1.3μm wavelength", IEEE J. Quantum Electron., vol.QE-15, pp.30-35, Jan. 1979.

1.46 C. W. Hurwite and J. J. Hsieh: "GaInAsP/InP avalanche photodiodes", Appl. Phys. Lett., vol.32, no.8, pp.487-489, Apr. 15, 1978.

1.47 Y. Takanashi and Y. Horikoshi: "InGaAsP/InP avalanche photodiode", Japan. J. Appl. Phys., vol.17, no.11, pp.2065-2066, Nov. 1978.

1.48 R. E. Yeats and S. H. Chiao: "III-V heterostructure avalanche photodiode modules for fiber optic communication links in the 1.0 to 1.3 micrometer spectral range", Interim Rep. 1, Sept. 1978 for Contract No. DAA B07-78-C-2402, U.S. Army ECOM, Fort Monmouth, NJ.

1.49 Hajime Imai and Takao Kaneda: "High-speed distributed feedback lasers and InGaAs avalanche photodiodes", J. of Lightwave Technology, vol.6, no.11, pp.1634-1642, Nov. 1988.

1.50 J. C. Campbell, S. Chandrasekhar, W. T. Tsang, G. J. Qua and B. C. Johnson: "Multiplication noise of wide-bandwidth InP/InGaAsP/InGaAs avalanche photodiodes", J. of Lightwave Technology, vol.7, no.3, pp.473-478, Mar. 1989.

1.51 C. R. Giles, E. Desurvire, J. L. Zyskind and J. R. Simpson: "Noise performance of Erbium-doped fiber amplifier pumped at 1.49 μm and application to signal preamplification at 1.8 Gbits/s", IEEE Photonics Technology Letter, vol.1, no.11, pp.367-369, Nov. 1989.

1.52 C. A. Burrus, A. G. Dentai and T. P. Lee: "InGaAsP P-I-N photodiodes with low dark current and small capacitance", Electron. Lett., vol.15, no.20, pp.655-656, Sept. 27, 1979.

1.53 R. E. Leheny, R. E. Nahory and M. A. Pollack: "In 0.53 Ga 0.47 As P-I-N photodiodes for long-wavelength fibre-optic systems", Electron. Lett., vol.15, no.22, pp.713-715, Oct. 25, 1979.

1.54 R. D. Maurer, presented at Conf. Trunk Telecommunications by Guided Waves, London, England, Sept. 1970.

1.55 J. E. Midwinter and J. R. Stern: "Propagation studies of 40km of graded-index fiber installed in cable in operational duct", IEEE Trans. Comm., vol.COM-26, pp.1015, 1978.

1.56 Suzanne R. Nagel: "Optical fiber - The expanding medium", IEEE Circuits & Devices Magazine, Mar. 1989, vol.5, no.2, pp.36-45.

1.57 B. J. Ainslie, K. J. Beales, C. R. Day and J. D. Rush: "The design and fabrication of monomode optical fiber", IEEE J. Quantum Electron., vol.QE-18, pp.514-523, 1982.

1.58 M. Horiguchi and H. Osanai: "Spectral losses of low-OH-content optical fibers", Electron. Lett., vol.12, pp.310-312, June 1976.

1.59 D. N. Payne and W. A. Gambling: "Zero material dispersion in optical fibers", Electron. Lett., vol.11, pp.176-178, Apr. 1975.

1.60 A. H. Gnauck, B. L. Kasper, R. A. Linke, R. W. Dawson, T. L. Koch, T. J. Bridges, E. G. Burkhart, R. T. Yen, D. P. Wilt, J. C. Campbell, K. C. Nelson and L. G. Cohen: "4Gb/s transmission over 103km of optical fiber using a novel electronic multiplexer/demultiplexer", Tech. Dig., Opt. Fiber Comm. Post Deadline Sess., San Diego, CA, 1985, PD-02.

1.61 L. C. Blank, L. Bickers and S. D. Walker, "220km and 230km transmission experiments over low-loss dispersion-shifted fiber at 140Mbit/s and 34Mbit/s", Tech. Dig., Opt. Fiber Comm. Post Deadline Sess., San Diego, CA, 1985, PD-07.

1.62 D. J. Malyon and A. P. McDonna: "102km unrepeatered monomode fiber system experiment at 140Mbit/s with an injection locked 1.52μm laser transmitter", Electron. Lett., vol.18, pp.445-447, 1982.

1.63 D. J. Malyon, T. G. Hodgkinson, D. W. Smith, R. C. Booth and B. E. Daymond-John: "PSK homodyne receiver sensitivity measurements at 1.55μm", Electron. Lett, vol.19, pp.144-146, 1983.

1.64 R. Wyatt, T. G. Hodgkinson and D. W. Smith: "1.52μm PSK heterodyne experiment featuring and external cavity diode laser local oscillator", Electron. Lett., vol.19, pp.550-551, 1983.

1.65 Isamu Kotaka, Koichi Wakita, Osamu Mitomi, Hiromitsu Asai and Yuichi Kawamura: "High speed InGaAlAs/InAlAs multiple quantum well optical modulators with bandwidths in excess of 20 GHz at 1.55μm", IEEE Photonics Tech. Lett., May 1989, vol.1, no.5, pp.100-101.

1.66 R. W. Tkach, A. R. Chraplyvy and R. M. Derosier: "Performance of a WDM network based on stimulated Brillouni Scattering", IEEE Photonics Tech. Lett., May 1989, vol.1, no.5, pp.111-113.

1.67 N. A. Olsson, J. Hegarty, R. A. Logan, L. F. Johnson, K. L. Walker and L. G. Cohen: "Transmission with 1.37Tbit-km/sec capacity using ten wavelength division multiplexed lasers at 1.5μm", Tech. Dig., Opt. Fiber Comm., San Diego, CA, 1985, WB6.

1.68 "Optical system for Indian Railways", Asian Comm., Mar. 1989, p.4.

1.69 "US-Japan fibre optic cable", Asian Comm., Mar. 1989, p.6.

1.70 "Undersea optical fibre cable systems", Asian Comm., Apr. 1989, pp.21-23.

1.71 "Optical communications systems for Indian Railway", Asian Comm., Apr. 1989, pp.25-26.

1.72 "Aerial fibre optic cable systems", Asian Comm., Apr. 1989, pp.28-29.

1.73 J. Erdmann and D.C. Soreide: "Fibre optic laser transit velocimeter", Appl. Opt., June 1982, 21(11), p.1876.

1.74 R.H. Stolen: "Fibre design for non-linear optics", Physics of fibre optics - advances in ceramics, Vol.II, American Ceramic Society, 1981.

1.75 A.J. Rojers: "The electrogyration effect in crystalline quartz", Proc. Roy. Soc. A, 1977, 353, p.117.

1.76 R.A. Bergh, H.C. Lefevre and H.J. Shaw: "All fibre gyroscope with inertial navigation sensitivity", Opt. Lett., Sept. 1982, 7, 9, p.454.

1.77 E. Hecht and A. Zajac: "Optics", p.502, Addison Wesley 1973.

1.78 G.C. Baldwin: "An Introduction to non-linear optics", Plenum Press, 1969.

1.79 R.A. Bergh, B. Culshaw, C.C. Cutler, H.C. Lefevre and H.J. Shaw: "Source statistics and the Kerr effect in fibre optic gyroscopes", Opt. Lett., 1982, p.563.

1.80 B. Culshaw and I.P. Giles: "Frequency modulated heterodyne optical fibre Sagnac interferometer", IEEE J. Quantum Electron., April 1982, 18(4), p.690.

1.81 V.T. Chitnis, S. Kumar and D. Sen: "Optical fiber sensor for vibration amplitude measurement", J. of Lightwave Technology, April 1989, vol.7, no.4, pp.687-691.

1.82 Thomas G. Giallorenzi: "Optical-fiber sensors challenge the competition", IEEE Spectrum, Sept. 1986, pp.44-49.

1.83 News of Electronics & Power IEE, Feb. 1986, p.111.

1.84 J. P. Dakin: "Optical fibre sensors - principles and applications", Proc. of Int. Conf. on Fibre Optics, IERE, March 1982, pp.39-52.

1.85 A. L. Harmer: "Optical fibre sensor markets", Proc. of 1st Int. Conf. on Opt. Fibre Sensors, April 1983, pp.53-56.

1.86 Peter McGeehin: "Optical sensors - developing the technology and the market", Electronics & Power, July 1986, pp.535-538.

1.87 A.D. Kersey, A. Dandridge and K.L. Dorsey: "Transmissive serial interferometric fiber sensor array", J. of Lightwave Technology, May 1989, vol.7, no.5, pp.846-854.

CHAPTER 2
DISTANCE MEASURING DEVICE USING INTENSITY SENSING TECHNIQUE

2.1 Introduction

Distance is a kind of measure in length. Measuring distance has been performed since very early in human history. Before the dawn of history, people used different methods to measure the length or the distance. For example, they used their hands, feet or other related objects for length measurement. Early records on units of length in the various countries of the world are most interesting and replete with native customs.

As the things in this modern world are going to be more and more fine and high precision, the slide caliper, the micrometer screw gauge and many other measuring instruments have been produced. Electronic devices for measuring length have also been promoted in the market. Optical lever is a potential displacement measuring device [2.1-2.4].

The optical lever mentioned in this chapter is actually an intensity sensor. It senses the change in the measurand by observing the change in intensity. It uses external modulation techniques.

2.2 Operation Principle of the Optical Displacement Sensing Device

The constructed optical displacement sensing device, or so called optical lever, determines the displacement by observing the intensity changed. The light from the light source is carried to the reflector by a source fibre, or source fibres. The reflected light is collected by a return fibre, or return fibres, and then is carried to a light detector. The distance between the fibre ends and the reflector is directly affecting the luminous flux collected by the return fibre.

To calculate the light power collected by the fibres, two methods with different assumptions will be mentioned in the following paragraphs. They have similar characteristic curve of received illuminous flux against distance, but they are not exactly the same. It is because of the difference in assumptions.

Cook and Hamm [2.5] simplified the visualization and mathematical analysis of the optical lever mechanism considerably by the assumption that uniangular electroluminescent energy is coupled into lossless, nondispersing, and ideal step-index fibres having negligible cladding thickness. And further assumed that the luminous intensities are only in a few directions. Multi-reflection was also not considered. Chu, Whitbread and Allen [2.6] simplified the problem by assuming the optical source fills the numerical aperture of the fibre completely. Only the illuminance at different coordinates is analyzed mathematically. In this chapter, the problem will be considered more deeply and counting the effect of multi-reflection in the mathematical analysis.

The simplified diagram of the setup of the fibre optic lever is shown in figure 2.1. The arrangement of the optical setup consists of light source, source fibre, reflector, return fibre and photodetector. The cross section view of the fibre bundle is shown in figure 2.2. Figure 2.3 shows the geometry associated with the fibres, reflector and the light cone for a certain angle of illumination. Figure 2.4 shows the plane of the fibre ends and the

intersect of the reflected light ring with the fibre. Although the real setup is a six-to-one fibre bundle structure, only one-to-one fibre bundle structure is considered in the mathematical analysis. It is because of the symmetry in the structure. The characteristic of the six-to-one structure can be easily obtained by multiplying the characteristic of the one-to-one structure by six.

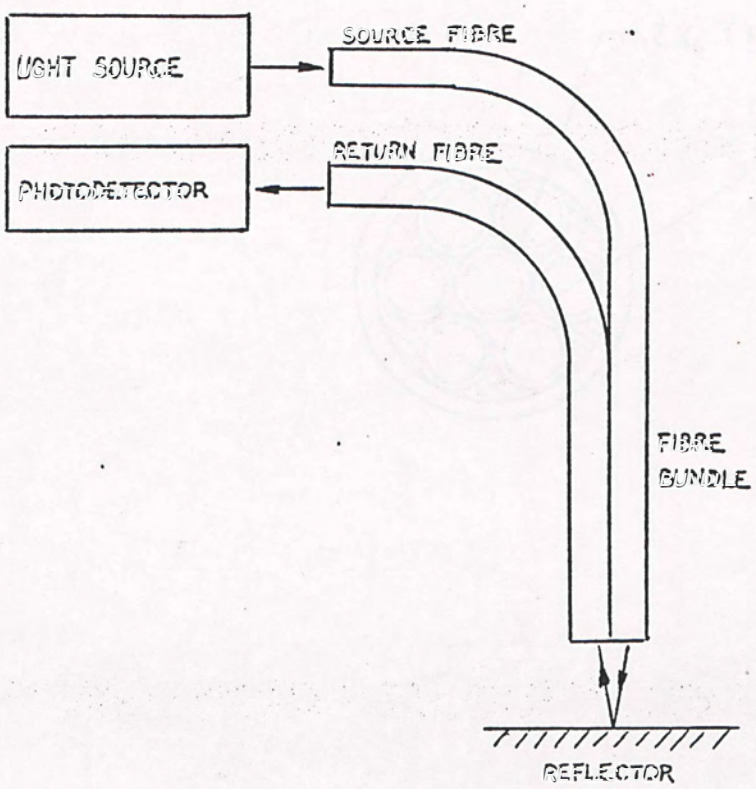

Fig. 2.1 Schematic diagram of the setup of fibre optic lever.

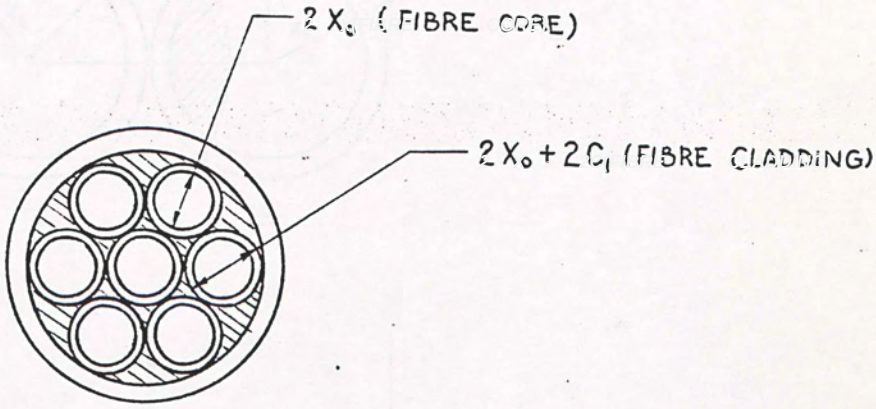

Fig. 2.2 Cross-sectional view of fibre bundle.

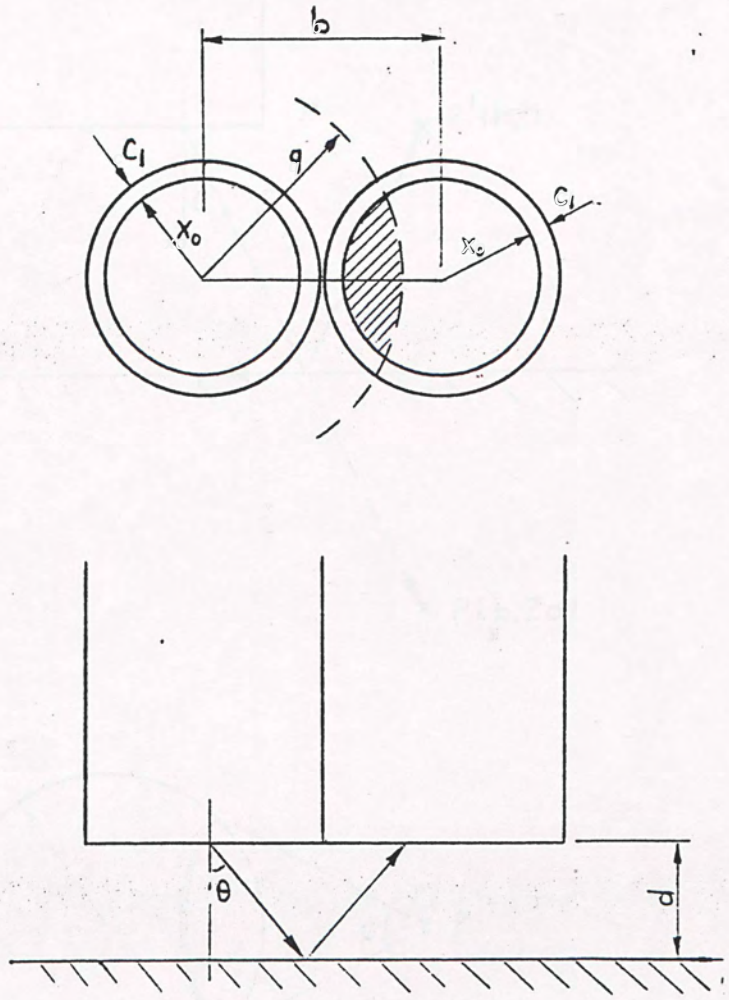

Fig. 2.3 Geometry associated with the fibres, the reflector and the light cone for a certain angle of illumination.

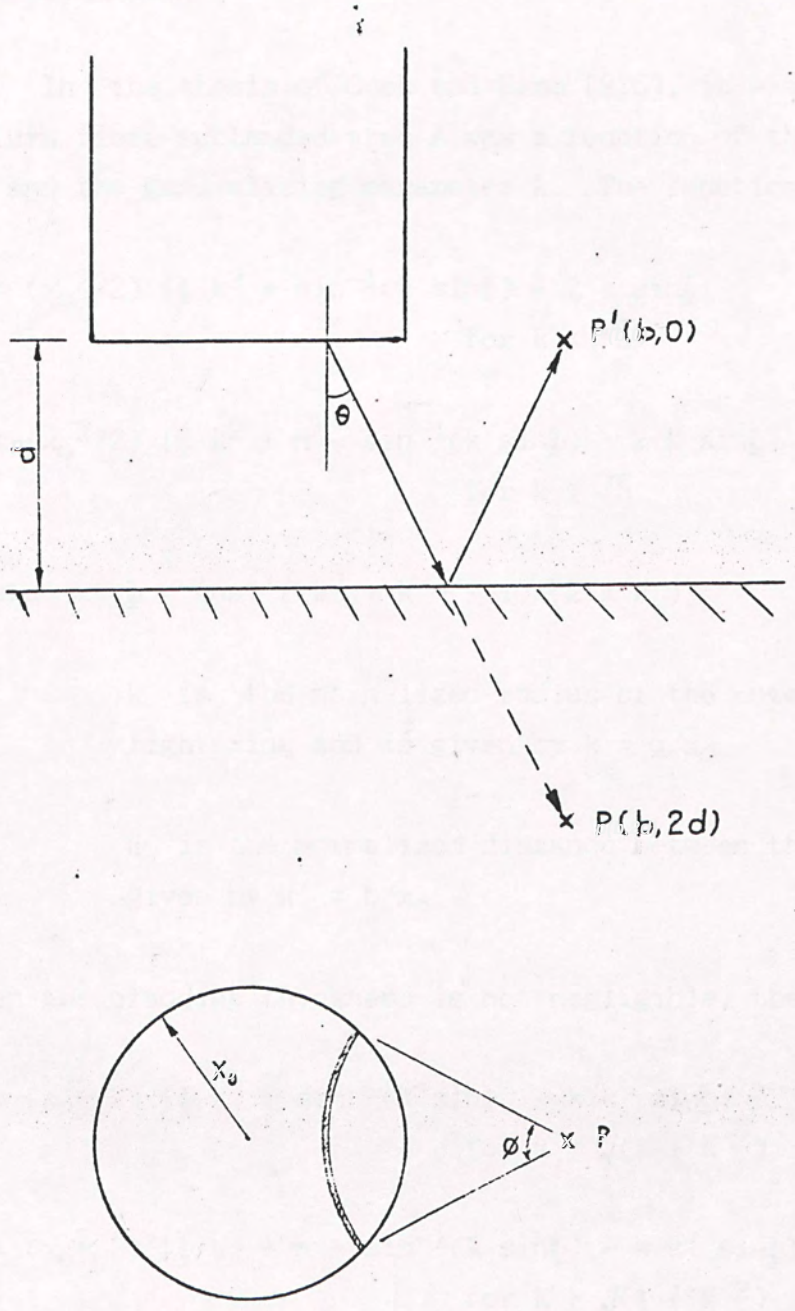

Fig. 2.4 Intersect of the reflected light ring with the fibre end surface.

2.2.1 Method 1

In the thesis of Cook and Hamm [2.5], it was proposed that the return fibre subtended area A was a function of the fibre core radius x_o and the generalizing parameter k. The function was:

$$A = (x_o^2/2)\,[\Phi\, k^2 + \sin^{-1}(k \sin\Phi) - 2\, k \sin\Phi] \quad \text{for } k \leq \sqrt{5} \qquad [2.1]$$

$$A = (x_o^2/2)\,[\Phi\, k^2 + \pi - \sin^{-1}(k \sin\Phi) - 2\, k \sin\Phi] \quad \text{for } k \geq \sqrt{5} \qquad [2.2]$$

where $$\Phi = \cos^{-1}[(k^2 + k'^2 - 1)/(2\, k\, k')] \qquad [2.3]$$

k is the normalized radius of the outer boundary of the light ring and is given by $k = q/x_o$ [2.4]

k′ is the normalized distance between the fibre axes and is given by $k' = b/x_o$ [2.5]

when the cladding thickness is not negligible, the function became:

$$A = (x_o^2/2)\,[\Phi\, k^2 + \sin^{-1}(k \sin\Phi) - k\, k' \sin\Phi] \quad \text{for } k \leq \sqrt{(1 + k'^2)} \qquad [2.6]$$

$$A = (x_o^2/2)\,[\Phi\, k^2 + \pi - \sin^{-1}(k \sin\Phi) - k\, k' \sin\Phi] \quad \text{for } k \geq \sqrt{(1 + k'^2)} \qquad [2.7]$$

The reflected illumination irradiance is

$$I_k = L\, I_o\, [(5 - k)/(4\, k + 4)] \quad \text{for } k \leq 3 \qquad [2.8]$$

$$I_k = L\, I_o\, [1/(4\, k - 4)] \quad \text{for } k \geq 3 \qquad [2.9]$$

The equations are further evolved in this chapter. The newly derived equations are as follows. The illuminance of the reflected light on the entrance plane of the return fibre can be approximated by (see

Appendix A for detail derivation)

$$f_I(k) = \begin{cases} C\, I_o/n\, [(5 - k)/(4\, k + 4)] & \text{for } k \leq 3, \quad [2.10] \\ C\, I_o\, /\, [n\, (4\, k - 4)] & \text{for } k \geq 3, \quad [2.11] \end{cases}$$

where C is an arbitrary constant counting for the deficiency of the reflecting surface and the fibre end surfaces

and n is the number of dividends of illumination angles

The function of the subtended area by the light cone with respect to different range of k is given by (see Appendix A for detail derivation)

$$f_A(k) = \begin{cases} 0; & \text{for } k \leq k'-1, \\ x_o^2\, \{\Phi\, k^2 + \sin^{-1}[k \sin \Phi] - k\, k'\, \sin \Phi\}; & \text{for } k'-1 < k \leq (k'^2+1)^{1/2}, \\ x_o^2\, \{\Phi\, k^2 + \pi - \sin^{-1}[k \sin \Phi] - k\, k'\, \sin \Phi\}; & \text{for } (k'^2+1)^{1/2} < k \leq k'+1, \\ x_o^2\, \{\pi - \Phi\, k^2 - \sin^{-1}[k \sin \Phi] + k\, k'\, \sin \Phi\}; & \text{for } k'+1 < k \leq (k'^2+1)^{1/2}+2 \\ x_o^2\, \{\sin^{-1}[k \sin \Phi] + k\, k'\, \sin \Phi - \Phi\, k^2\}; & \text{for } (k'^2+1)^{1/2}+2 < k < k'+3 \\ 0; & \text{for } k'+3 \leq k. \end{cases}$$

[2.12]

The luminous flux collected by the return fibre from an angle of illuminance Θ at the source fibre is given by

$$f_r(k) = f_I(k)\, f_A(k) \qquad [2.13]$$

The total luminous flux collected by the return fibre from the source fibre is given by

$$F_r(k) = \lim_{n \to \infty} \sum_{\theta_{min}}^{\theta_{max}} f_r(k) \qquad [2.14]$$

2.2.2 Method 2

The light intensity I_p at a point d from a source fibre tip and b from the fibre axis due to the whole source fibre is given by Chu, Whitbread and Allen [2.6] as

$$I_p = \int_{\theta_{min}}^{\theta_o} \{4\ I_o \cos^{-1}[(4\ d^2 \tan^2\theta + b^2 - x_o^2)/(4\ d\ b \tan\theta)] \sin\theta \cos\theta\}\ d\theta \qquad [2.15]$$

where
$$\theta_{min} = \tan^{-1}[(b - x_o)/(2\ d)] \quad \text{for } b > x_o$$
$$= 0 \quad \text{for } b < x_o \qquad [2.16]$$

$$\theta_o = \sin^{-1}(NA) \qquad [2.17]$$

To investigate the illuminance connected by the whole return fibre due to the whole source fibre, a set of equations is derived (see Appendix B). The luminous flux collected by the return fibre from the source fibre is given by

$$I_r = \int_{b_{min}}^{b_{max}} I_p\ \emptyset\ b\ db \qquad [2.18]$$

where

$$I_p = \int_{\theta_{min}}^{\theta_{max}} \{2\ C\ I_o \cos^{-1}[(4\ d^2 \tan^2\theta + b^2 - x_o^2)/(4\ d\ b \tan\theta)] \sin\theta \cos\theta\}\ d\theta \qquad [2.19]$$

$$\theta_{min} = \tan^{-1}[(b - x_o)/(2\ d)] \qquad [2.20]$$

$$\theta_{max} = \begin{cases} \sin^{-1}(NA) & \text{for } NA/\sqrt{(1-NA^2)} \leq (b+x_o)/(2d) \\ \tan^{-1}[(b+x_o)/(2d)] & \text{for } NA/\sqrt{(1-NA^2)} > (b+x_o)/(2d) \end{cases}$$

[2.21]

2.3 Calculated Result and Experimental Result

In the calculations, the parameters of the fibres are using those fibres used in the experiment. The radius of the fibre core is 50 μm. The thickness of the cladding is 75 μm. The theoretical relationship of the received luminous flux against the distance between the reflecting surface and the fibre end surface is shown in figure 2.5. It is calculated by using equation 2.10 - 2.14 in method 1. The relationship is plotted from distance of 0 mm to distance of 10 mm for fibre end surface reflection coefficient of 0, 0.05, 0.1 and 0.2. The multi-reflection phenomenon is considered. The intensity is normalized by the peak intensity of the characteristic curve with fibre end surface reflection coefficient of 0. Figure 2.6 shows the relationship from distance of 0 mm to 1.25 mm. It is easy to observed that a small portion the linear region of the characteristic curve near the starting of the curve has been distorted when multi-reflection is allowed. The distortion in the linear region in the characteristic curve is increased with the increase in the reflection coefficient. The effect of using a reflector having a reflection coefficient less than 100% can be counted by using the resultant reflection coefficient, which is the product of the reflection coefficients of the reflector and the end surface of the fibres, in the calculation.

The calculated characteristic curve for a system using fibres having no cladding is shown in figure 2.7. It is shown that multi-reflection do not affect much on the characteristic curve. The characteristic curve for a practical system having light transmitted both in cladding and core can be obtained by combining the no-cladding system characteristic and the ideal-cladding system characteristic. As the light transmitted in the cladding is much less than that in the core, the light transmitted in the cladding can be neglected.

By using equation 2.18 - 2.21 in method 2, the illumination at each point can be calculated. The relationship of luminous flux collected by the return fibre against the distance with reflection

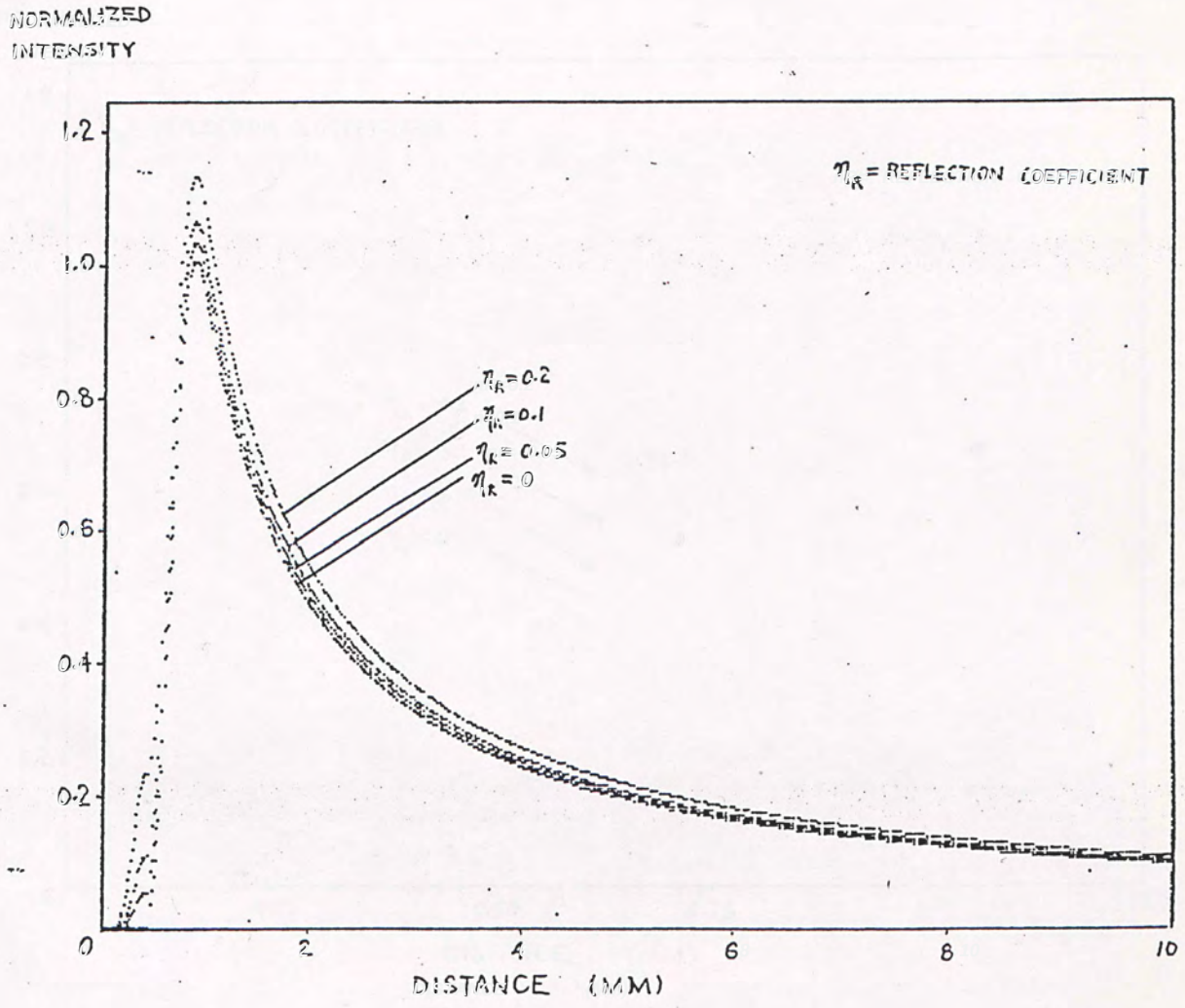

Fig. 2.5 Theoretical relationship of the normalized received luminous flux against the distance between the reflecting surface and the fibre end surface calculated by method 1. The distance is from 0 mm to 10 mm. The intensity is normalized by the peak intensity of the characteristic curve with fibre end surface reflection coefficient of 0.

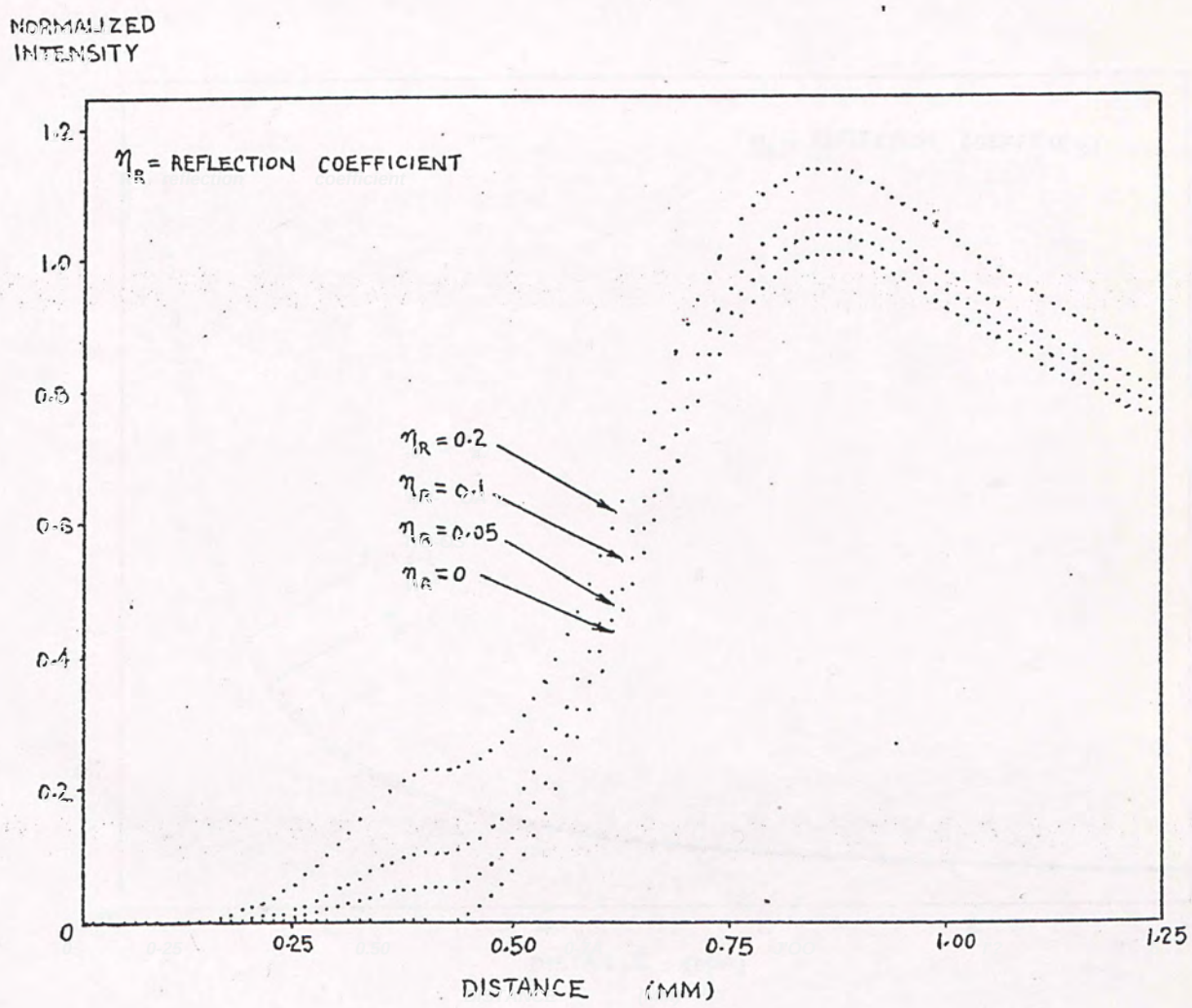

Fig. 2.6 Theoretical relationship of the normalized received luminous flux against the distance between the reflecting surface and the fibre end surface calculated by method 1. The distance is from 0 mm to 1.25 mm. The intensity is normalized by the peak intensity of the characteristic curve with fibre end surface reflection coefficient of 0.

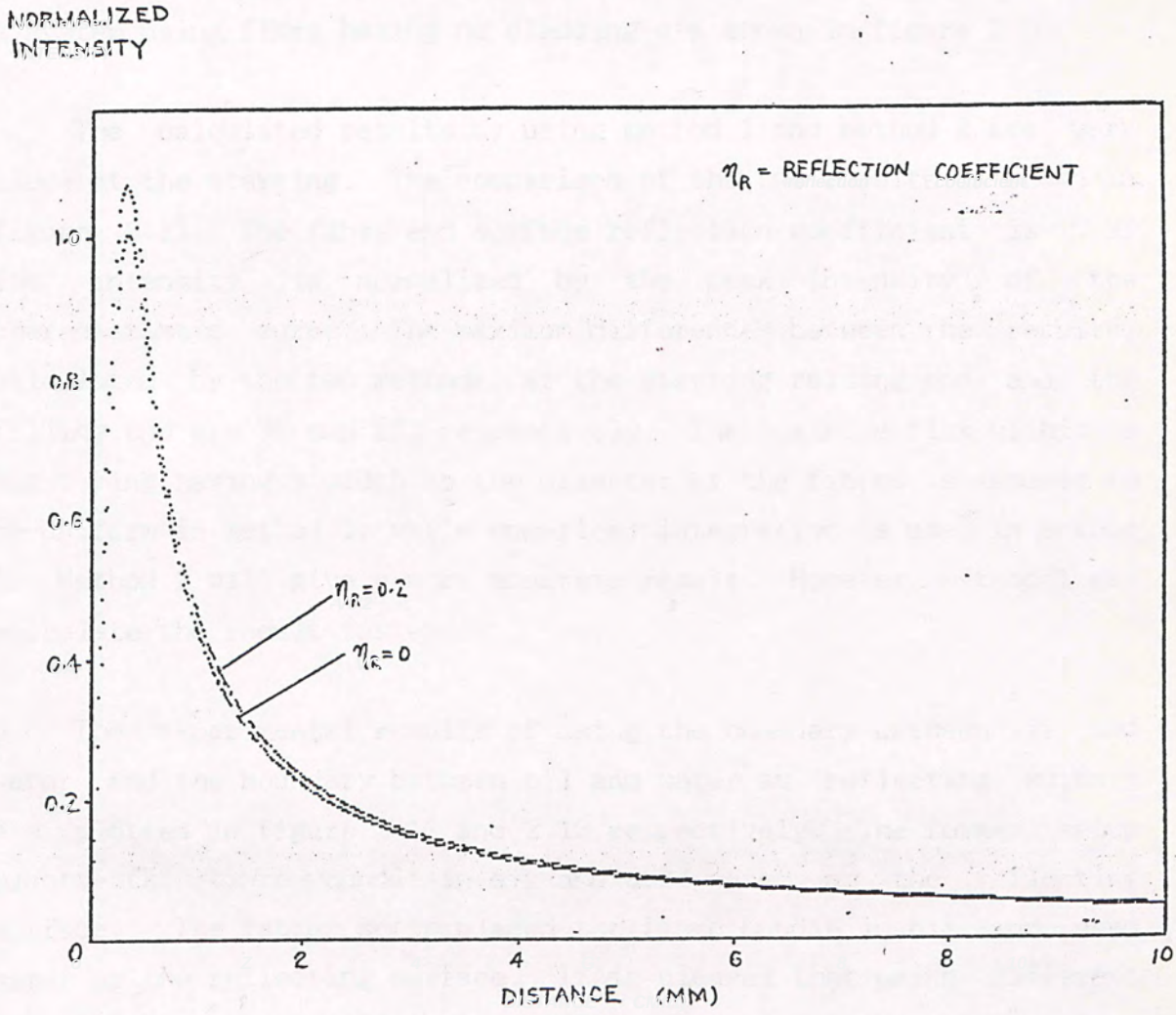

Fig. 2.7 Theoretical relationship of the normalized received luminous flux against the distance between the reflecting surface and the fibre end surface calculated by method 1. Cladding thickness is neglected. The distance is from 0 mm to 10 mm. The intensity is normalized by the peak intensity of the characteristic curve with fibre end surface reflection coefficient of 0.

coefficient of 0, 0.05, 0.1 and 0.2 is shown in figure 2.8 and 2.9 for distance of 0 mm to 10 mm and 0 mm to 1.25 mm respectively. The multi-reflection phenomenon is considered. The intensity is normalized by the peak intensity of the characteristic curve with fibre end surface reflection coefficient of 0. The characteristic of a system using fibre having no cladding are shown in figure 2.10.

The calculated results by using method 1 and method 2 are very close at the starting. The comparison of the two results is shown in figure 2.11. The fibre end surface reflection coefficient is 0.2. The intensity is normalized by the peak intensity of the characteristic curve. The maximum differences between the results, calculated by the two methods, at the starting raising end and the falling end are 3% and 23% respectively. The luminous flux within a light ring having a width as the diameter of the fibres is assumed to be uniform in method 1, while numerical integration is used in method 2. Method 2 will give a more accurate result. However, method 1 can calculate the result faster.

The experimental results of using the boundary between air and water and the boundary between oil and water as reflecting surface are plotted in figure 2.12 and 2.13 respectively. The former setup placed the fibre bundle in air and used water as the reflecting surface. The latter setup placed the fibre bundle in oil and used water as the reflecting surface. It is cleared that using different reflecting surface will obtain different sensitivities. Deviations in the characteristic curves were due to the imperfect in the fibre bundle. Off center, non-uniform spacing among fibres, inclination in the axis of the fibre bundle and the difference in medium caused the shift in the characteristic curve and differences in intensity. A photograph of the experimental setup is shown in figure 2.14. A photograph of the end surface of the fibre bundle is shown in figure 2.15.

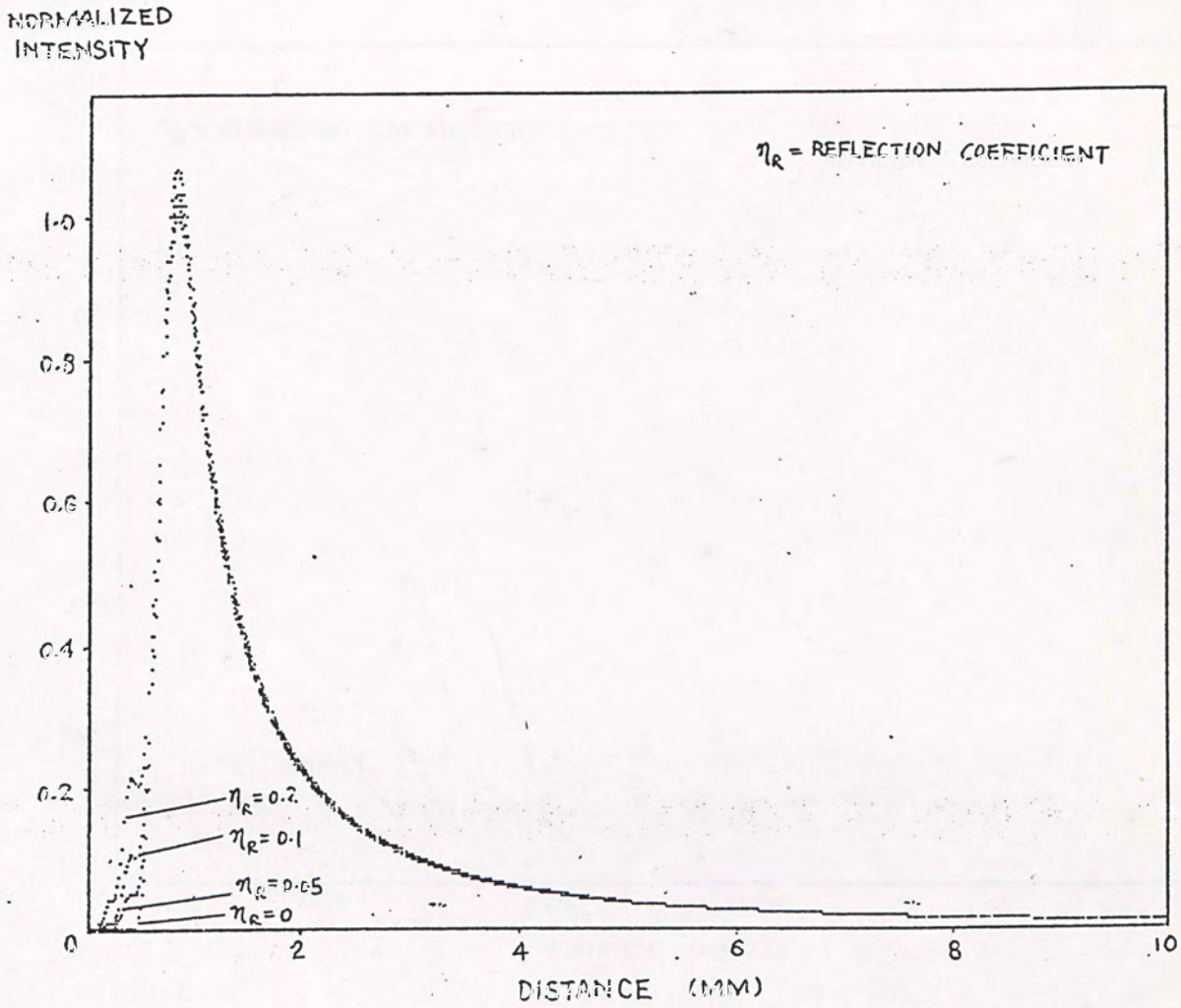

Fig. 2.8 Theoretical relationship of the normalized received luminous flux against the distance between the reflecting surface and the fibre end surface calculated by method 2. The distance is from 0 mm to 10 mm. The intensity is normalized by the peak intensity of the characteristic curve with fibre end surface reflection coefficient of 0.

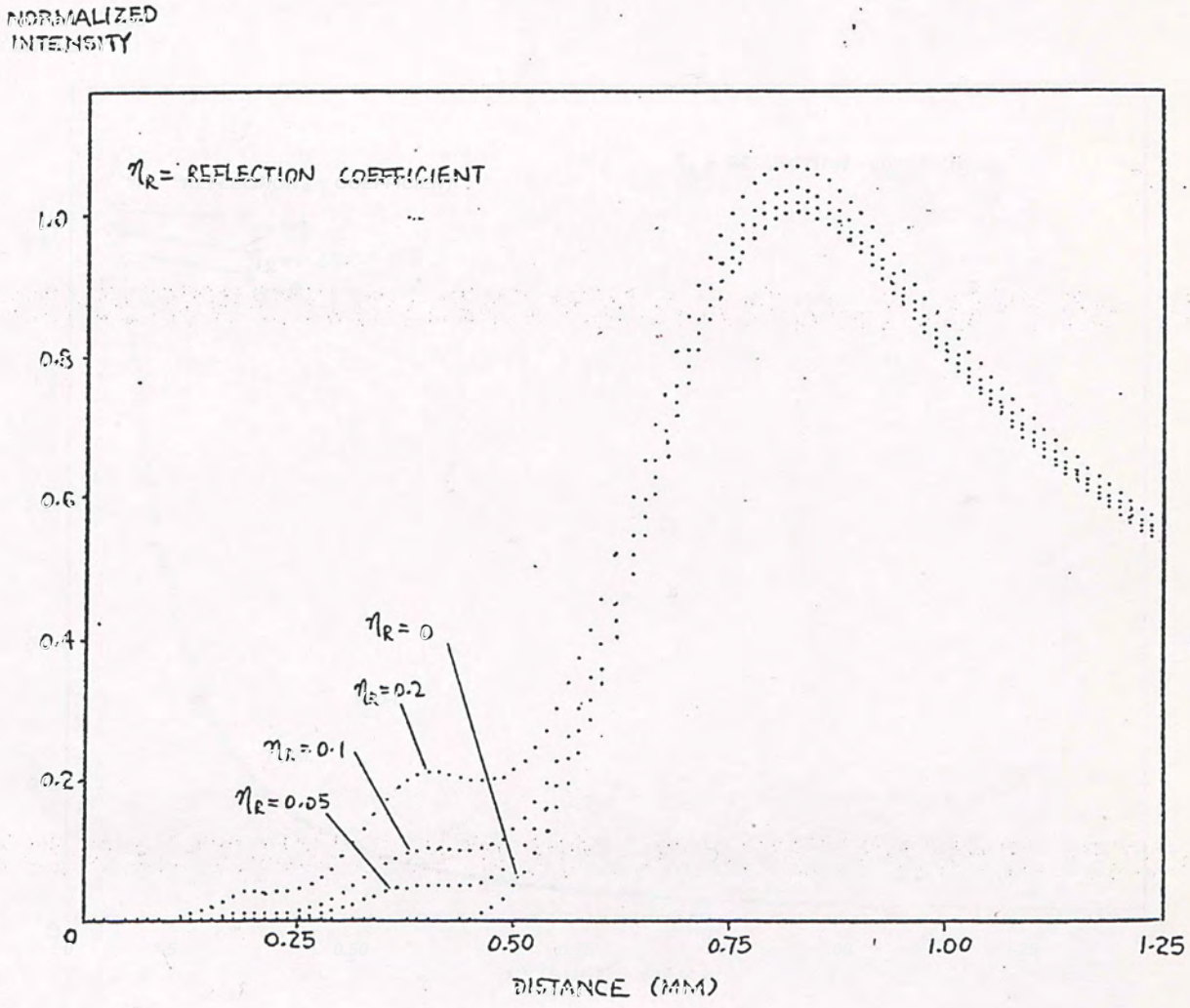

Fig. 2.9 Theoretical relationship of the normalized received luminous flux against the distance between the reflecting surface and the fibre end surface calculated by method 2. The distance is from 0 mm to 1.25 mm. The intensity is normalized by the peak intensity of the characteristic curve with fibre end surface reflection coefficient of 0.

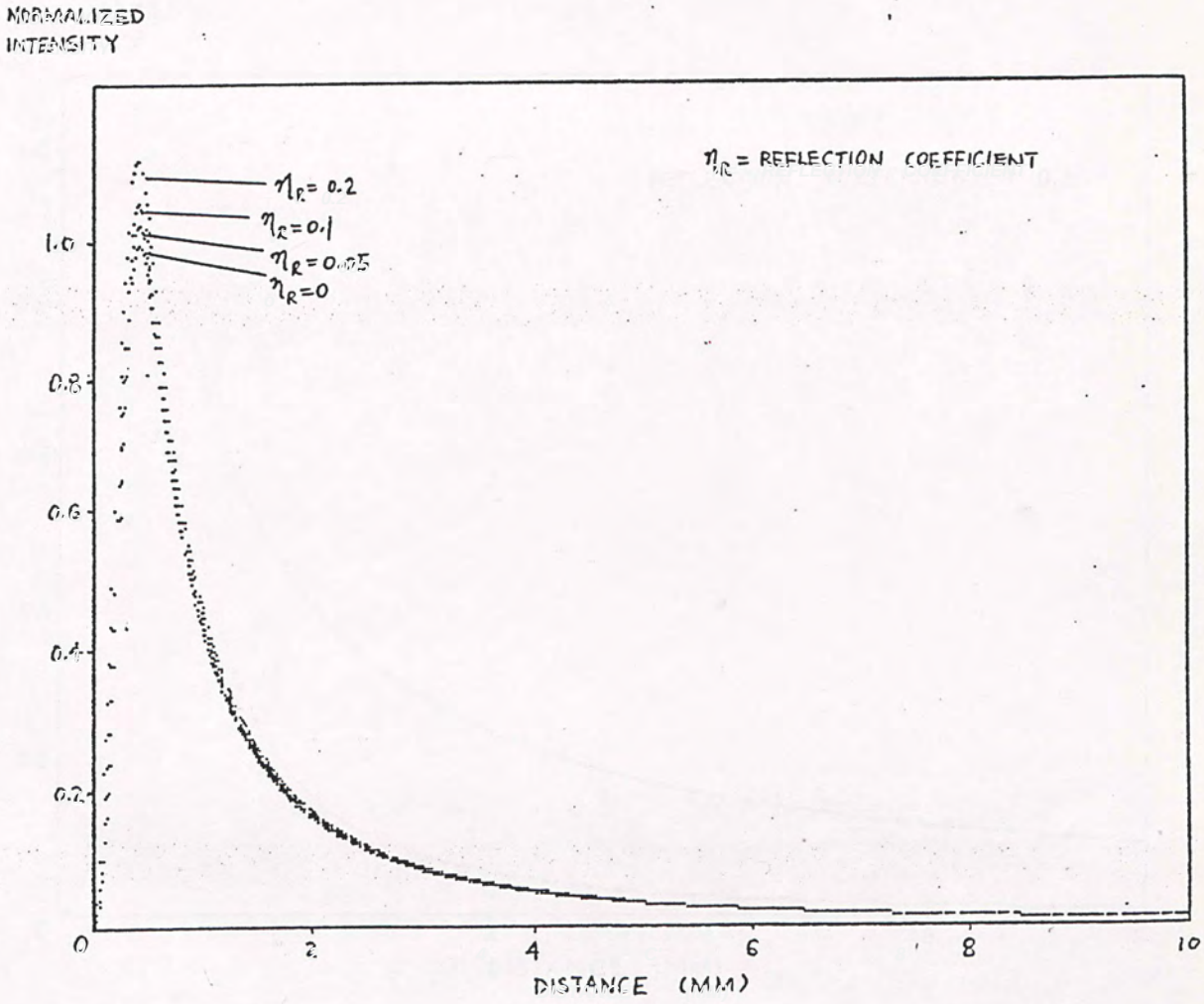

Fig. 2.10 Theoretical relationship of the normalized received luminous flux against the distance between the reflecting surface and the fibre end surface calculated by method 2. The cladding thickness is neglected. The distance is from 0 mm to 10 mm. The intensity is normalized by the peak intensity of the characteristic curve with fibre end surface reflection coefficient of 0.

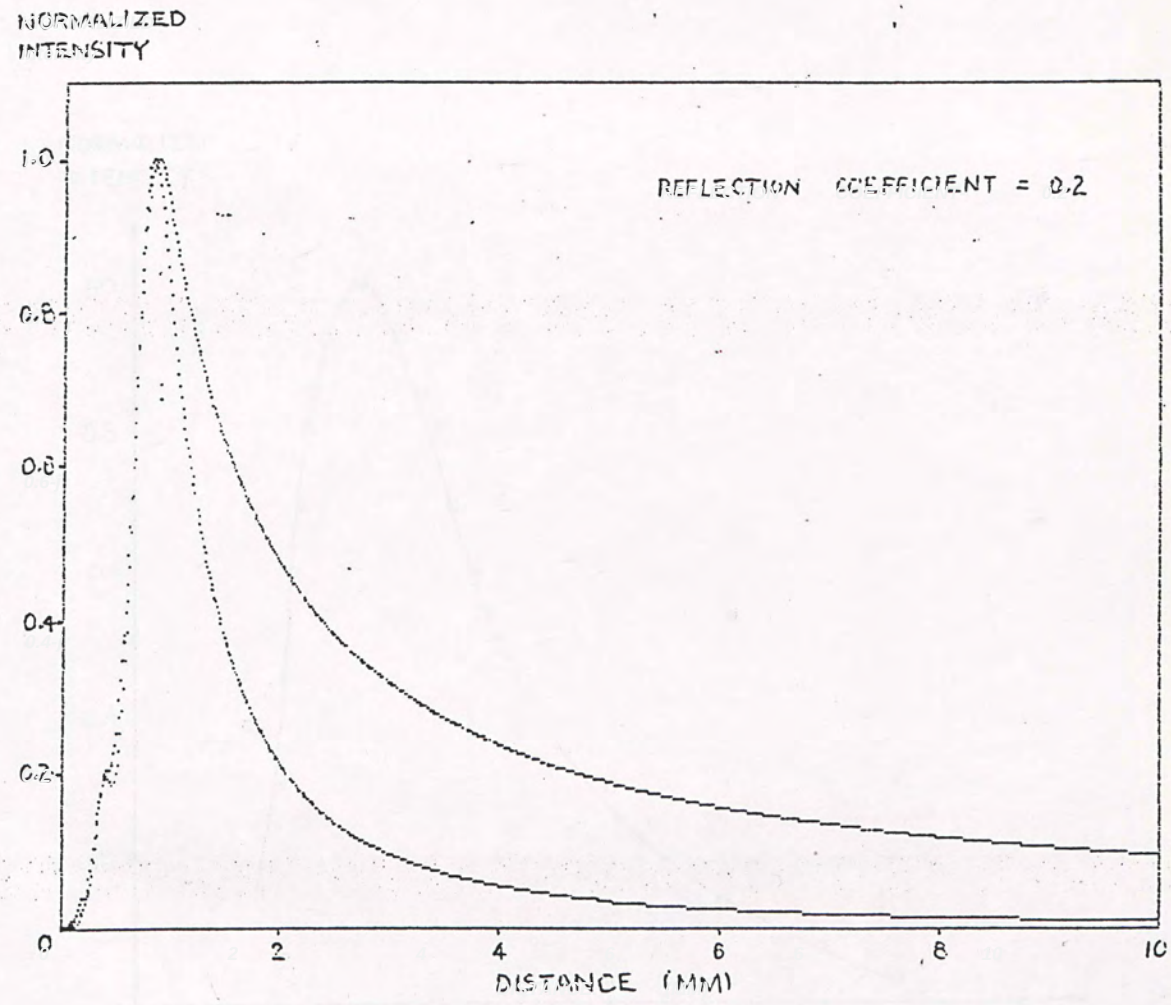

Fig. 2.11 Theoretical relationship comparison of the normalized received luminous flux against the distance between the reflecting surface and the fibre end surface in method 1 and method 2. The distance is from 0 mm to 10 mm. The fibre end surface reflection coefficient is 0.2. The intensity is normalized by the peak intensity of the characteristic curve.

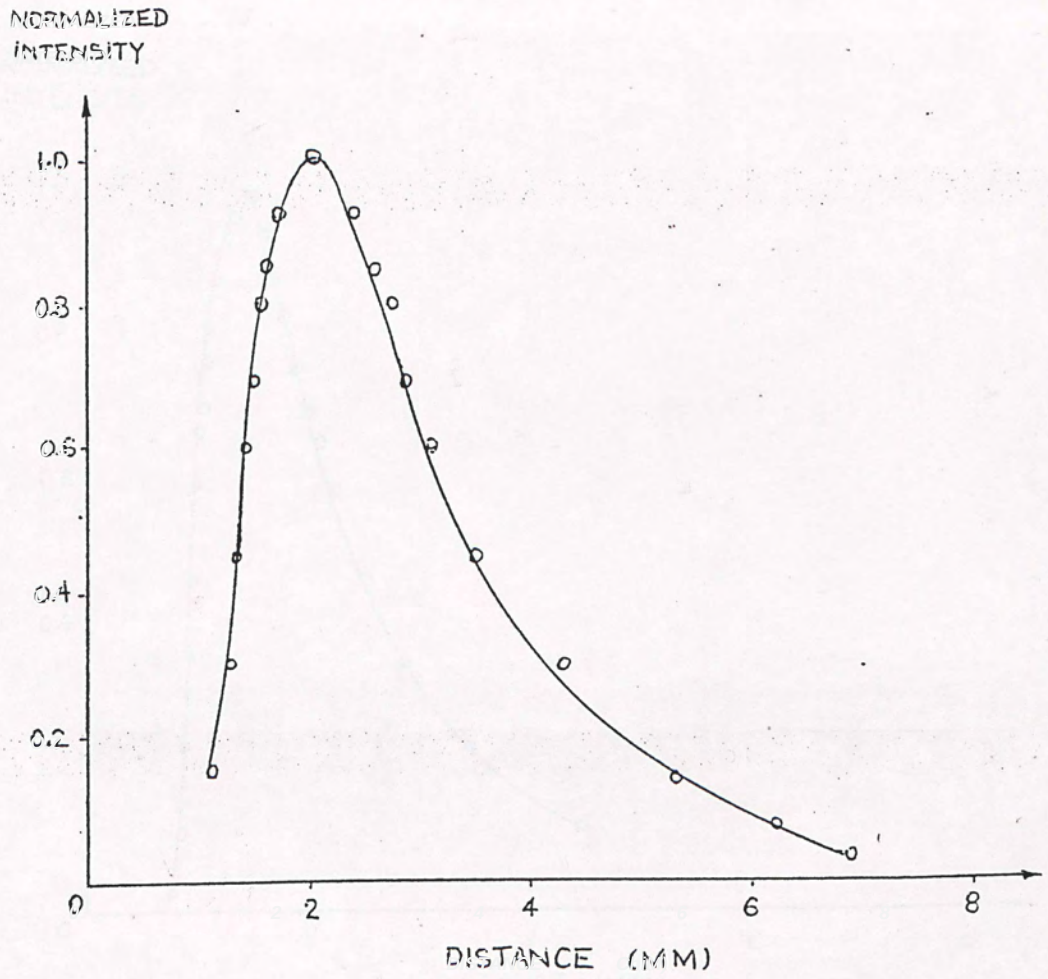

Fig. 2.12 Experimental result of placing the fibre bundle in air and using water as reflecting surface.

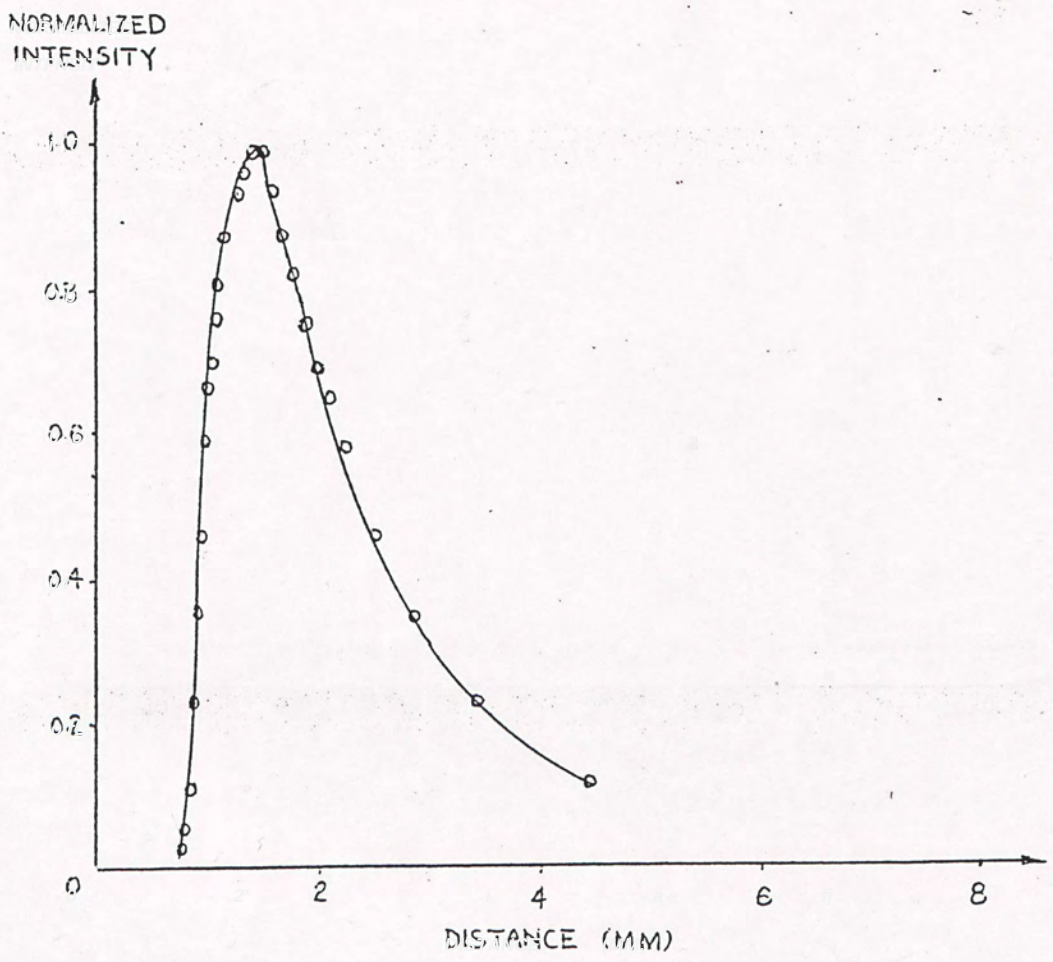

Fig. 2.13 Experimental result of placing the fibre bundle in oil and using water as reflecting surface.

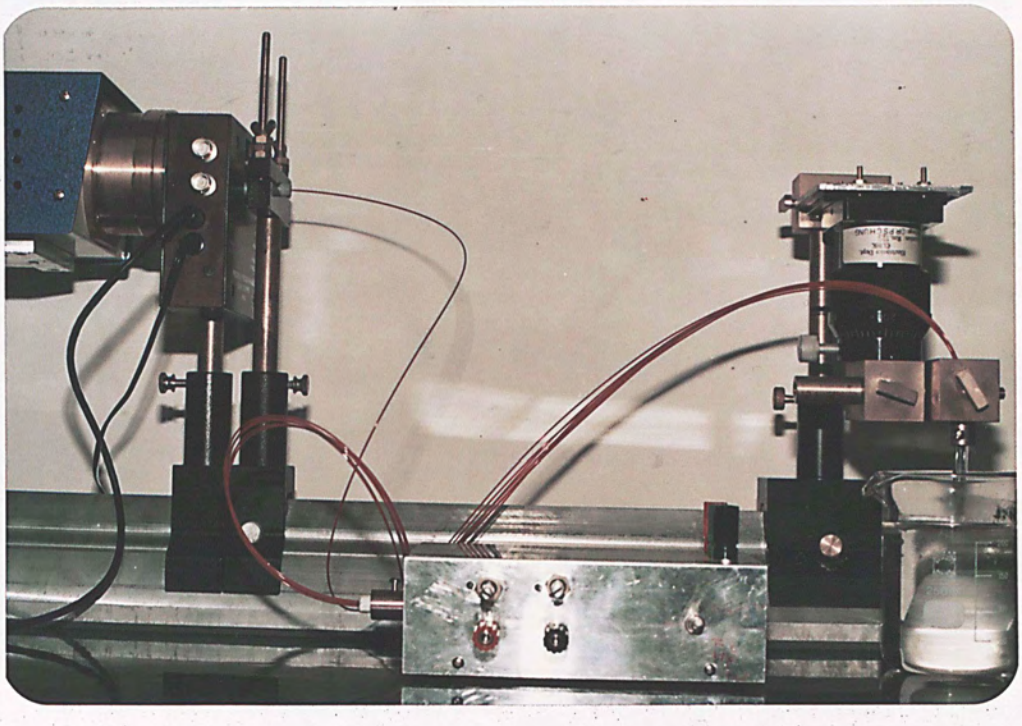

Fig. 2.14 Experimental setup of the displacement measuring system.

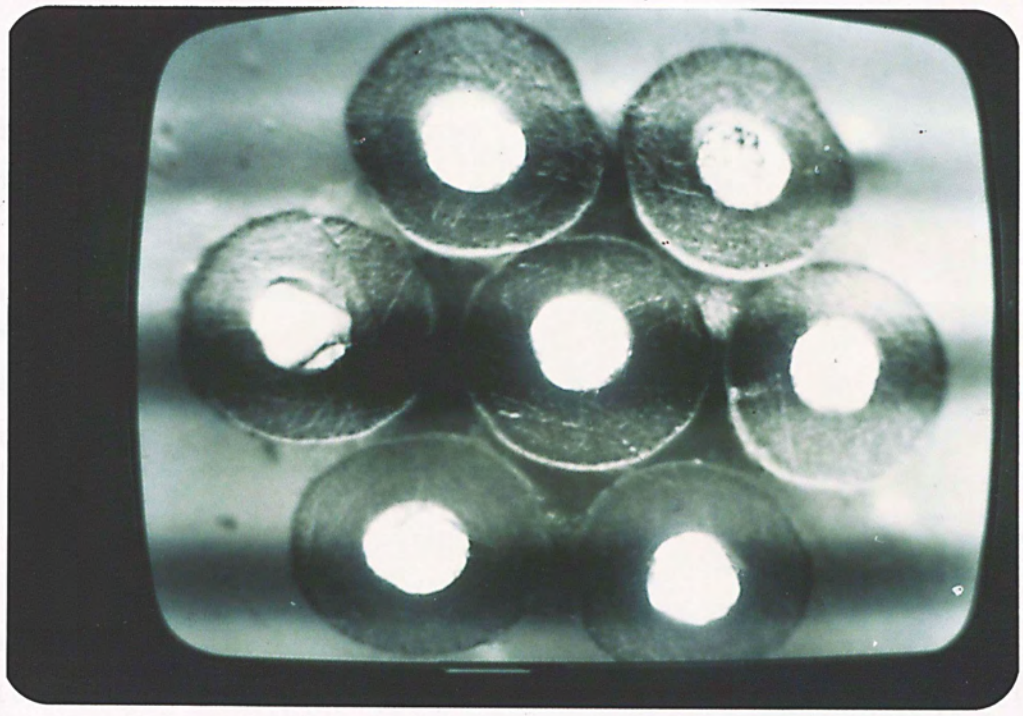

Fig. 2.15 End surface view of the fibre bundle.

2.4 Conclusion

An optical displacement measuring device is built by multimode fibres. All the components in the setup are cheap and common available materials. Using optical fibre to build a cheap and accurate distance measuring device is realized. Formulas are proposed for theoretical analysis on the characteristic of the optical displacement measuring device.

Although theoretical analysis is developed, the variation in practical parameters causes the difference in theoretical calculation and practical result.

At present moment, electronic displacement sensors are undoubtly cheaper and more accurate than optical fibre displacement sensor. However, optical fibre displacement sensors have their advantages in hazard area and poor environment.

There is a sharp peak in the characteristic curve. Its position is depended on the physical dimensions and positions of the fibres in the fibre bundle. Using a servo motor with the detector output voltage as feedback, the peak can be chased time to time, while the reflector is moved. Hence, the displacement of the reflector can be measured. This can be one of the various applications of the sensing system.

Reference

2.1 J. Simon: "New Noncontact Devices for measuring small Microdisplacements", Applied Optics, October, 1970, vol.9, no.10, pp.2337-2340.

2.2 Geza J. Jako, Kenneth E. Hickman, Lewis A. Marots and Sandor Holly: "Recording of the Movement of the Human Basiler Membrane", J. of the Acoustical Society of America, 1967, vol.41, no.6, p.1578.

2.3 R.O. Cook, T. Komishi, C. W. Hamm, and A.H. Yankwich: "Relationship of SPL, CM, and umbo displacement under fre-field closed bulla conditions in guinea pig", J. of Acoustical Society of America, vol. 58, Suppl. no.1, p.S104, YY7.

2.4 R.O. Cook, T. Komishi, C.W. Hamm, and A.H. Yankwich: "Relationship of ossicular chain displacement and CM resulting from stimulation with direct contact piezoelectric", J. of Acoustical Society of America, vol.58, Suppl. no.1, p.S104, YY8.

2.5 R.O. Cook and C.W. Hamm: "Fiber optic lever displacement transducer", Applied Optics, vol.18, no.19, pp.3230-3241, October, 1979.

2.6 P.L. Chu, T. Whitbread and P.M. Allen: "Fibre Optic Lever Sensors",pp.976-979.

CHAPTER 3
OPTICAL WEIGHT SENSOR USING INTENSITY SENSING TECHNIQUE

3.1 Introduction

Weight measuring devices are absolutely necessary in a commercial society. In all trading and manufacturing processes, the quantities of the goods or materials used must be specified. Weight is one of the various kinds of measurement. It is so important in markets that weight measuring methods were developed at the early history in human lives. Modifications and developments are going on time to time.

Traditional weight measuring devices have their own deficiencies. For example, some of them cannot be used in corrosive environment. Some of them have not a large dynamic range. Some of them have not a high precision. It is still necessary to develop new weight measuring devices for the fast-developing world. Optical weight measuring device is one of the unlimited solutions for weight measuring problems. In this chapter, an optical weight measuring sensor is introduced.

3.2 Principle of Optical Weight Measuring Sensor

The proposed optical weight measuring sensor is in fact a modification of the optical displacement sensor introduced in chapter 2. It is so modified that it can be used for measuring weight. The schematic diagram of the optical weight measuring sensor and the photograph of the setup are shown in figure 3.1 and 3.2 respectively. The light from the light source is transmitted by the source fibre to the reflecting surface mounted on a hydraulic system. The return fibre collects a part of the reflected light and then transmitted to the light detector. The fibre bundle is mounted on the piston of secondary cylinder in the hydraulic system. As described in chapter 2, the electrical output at the photodetector is related to the distance between the fibre end and the reflecting surface. By using a simple hydraulic system, the level of the fibre end surface can be related to the length of the control spring. The change in length of the control spring depends on the weight of the object put on the container at the piston of primary cylinder in the hydraulic system. Here-on the weight of the measured object is related to the electrical output of the photodetector.

As the relationship of the luminous flux collected by the return fibre and the distance between the fibre end and the reflector is mentioned in chapter 2, only the theory of the hydraulic system and the control spring will be discussed in Appendix C. The arrangement of the hydraulic system and the control spring is shown in figure 3.3. The weight of the measured object is expressed as

$$W = [\rho g (A_1 + A_2) + k A_2/A_1] (y - y_0) \qquad [3.1]$$

As ρ, g, k, A_1 and A_2 are constants, the weight of the measured object is proportional to the distance between the sensing head and the reflecting surface. The equation 3.1 can be written as

$$W = m \varepsilon y \qquad [3.2]$$

where $$m = \rho g (A_1 + A_2) + k A_2/A_1 \qquad [3.3]$$

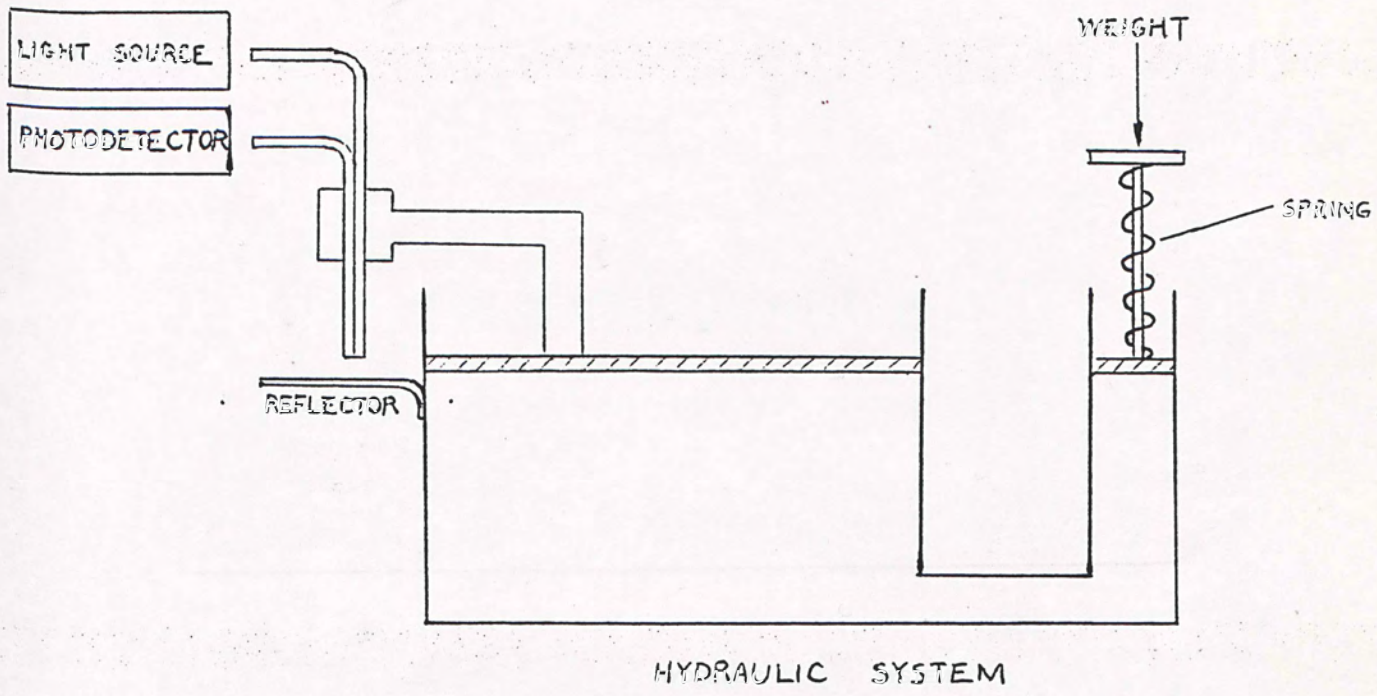

Fig. 3.1 Schematic diagram of the optical weight measuring sensor.

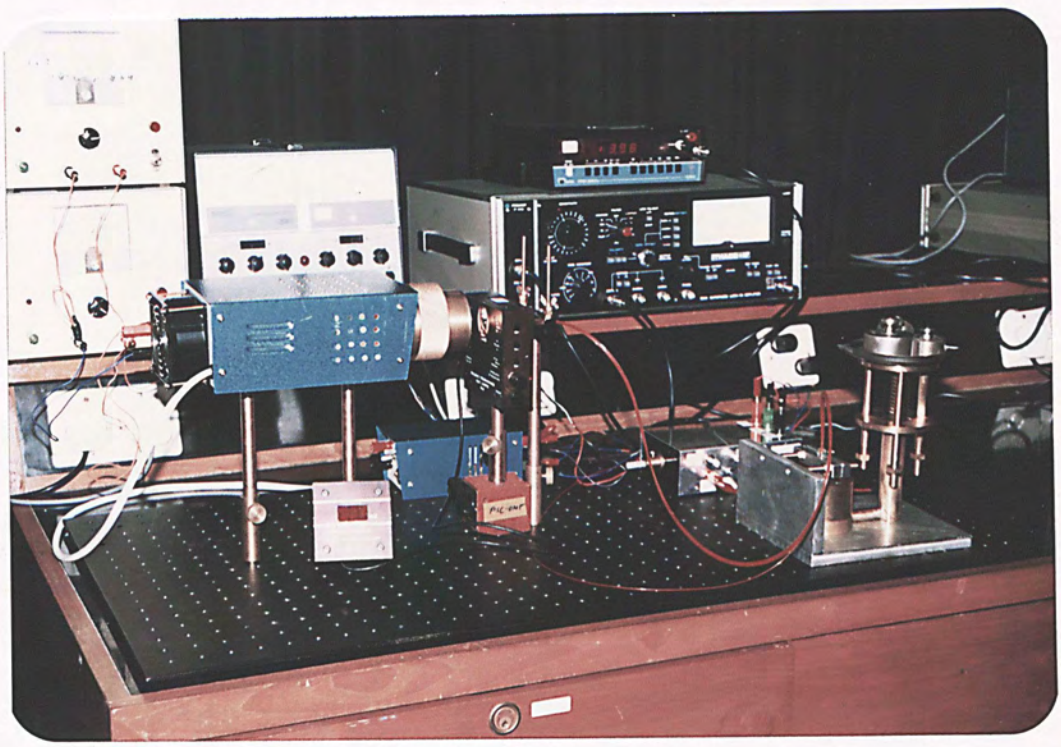

Fig. 3.2 Photograph of the experimental setup of the optical weight measuring sensor.

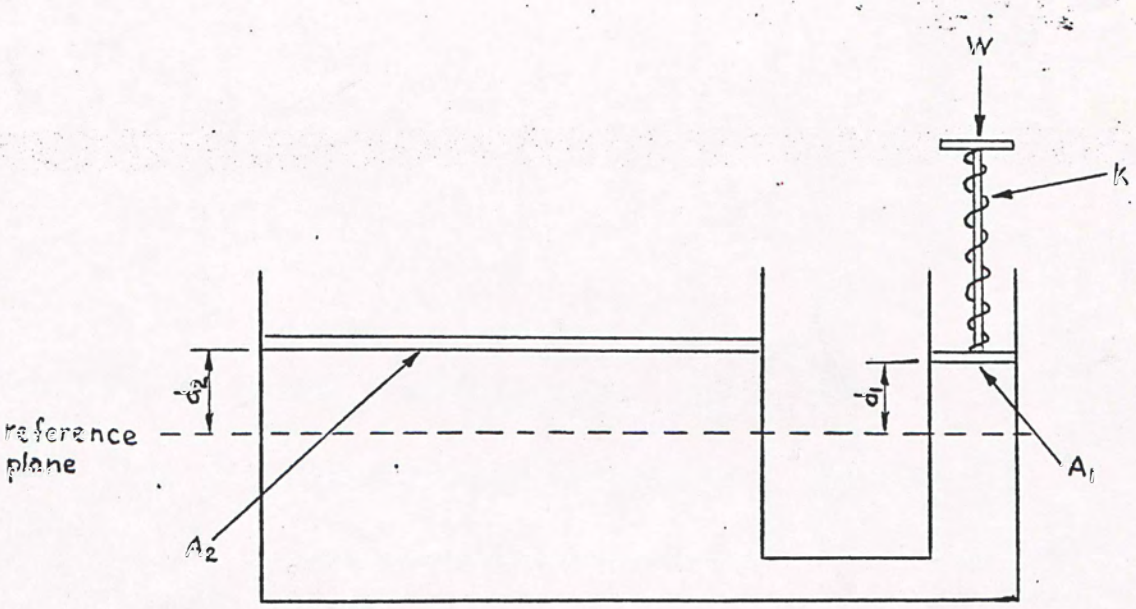

Fig. 3.3 Arrangement of the hydraulic system and the control spring.

$$\varepsilon y = y - y_0 \qquad [3.4]$$

The characteristic curve of the optical weight sensing device can be obtained by extracting the respective portion from the characteristic curve of the optical displacement sensor and multiplying by the constant m.

3.3 Experimental Result

The internal radius of the primary cylinder and the secondary cylinder are 6.35 mm and 25.4 mm respectively. The solution used in the hydraulic system is glycerine. The density of glycerine is 234 kg/m^3 [3.1-3.4]. g is 9.81 m/s^2. The calibration curve in figure 3.4 shows that the spring constant is found to be 47 kg/m. From equation 3.2, the weight of the measured object is given by

$$W = 757 \times (y - y_o) \qquad [3.5]$$

where y is in meter.

The experimental characteristic curve of the optical weight measuring sensor was plotted in figure 3.5. The measuring range was 2.6 kilogram. The curve may be divided into three portions. The first part of the curve (0 g to 300 g) has a rising slope with a low sensitivity. The second part of the curve (400 g to 800 g) has also a rising slope but with a high sensitivity. The third part of the curve (1400 g to 2600 g) has a falling slope with a low sensitivity.

By using least-square-error fit method, the following statistical figures were obtained. The sensitivity of the first part of the characteristic was 2.625 V/kg. The mean error at this part was 43.75 mV. The standard deviation was 63.43 mV. At the second part of the characteristic, the sensitivity was 26.44 V/kg. The mean error at this part was 0.7181 V. The standard deviation was 0.6892 V. The sensitivity of the third part of the characteristic was -5.33 V/kg. The mean error and the standard deviation at this part were 0.2477 V and 0.1532 V respectively.

For further detail analysis on each part of the characteristic of the measuring device, three sets of tests were carried out separately. The three sets of tests were individually stressed on the three portions of the characteristic curve.

The experimental testing result for examining the first part was

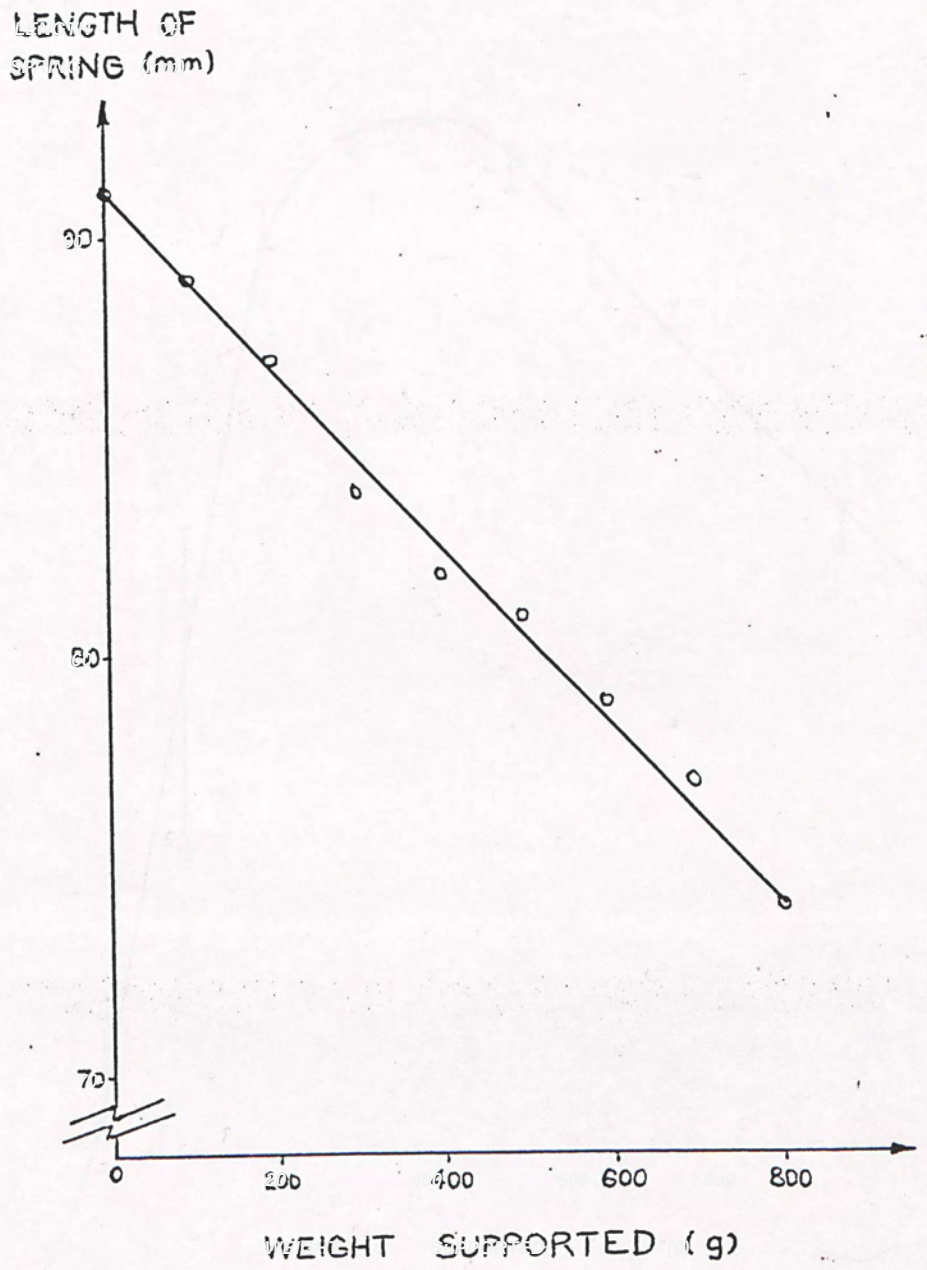

Fig. 3.4 Calibration curve for the spring used in the experiment.

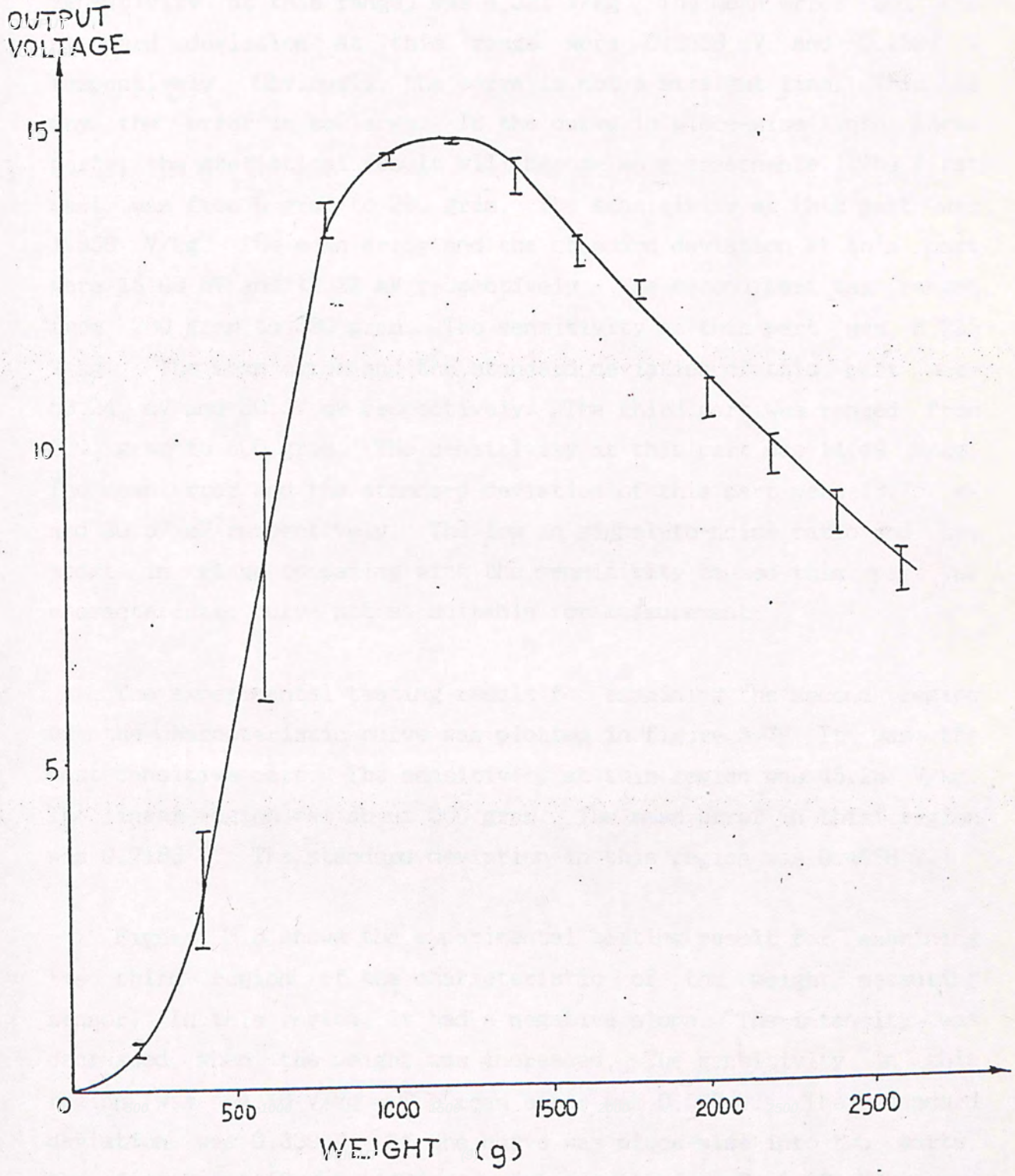

Fig. 3.5 Characteristic curve of the optical weight measuring sensor with a measuring range of 2.6 kg.

plotted in figure 3.6. In this part, the sensitivity was very low. The range shown in the figure was 600 gram. If the whole curve was fitted for a straight line, the slope of the straight line (i.e. sensitivity at this range) was 4.321 V/kg. The mean error and the standard deviation at this range were 0.2356 V and 0.1597 V respectively. Obviously, the curve is not a straight line. This is why the error is so large. If the curve is piece-wise into three parts, the statistical result will become more reasonable. The first part was from 0 gram to 280 gram. The sensitivity at this part was 1.656 V/kg. The mean error and the standard deviation at this part were 15.69 mV and 12.22 mV respectively. The second part was ranged from 280 gram to 530 gram. The sensitivity at this part was 6.255 V/kg. The mean error and the standard deviation of this part were 53.24 mV and 30.57 mV respectively. The third part was ranged from 530 gram to 600 gram. The sensitivity at this part was 14.49 V/kg. The mean error and the standard deviation of this part were 43.75 mV and 30.57 mV respectively. The low in signal-to-noise ratio and the short in range comparing with the sensitivity caused this part of characteristic curve not so suitable for measurement.

The experimental testing result for examining the second region of the characteristic curve was plotted in figure 3.7. It was the most sensitive part. The sensitivity at this region was 45.23 V/kg. The linear region was about 300 gram. The mean error in this region was 0.7186 V. The standard deviation in this region was 0.4636 V.

Figure 3.8 shows the experimental testing result for examining the third region of the characteristic of the weight measuring sensor. In this region, it had a negative slope. The intensity was decreased when the weight was increased. The sensitivity in this region was -4.16 V/kg. The mean error was 0.562 V. The standard deviation was 0.339 V. If the curve was piece-wise into two parts, the first part (0 g to 1400 g) had a sensitivity of -5.28 V/kg and the second part (1400 g to 2800 g) had a sensitivity of -2.66 V/kg. The mean error and the standard deviation at the first part were 0.324 V and 0.222 V respectively. The mean error and the standard deviation at the second part were 0.289 V and 0.183 V respectively.

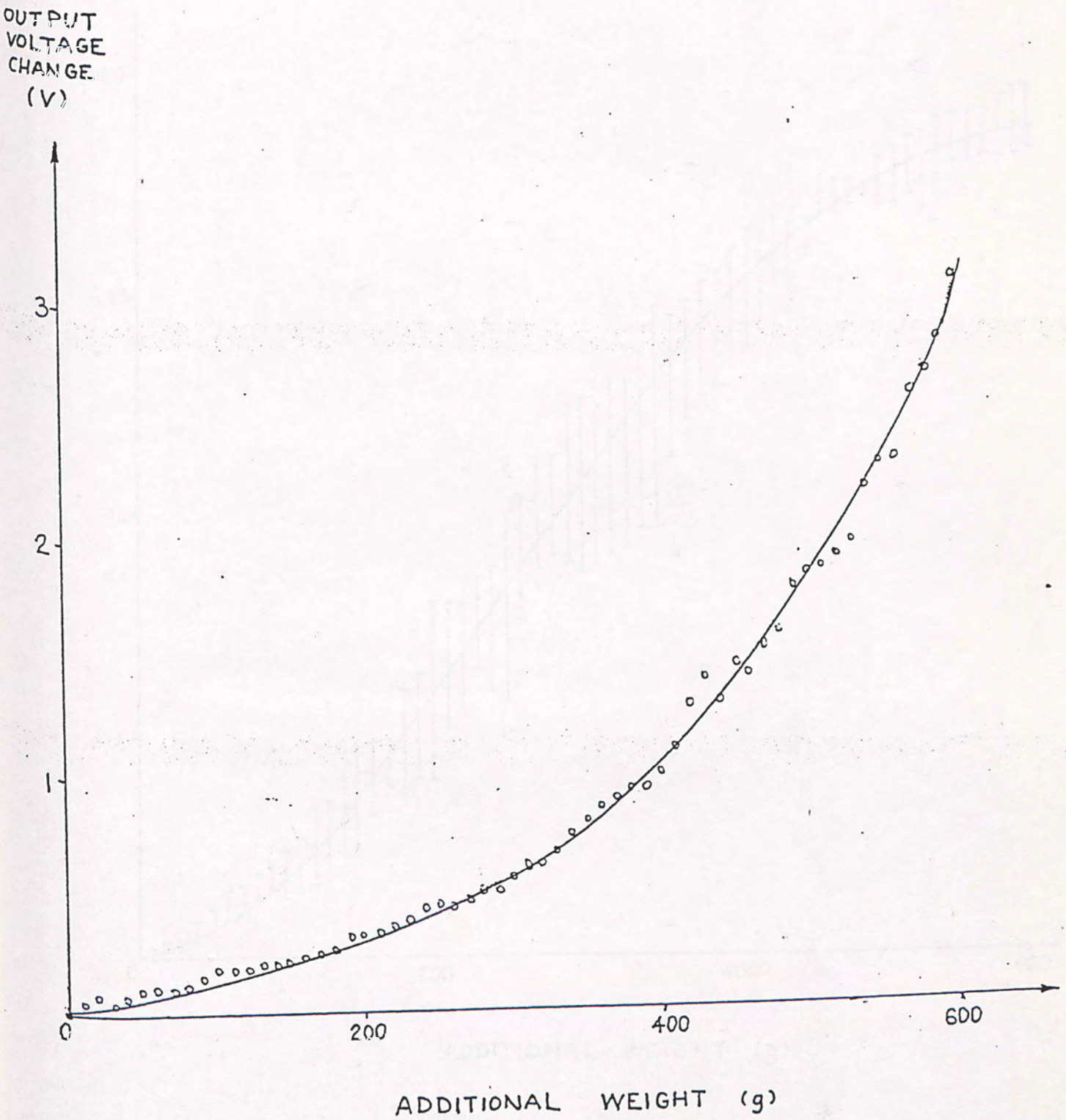

Fig. 3.6 Experimental result of the first portion of the characteristic curve.

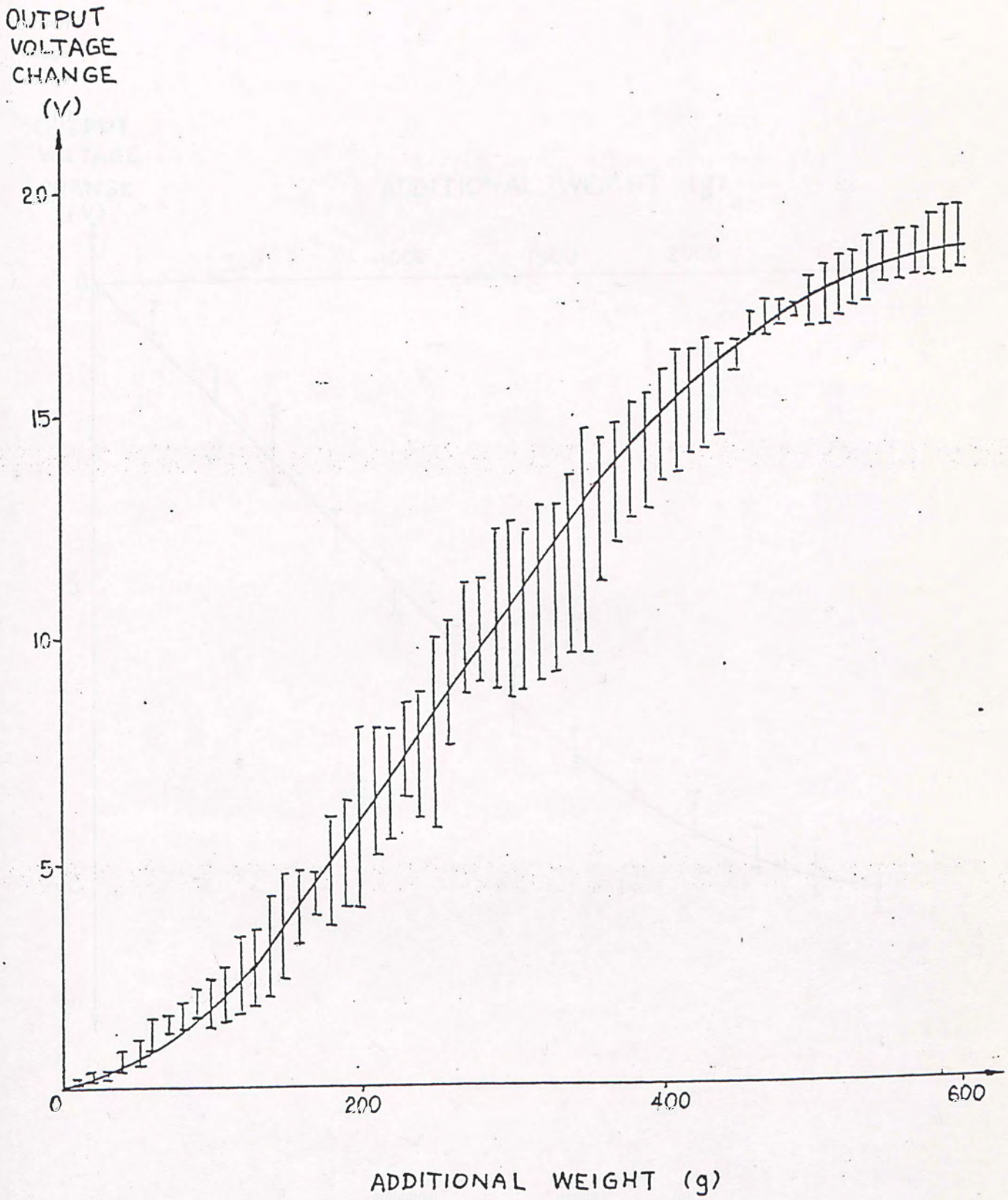

Fig. 3.7 Experimental result of the second portion of the characteristic curve.

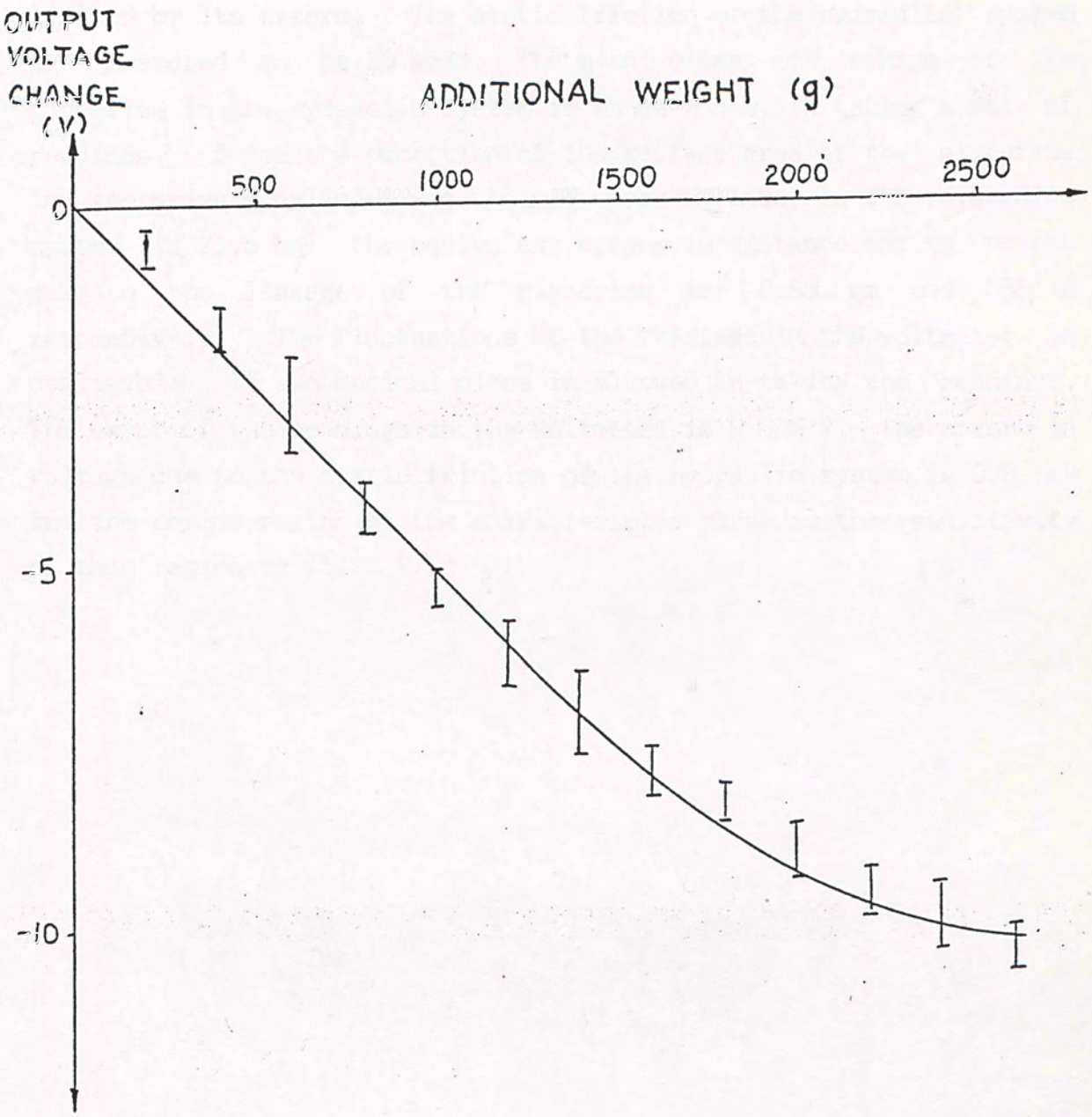

Fig. 3.8 Experimental result of the third part of the characteristic curve.

The error of this sensing device is mainly due to the static friction at the pistons in the cylinders and the leakage of glycerine in the hydraulic system. The resolution of this sensing device is limited by its errors. The static friction of the hydraulic system was measured to be 20 gram. The mean volume of leakage of the glycerine in the hydraulic system is about 2 c.c. in taking a set of readings. Since the summation of the surface area of the glycerine in the primary cylinder and the secondary cylinder in the hydraulic system is 21.5 cm^2, the equivalent errors in distance and in weight due to the leakage of the glycerine are 0.93 mm and 388 g respectively. The fluctuations of the readings in the voltmeter is negligible, if two decimal place is allowed in taking the readings. The error of the readings in the voltmeter is 0.005 V. The error in voltage due to the static friction of the hydraulic system is 0.9 mV in the second region of the characteristic curve as the sensitivity of this region is 45.23 V/kg.

3.4 Conclusion

An optical weight sensor is demonstrated and its performance is shown in this chapter. Of course, it will not be as cheap as spring balance or other common weight measuring device. However, if it is applied in some hazardous area or corrosive area, it has a potential to be a comparative cheap and accurate measuring device. Theoretical prediction on the characteristic is also proposed. However, the practical starting point in the characteristic curve is difficult to predict unless a very accurate manufacturing procedure is used to fabricate the optical sensor. And also, it shall cost more to prevent leakage and reduce friction.

By increasing the ratio of the diameters of the hydraulic cylinders or using a spring having a larger stiffness, the measuring range can be increased.

Reference

3.1 Victor L. Streeter: "Handbook of Fuild Dynamics", McGraw-Hill Book Company, 1961.

3.2 G.W.C. Kaye and T.H. Laby: "Tables of Physical and Chemical Constant", Longmans, 1911.

3.3 John Robson: "Basic Tables in Physics", McGraw-Hill, 1967.

3.4 Victor J. Johnson: "Properties of Materials at Low Temperature", Perganon Press, 1961.

CHAPTER 4
OPTICAL TENSION SENSOR USING MODAL SENSING TECHNIQUE

4.1 Introduction

The phase change of a light wave travelling in an optical fibre is very sensitive to external influence. In the previous two chapters, intensity sensors have been discussed. They are using external modulation technique. Phase sensors usually employ internal modulation technique. There is no such a need to break the sensing fibre into two parts - source fibre and return fibre - as in intensity sensors.

Phase modulation of light as a highly sensitive monitor of environmental changes has been increasingly exploited over the past hundred years [4.1]. An optical fibre phase-sensitive device requires some forms of interferometer to perform the phase detection process [4.2, 4.3]. The traditional form of interferometer is using the Mach Zehnder interferometric technique, which employs one optical fibre as the sensing arm and another optical fibre as the reference arm. The technique is in the same form of a heterodyne system [4.4]. When this kind of sensors is used for measuring strain, it has a sensitivity of about 11 radians/longitudinal microstrain and 6 radians/radial microstrain [4.5].

The proposing modal sensing technique in this chapter employs the interference between the core mode and the cladding mode to obtain the phase change. The simplicity in structure and the sensitivity in characteristic give this sensing technique a possibility to challenge the traditional phase sensing technique.

The practical application of the modal sensing technique in here is to measure the tension in an optical fibre. Tension is also a kind of force. Different with weight measuring device and compression measuring device, the direction of force applied on it is pointing out instead of pointing in. It causes a tension measurement more difficult comparing with a compression measurement.

Primitive tension meters used a spring to hang the tested object. Observing the extended length of the spring, the tension in the measured object can be calculated. Many other kinds of tension meters are using a similar operating principle. As things are trending towards electronics, industrialists have also pushed this kind of measurement to have an electronic revolution. According to the advantages of using optical fibre, optical tension measuring devices will also be one of the competitors in the market of tension measuring instruments [4.6], especially used in optical communication systems.

4.2 Principle of Modal Sensing Technique

Modal sensors are those sensors in which the information of the measurand is obtained by the interference between different modes. Generally, optical fibre sensors employ the intensity sensing technique and the phase sensing technique (Mach Zehnder Interferometric technique) [4.7, 4.8]. Although modal sensing technique had been proposed [4.9] and built in prototype [4.10-4.13], this technique is still in a research stage. No commercial product is available in the market. The main problem is that the different modes cannot be controllably injected into a fibre and then received separately.

The proposing modal sensing technique employs the interference between the core mode and the cladding mode of the sensing fibre to measure the environmental change acting on the sensing fibre. In the experiment, the tension on the fibre was the measurand. The tension in a fibre will change the dimension of the fibre. Hence, the phase of the detected light beam will be changed. The interfered light is detected by a photodetector.

As the fibre is a single-mode fibre, only the fundamental mode will propagate inside the core of a fibre having a good cutting edge and it can be expressed as

$$E = E_c \sin(\omega t - \beta_c z) \qquad [4.1]$$

Consider only one mode dominant in the cladding (see Appendix D for more than one mode dominant in the cladding) and it is expressed as

$$E = E_{cln} \sin(\omega t - \beta_{cln} z) \qquad [4.2]$$

The detected intensity of the interfered light beams is given by

$$I = (1/nT) \int_0^{nT} E_R 2 \, d(\omega t) \qquad [4.3]$$

where E_R is the resultant electric field at the detecting point, T is the wavelength of the light beam, and n is an arbitrary constant. From equation 4.1, 4.2 and 4.3, the intensity obtained at the detecting point is given by

$$I = 0.5\ E_c^2 + 0.5\ E_{cln}^2 + E_c\ E_{cln} \cos(\beta_{cln} - \beta_c)z \qquad [4.4]$$

It is obvious that the equation is quite similar to that of a phase sensor using an optical fibre Mach Zehnder interferometer. It is because of that both techniques are detecting the phase change by interfering the light beams. The only difference is that the phase constant of the intensity in an optical fibre Mach Zehnder interferometer is β while the phase constant of the intensity in the proposing modal sensor is $(\beta_{cln} - \beta_c)$. The applied stress changes the dimensions of the cross-section and the refractive index of the stressing fibre so small that it can be neglected. Therefore, only the change in the detected intensity due to the change in the length of the stressing fibre is considered. The sensitivity of the proposing modal sensor can be obtained by differentiating the equation 4.4 with respect to the applied tension T. The sensitivity at the linear region is given by

$$dI/dT = E_c\ E_{cln}\ (\beta_c - \beta_{cln})\ (dz/dT) \qquad [4.5]$$

while the sensitivity of an optical fibre Mach Zehnder interferometer at the linear part is given by

$$dI/dT = E_c\ E_f\ \beta_c\ (dz/dT) \qquad [4.6]$$

Although the sensitivity of a modal sensor is lower than that of an optical fibre Mach Zehnder interferometer, the proposing modal sensor is still having a high sensitivity.

4.3 Theoretical Prediction of Tension Measuring Performance

For a mass of m kg is applied by the spring balance on the fibre, the force is given by

$$F = m g \qquad [4.7]$$

where g is the constant of gravity. For an angle of inclination θ between the axis of the spring balance and the fibre, the tension in the fibre will be reduced by a certain portion. The actual tension in the fibre is given by

$$F' = F / (2 \cos\theta)$$

$$= m g / (2 \cos\theta) \qquad [4.8]$$

As the plastic jacket is much more soften than the silica fibre [4.14], for simplicity, the force is assumed to be applied on the silica fibre only. Hence, the stress on the fibre is given by

$$S = F' / A$$

$$= m g / (2 A \cos\theta) \qquad [4.9]$$

where A is the cross sectional area of the fibre. The strain of the fibre is given by

$$E = S / E$$

$$= m g / (2 A E \cos\theta) \qquad [4.10]$$

where E is the Young's modulus. For the strain is applied over a part of the fibre which length is l, the change in length εl of the fibre is given by

$$\varepsilon l = l E$$

$$= m g l / (2 A E \cos\theta) \qquad [4.11]$$

The phase change of the resultant light intensity detected is given by

$$\phi = (\beta_c - \beta_{cln}) \varepsilon l$$

$$= (\beta_c - \beta_{cln}) m g l / (2 A E \cos\theta) \qquad [4.12]$$

The parameters of the silica fibre used is [4.14, 4.15, 4.16]

$n_1 \simeq n_2 = 1.46$
$\Delta n = 0.005$
Young's modulus = 1.9×10^{11} N/m^2
Poisson's ratio = 0.17
diameter of core = 10 μm
diameter of cladding = 150 μm

The dimensions of the setup A are shown in figure 4.1. The length of the fibre used was 0.78 meter. The angle of inclination of the fibre was 44°. From the above parameters, it can be calculated that

$$\beta_c - \beta_{cln} = 49.7 \times 10^3 \text{ rad/m}$$

$$A = (\pi/4) \times (150 \times 10^{-6})^2$$

$$= 1.77 \times 10^{-8}$$

Hence from the equation 4.6, the phase change due to one gram of mass is given by

$$\phi = (49.7 \times 10^3 \times 10^{-3} \times 9.81 \times 0.78)/(2 \times 1.77 \times 10^{-8} \times 1.9 \times 10^{11} \times \cos 44°)$$

$$= 78.6 \times 10^{-3} \text{ rad}$$

The mass required to have a whole period of change in resultant light intensity detected is

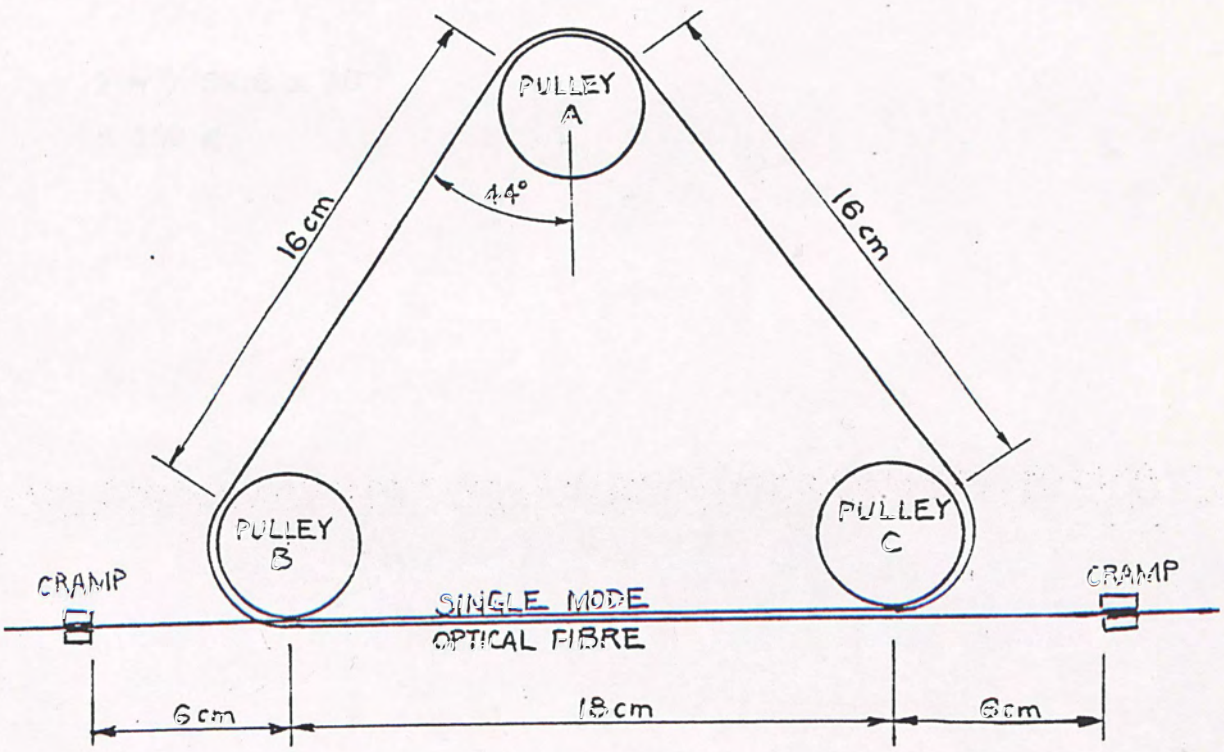

Fig. 4.1 Dimensions of the setup A.

$2\pi / 78.6 \times 10^{-3}$

$= 79.9$ g

The dimension of the setup B is shown in the figure 4.2. The length of the fibre used was 0.51 meter. The angle of inclination of the fibre is 21°. From these parameter, the predicted value can be calculated similarly. The phase change due to one gram of mass is

$$\phi = (49.7\times10^{3}\times10^{-3}\times9.81\times0.51)/(2\times1.77\times10^{-8}\times1.9\times10^{11}\times\cos21°)$$
$$= 39.6 \times 10^{-3} \text{ rad}$$

The mass required to have a whole period of change in the resultant light intensity detected is

$2\pi / 39.6 \times 10^{-3}$

$= 159$ g

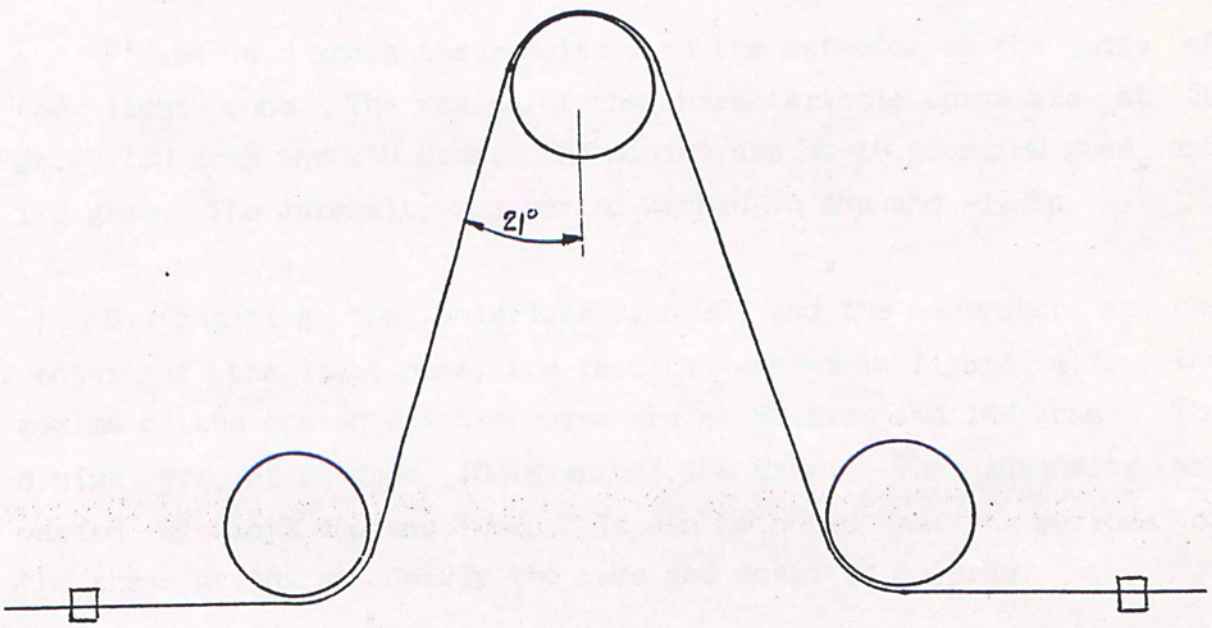

Fig. 4.2 Dimension of the setup B.

4.4 Experimental Result

A photograph of the experimental setup is shown in figure 4.3. Photographs of the light cone, with different tension applied on the fibre, are shown in figure 4.4.

Figure 4.5 shows the result of the tension measurement using setup A with a range of 210 g change. The detector was put in the center of the light cone. The maxima of the characteristic curve are at 10 gram, 90 gram and 170 gram. The minima are at 50 gram and 130 gram. The period is 80 gram, which is very closed to the predicted value in the theoretical calculation. The intensity was varied within -1 dBμ and -17 dBμ.

Figure 4.6 shows the results with the detector at the edge of the light cone. The maxima of the characteristic curve are at 50 gram, 130 gram and 210 gram. The minima are at 10 gram, 90 gram and 170 gram. The intensity was varied within -5 dBμ and -12dBμ.

By rotating the polarizer with 90° and the detector at the center of the light cone, the results were as in figure 4.7. The maxima of the characteristic curve are at 60 gram and 140 gram. The minima are at 20 gram, 100 gram and 180 gram. The intensity was varied within 2 dBμ and 10dBμ. It can be noted that the periods of the three graphs are nearly the same and equal to 80 gram.

The period of the characteristic of the modal sensor can be shifted. Comparing the maxima and the minima in figure 4.5 with those in figure 4.6, it was found that the characteristic curve was shifted by 180°, i.e. half period. Comparing the maxima and the minima in figure 4.5 and those in figure 4.7, it was found that the characteristic curve was shifted by 135°. The characteristic curve was shifted by moving the light detector, because the geometrical position was changed. When the polarizer was rotated, the polarization component of cladding mode interacting with core mode was changed from one axis to another axis. Then, the characteristic curve was shifted. By rotating the polarizer or moving the light

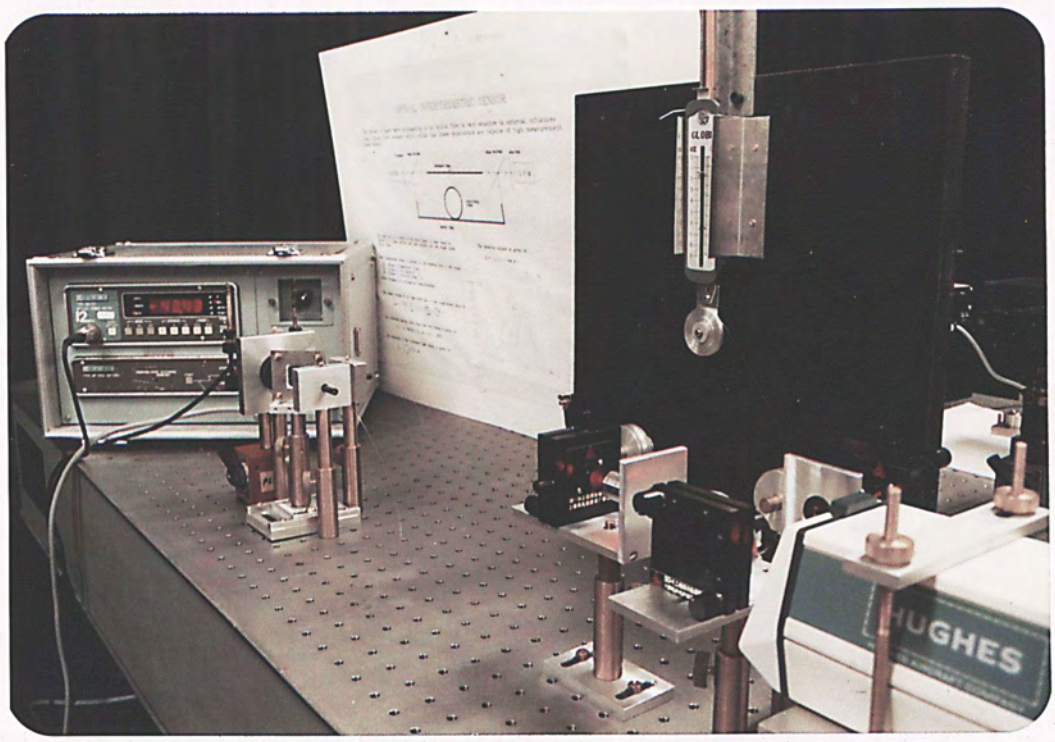

Fig. 4.3 Photograph of the experimental setup.

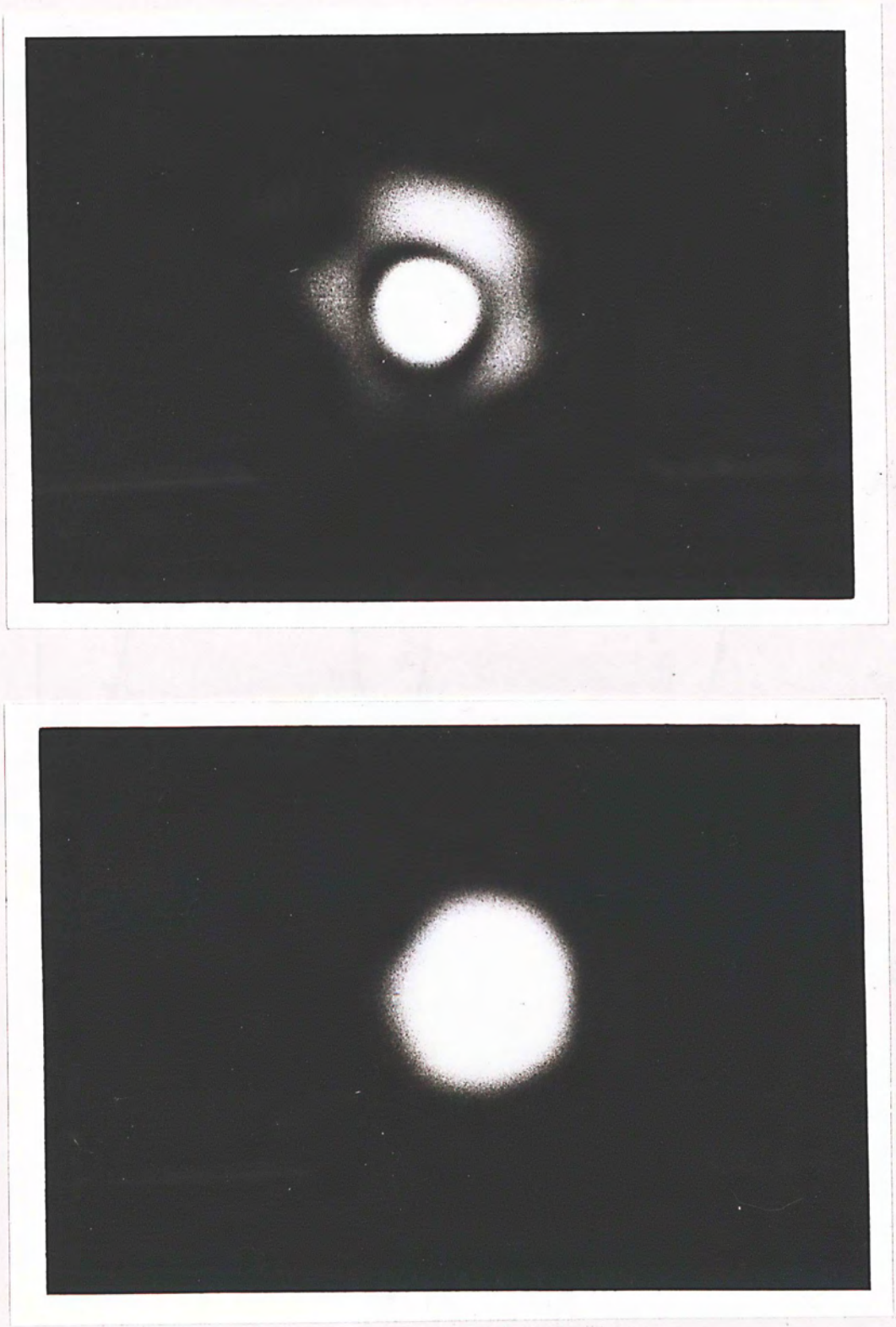

Fig. 4.4 Photographs of light cone when different tension was applied.

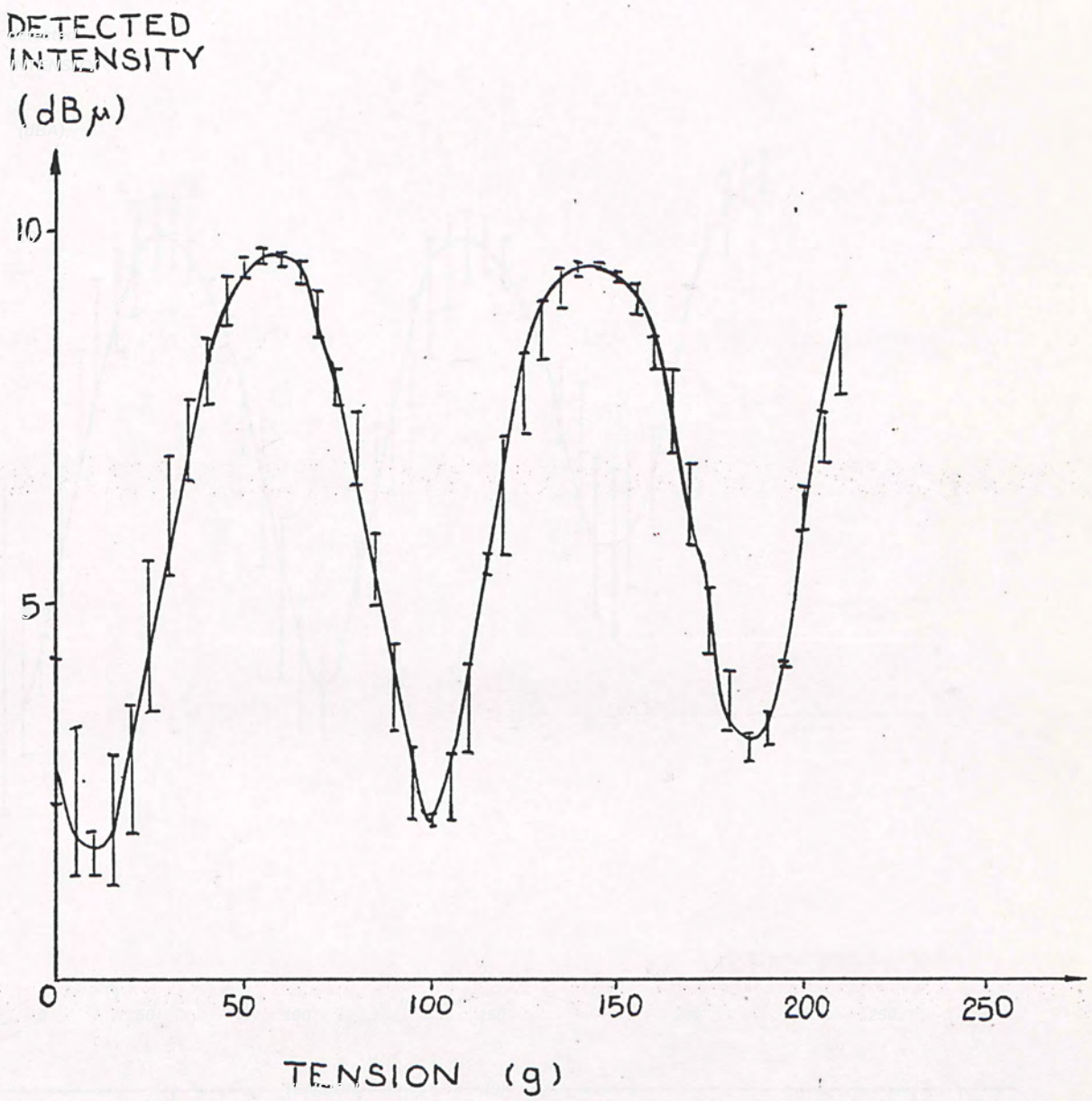

Fig. 4.5 Results of the set A tension measurement within a range of 210 g change (the detector was put at the center of the light cone).

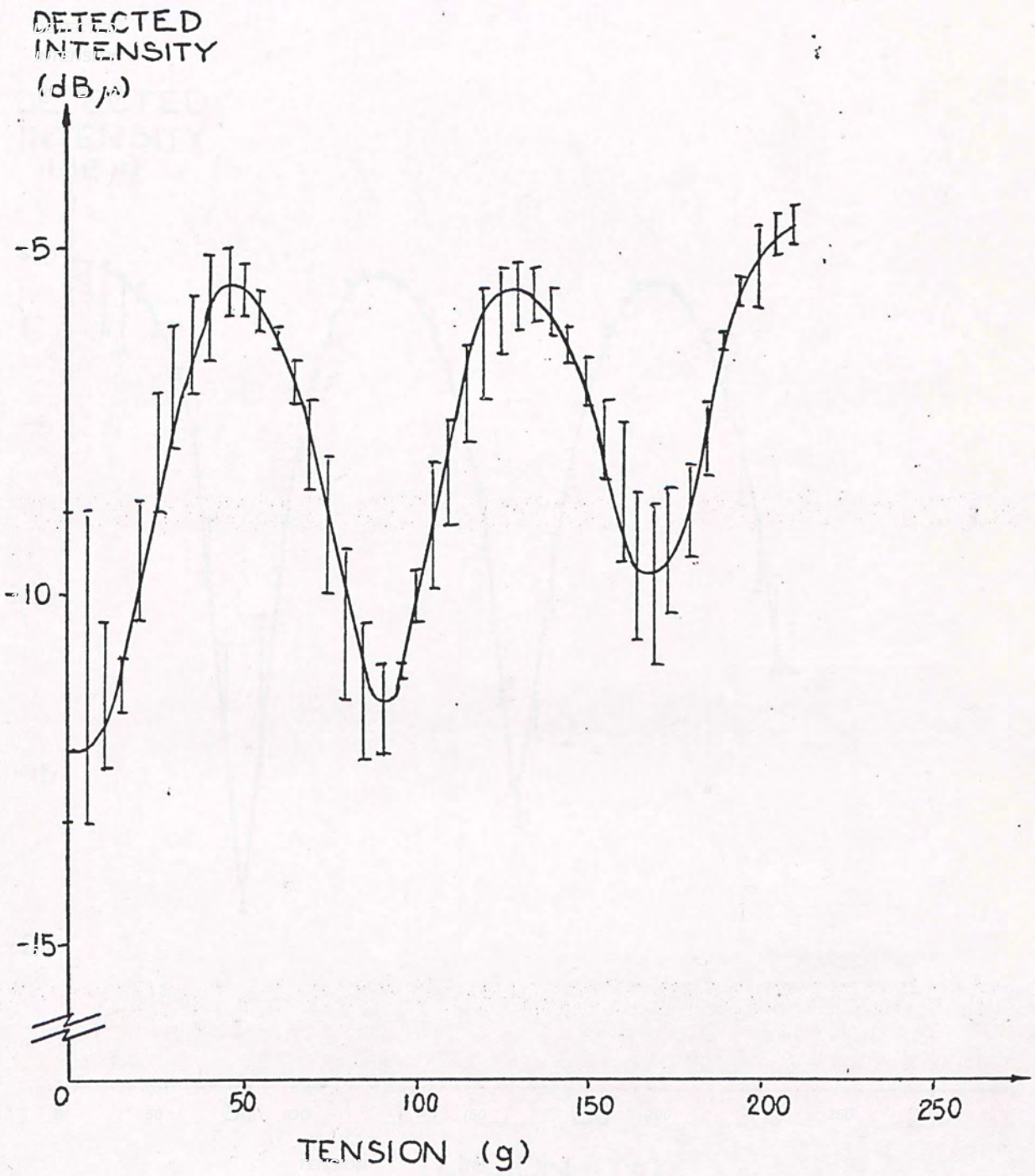

Fig. 4.6 Results of the setup A tension measurement within a range of 210 g (the detector was put at the edge of the light cone).

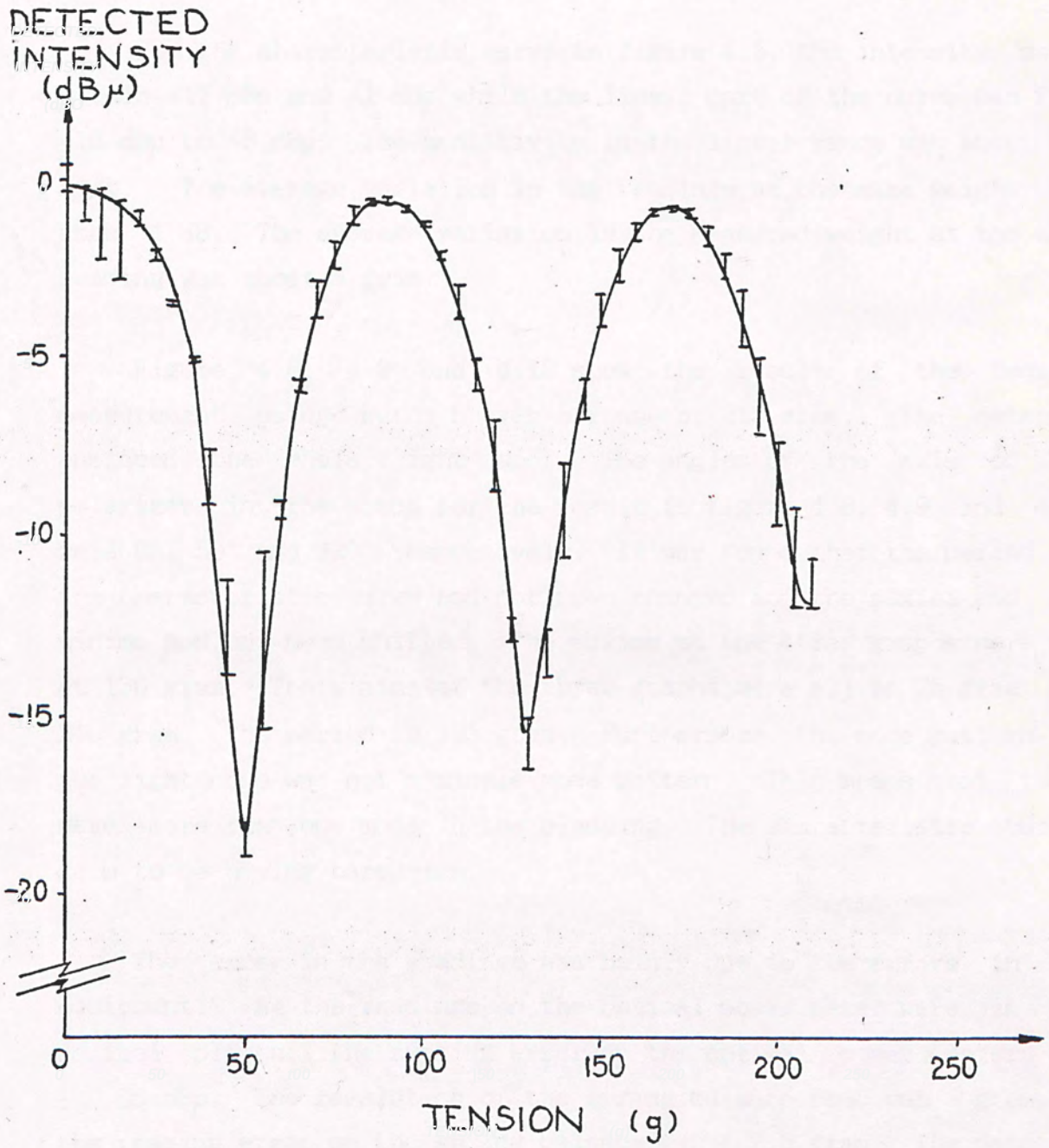

Fig. 4.7 Results of the setup A tension measurement within a range of 210 g (the detector was put at center of the light cone and the polarizer was rotated by 90°).

detector, the characteristic curve can be shifted. Here-of, the linear region of the curve can be shifted as required.

For the characteristic curve in figure 4.5, the intensity swang within -17 dBμ and -1 dBμ while the linear part of the curve was from -16 dBμ to -3 dBμ. The sensitivity in the linear range was about 0.7 dB/g. The average variation in the readings at the same weight was about 1 dB. The average variation in the measured weight at the same reading was about 5 gram.

Figure 4.8, 4.9 and 4.10 show the result of the tension measurement using setup B over a range of 215 gram. The detector enclosed the whole light spot. The angles of the axis of the polarizer in the setup for the result in figure 4.8, 4.9 and 4.10 were 0°, 50° and 320° respectively. It was found that the period of the characteristic curve had not been changed and the maxima and the minima had not been shifted. The maxima at the three graphs were all at 130 gram. The minima at the three graphs were all at 25 gram and 210 gram. The period is 185 gram. Furthermore, the mode pattern of the light cone was not a single mode pattern. This means that there were more than one mode in the cladding. The characteristic curves seem to be having harmonics.

The error in the readings was mainly due to the errors in the equipment. As the readings on the optical power meter were in one decimal places, the reading error on the optical power meter was ± 0.05 dBμ. The resolution of the spring balance used was 5 gram, so the reading error on the spring balance was ± 2.5 gram. The detected power fluctuations were 0.2 dBμ, 0.6 dBμ and 1.3 dBμ at the lightest, medium and darkest intensity respectively. The practical error of the sensor was less than the sum of all these errors.

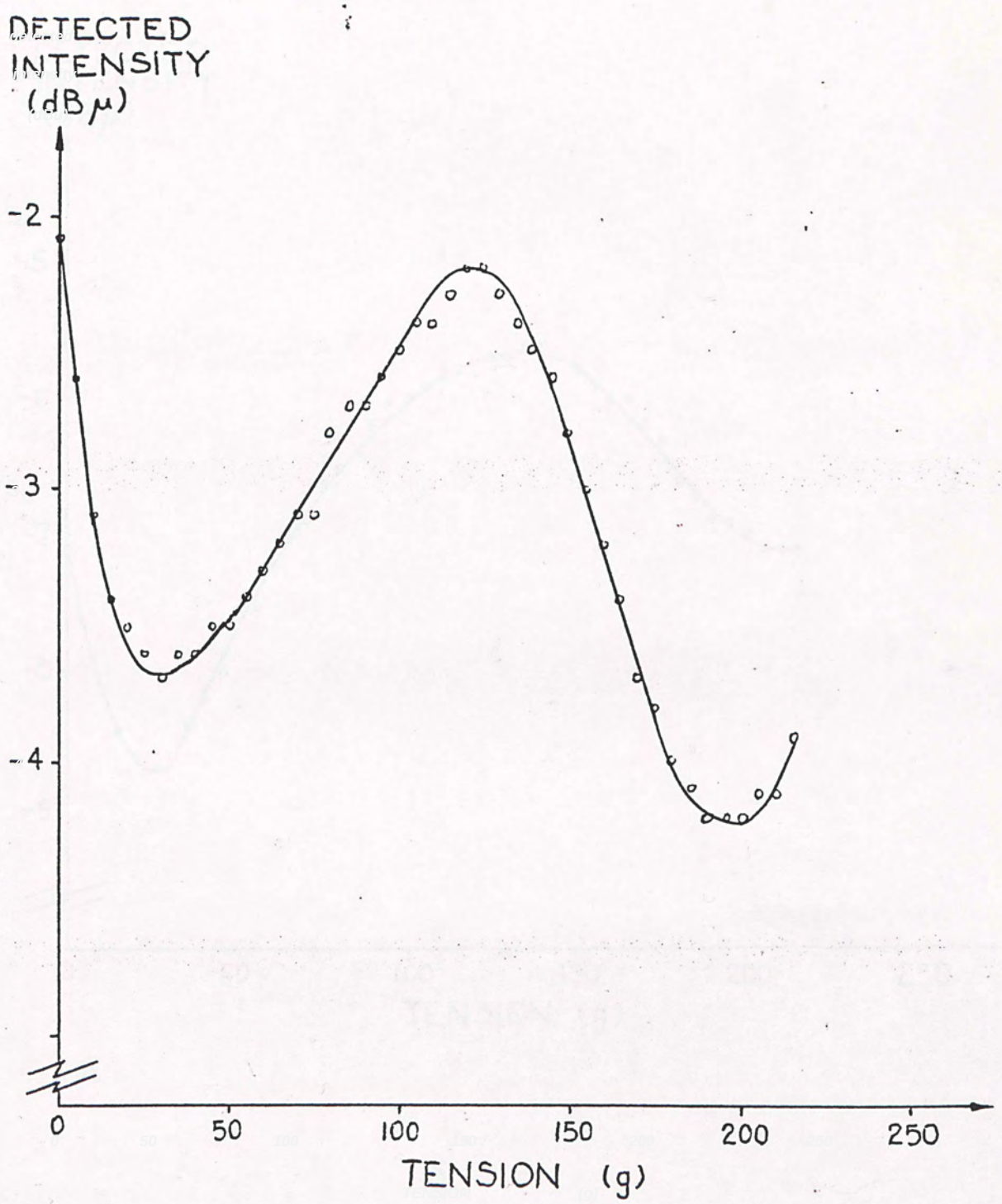

Fig. 4.8 The result of the setup B tension measurement over a range of 215 g with the detector enclosing the whole light spot and the polarization angle of 0°.

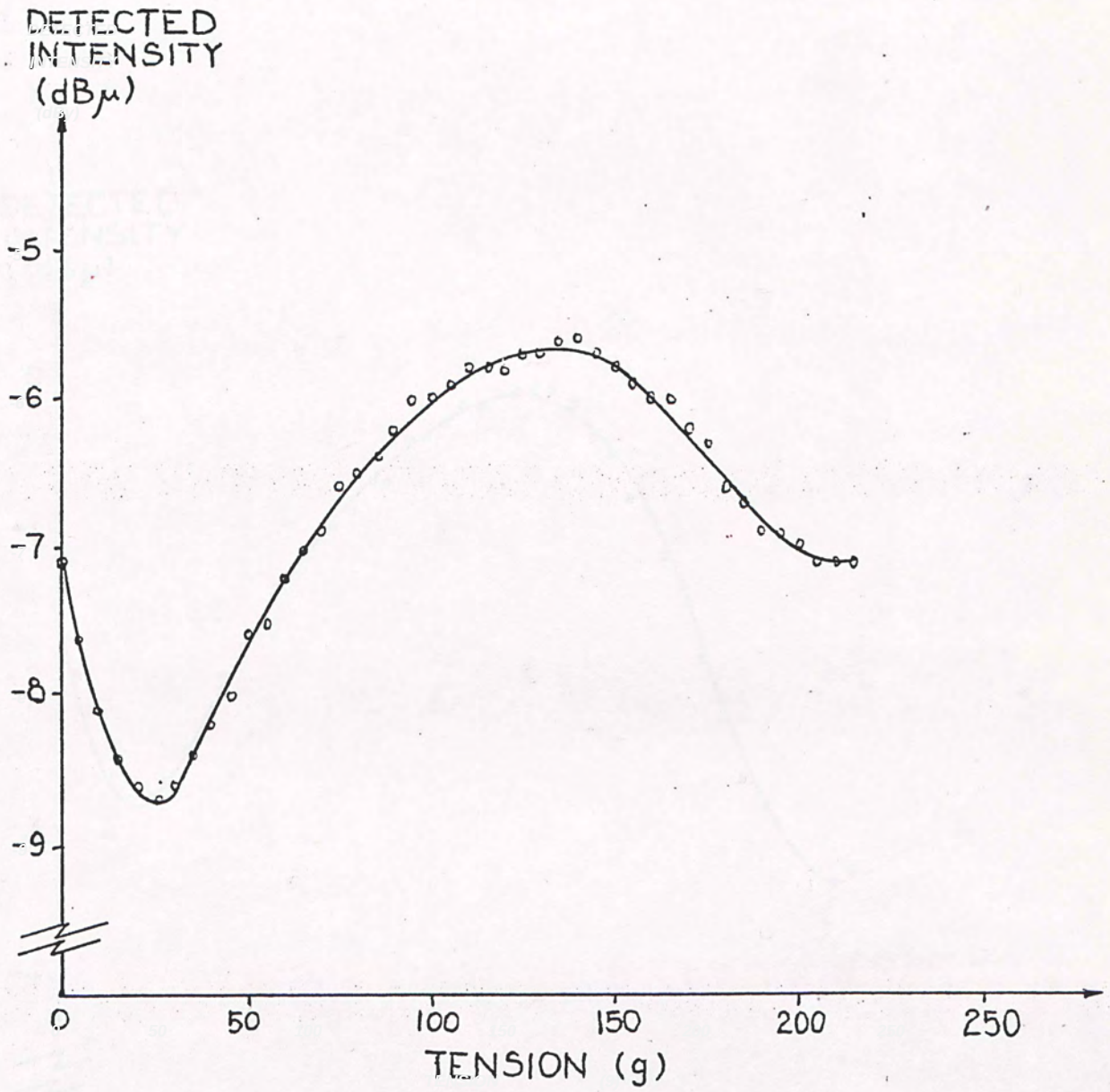

Fig. 4.9 The result of the setup B tension measurement over a range of 215 g with the detector enclosing the whole light spot and the polarization angle of 50°.

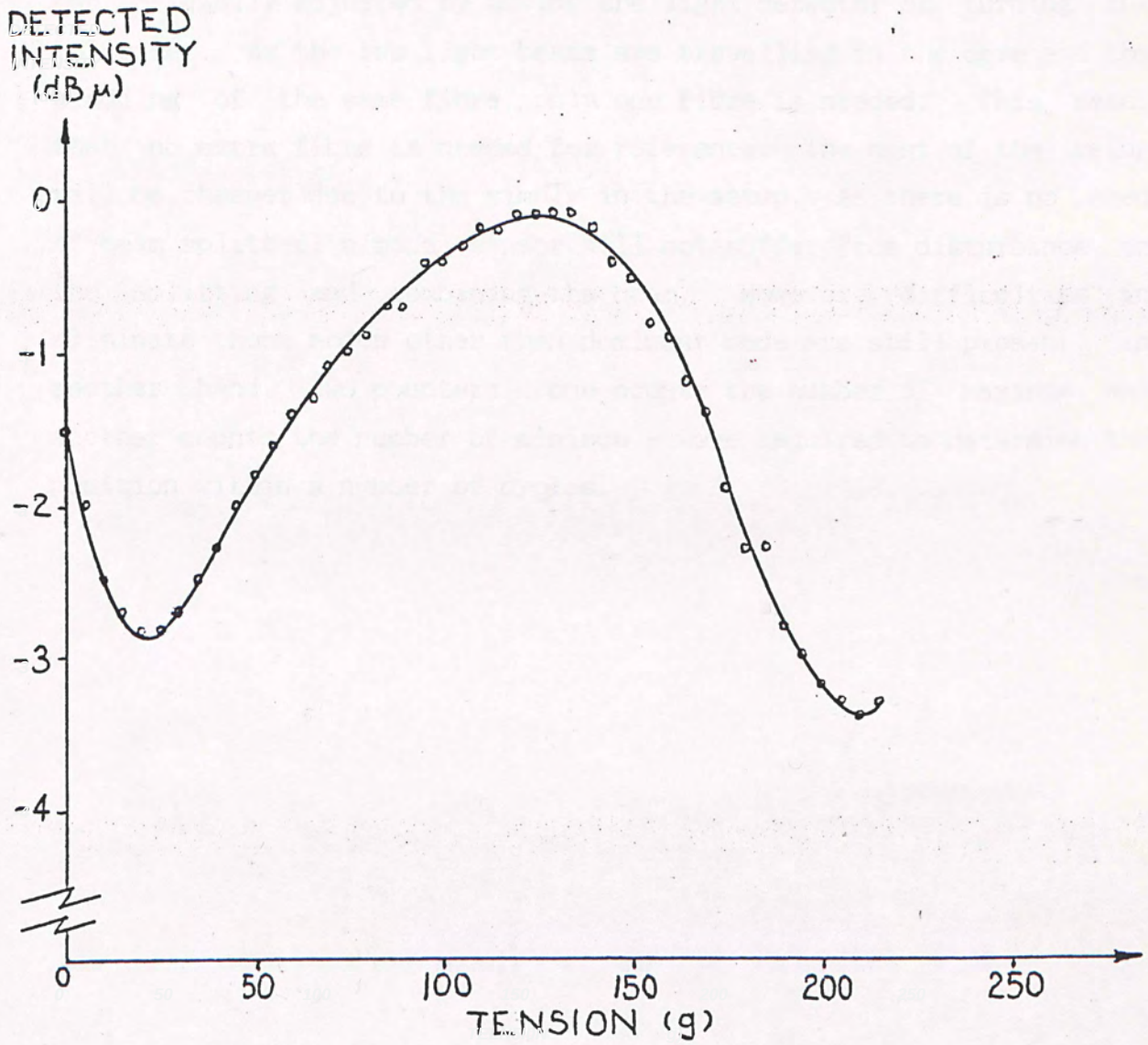

Fig. 4.10 The result of the setup B tension measurement over a range of 215 g with the detector enclosing the whole light spot and the polarization angle of 320°.

4.5 Conclusion

Concluding the previous analysis on the proposing modal sensing technique, it is proved that the modal sensor has a higher sensitivity. The sensitivity and the linear range of a modal sensor can be easily adjusted by moving the light detector or turning the polarizer. As the two light beams are travelling in the core and the cladding of the same fibre, only one fibre is needed. This means that no extra fibre is needed for reference. The cost of the setup will be cheaper due to the simply in the setup. As there is no need of beam splitter, a modal sensor will not suffer from disturbance in the splitting and combining the beam. However, difficulties in eliminate those modes other than dominant mode are still present. In another hand, two counters - one counts the number of maximum and another counts the number of minimum - were required to determine the position within a number of cycles.

Reference

4.1 M. Born and E. Wolf: "Principles of optics", Pergamon Press, 1975, Chapter 7.

4.2 C.D. Butter and G.B. Hocker: "Fiber optics strain gauge", Applied Optics, vol.17, no.18, 15 September, 1978, pp.2867-2869.

4.3 G.B. Hocker and W.K. Burns, IEEE J. Quantum Electron., vol. QE-11, 270 (1975).

4.4 Tsuneo Horiguchi, Toshio Kurashima and Mitsuhiro Tateda: "Tensile strain dependence of Brillouni Frequency Shift in silica optical fibers", IEEE Photronics Technology Letters, May 1989, vol.1, no.5, pp.107-108.

4.5 J.E. Donovan, T.G. Giallorenzi, J.A. Bucaro and V.P. Simmons: "Applications of fibre optics in sensors", Electro/'81 Conference Record (Electron. Conventions, El Segundo, Ca, USA), 7-9 April 1981, N. York, 8B/4/pp.1-14.

4.6 C.K. Asawa, S.K. Yao, R.C. Stearns, N.L. Mota and J.W. Downs: "High-sensitivity Fibre-optic Strain Sensors for Measuring Structural Distortion", Electronics Letters, 29th April, 1982, vol.18, no.9, pp.362-364.

4.7 B. Culshaw, D.E.N. Davies and S.A. Kingsley: "Fibre Optic Strain Pressure and Temperature Sensors", Optical Fiber Technology II, IEEE Press, pp.226-237.

4.8 W.B. Sprillman, Jr. and D.H. McMahon: "Multimode Fibre Optic Sensors", First International Conference on Optical Fibre Sensors, 26-28 April, 1983, pp.160-163.

4.9 Ivan P. Kaminow: "Polarization in Optical Fibers", IFEE J. of Quantum Electronics, vol.QE-17, no.1, January 1981, pp.15-22.

4.10 Xinnda Dai, P.L. Chu and K.C. Chiang: "Optical Fibre Sensor Using Modal Noise Effect",

4.11 D.E.N. Davies and S.A. Kingsley: "Method of Phase-modulating Signals in Optical Fibres: Application to Optical-Telemetry Systems", Electronics Letters, 24th January, 1974, vol.10, no.2, pp.21-22.

4.12 B. Culshaw, D.E.N. Davies, S.A. Kingsley: "Acoustic Sensitivity of Optical-Fibre Waveguides", Electronics Letters, 8th December, 1977, vol.13, no.25, pp.760-761.

4.13 M.R. Layton and J.A. Bucaro: "Optical Fiber Acoustic Sensor Utilizing Mode-Mode Interference", Optical Fiber Technology II, IEEE Press, pp.238-242.

4.14 G.W.C. Kaye and T.H. Laby: "Tables of Physical and Chemical Constant", Longmans, 1911.

4.15 John Robson: "Basic Tables in Physics", McGraw-Hill, 1967.

4.16 B. Culshaw: "Optical Fibre Sensing and Signal Processing", Peter Peregrinus Ltd., 1984, Chapter 7.

CHAPTER 5
POLARIZATION-DIVISION-MULTIPLEXING

5.1 Introduction

The development in the lightwave technology has been dramatic since 1970. The bandwidth-distance product has been doubling about every two years for the last decade, as observed by Chynoweth [5.1]. This rate of progress is strikingly similar to that taken by the silicon technology in the famous Moore's Law.

Efforts are still being put to further increase the repeater spacing and to improve the information capacity of the optical communications channels. The use of multimode graded-index fibres and now the 1.3 μm and the 1.55 μm single-mode silica fibres has increased the channel capacity by more than an order of magnitude. The recent development of mid-IR fluoride-based glass fibres promises an intrinsic loss of the order of 0.001 dB/km [5.2], indicating possible unrepeatered spans of more than 1000 km. The path taken to improve the channel capacity has gone in two directions, viz. a higher data rate in the time-division multiplexing (TDM) level and a viable wavelength-division multiplexing (WDM) system. It seems that electronic capability limits the maximum TDM bit rates over a fibre link to about 4 Gbit/s [5.3,5.4]. In WDM, an over 1 Tbit.km/s transmission system was demostrated [5.5] over a 68 km single-mode fibre using 10 WDM-lasers in the 1.55 um range, each laser being modulated at 2 Gbit/s. A Duplex-diplex optical transmission system [5.6] using wavelength division multiplex in the 1300 nm and 1500 nm fibre widows have been installed.

The progress in recent years using phase modulation and polarization modulation instead of the conventional direct detection/amplitude modulation has provided a new horizon for lightwave development. This is mainly due to the successful fabrication of various types of polarization-maintaining fibres since 1980 [5.7]. A conventional circular single-mode fibre can not maintain the polarizations of the light in the fibre due to the

variations in the diameter and the refractive index of the fibre caused by some uncontrolled external perturbations. The successful development in the polarization-state controller has led to the realization of coherent transmission system over an unrepeatered spacing of more than 250 km [5.8].

The use of the orthogonal polarization property of optical fibres to increase the information capacity has also been proposed [5.9]. Not much development on polarization-division multiplexing has been reported. Li and Jian [5.10] reported an experiment using two He-Ne lasers coupled into a short-length elliptical-core fibre with a crosstalk coupling of - 25 dB. But no information was given whether the two light sources, being identical He-Ne lasers, were coupled into the fibre at the same time. Bi-directional transmission using polarized light was reported by Sasaki et al [5.11]. A signal of 100 Mbit/s was transmitted over a 13.6 km PANDA fibre. The bit-error-rate of the system was less than 10^{-9}.

5.2 Fibre Structures and Multiplexing Theory

In many optical applications, the state of polarization of the propagating modes in a fibre has to be strictly controlled. Practical fibres cannot be made perfectly circularly symmetric, thus external perturbations such as bends, stress and changes of temperature will decompose an input linearly-polarized light into two orthogonal components with different phase velocities along the two principal transverse planes. Coupling between these two orthogonal components will therefore cause the state of polarization to vary along the fibre in an unpredictable manner.

Polarization-maintaining fibres are normally classified into two categories, viz. low-birefringent (LB) and high birefringent (HB) fibres. For HB fibres, the linear-polarized state is maintained or stabilized by reducing the amount of coupling between the two orthogonal linear-polarized components through the introduction of strong linear birefringence into fibres as shown in different schemes illustrated in figure 5.1. See appendix E for classification of PM fibres.

A parameter B is usually used to express the difference of the effective refractive index between orthogonal linear-polarization modes. The beat length L_p is the difference of propagation constant between the orthogonal modes and is given as

$$L_p = \lambda / B = 2\pi / \beta B \qquad [5.1]$$

where λ is the wavelength. The group delay-time difference t_p is given by

$$t_p = B / c \qquad [5.2]$$

where c is the light velocity in a vacuum.

In a polarization-maintaining fibre, bow-tie fibre or PANDA fibre, there are major axis and minor axis. In the proposed

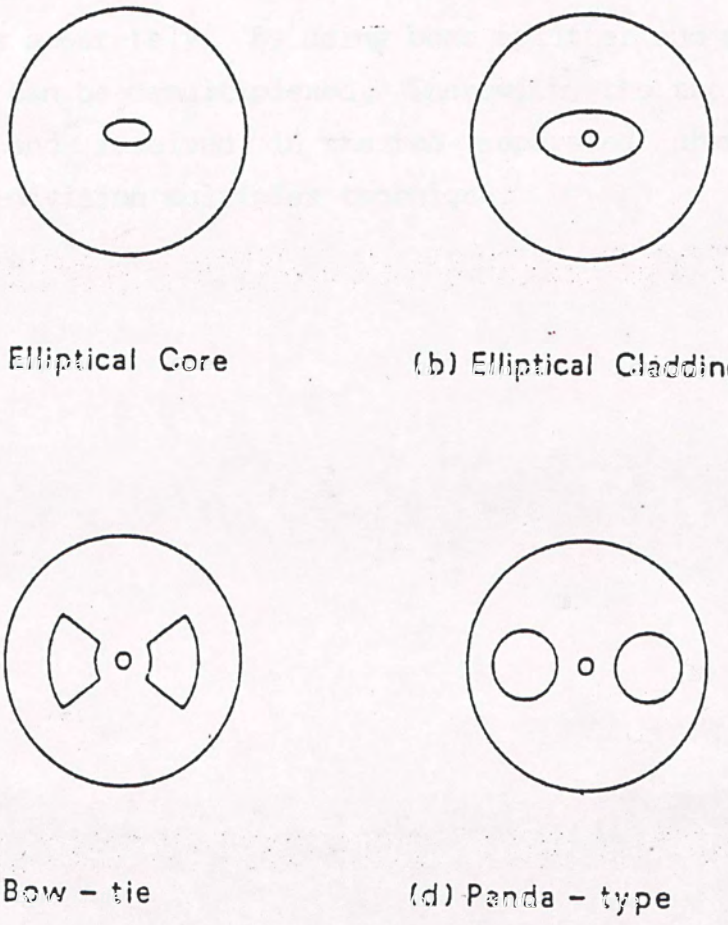

Fig. 5.1 Various forms of polarization-maintaining fibres.

polarization-division-multiplexing technique [5.12], the x-channel and the y-channel occupy the two axes of the fibre. The signals are polarized before they are injected into the fibre. As an important property of a polarization-maintaining fibre is the ability to maintain the state of polarization of the light in the fibre, the light output of the fibre is still in two polarizations, with which the signals in the x-channel and the y-channel are carried in the two polarizations separately. By using beam splitter and polarizers, the two channels can be demultiplexed. Therewith, the two signals can be transmitted and received in the two separated channel by using polarization-division multiplex technique.

5.3 Experimental Result

In the experiment of the polarization-division multiplexing, the light sources of the two channels - a video channel and a voice channel - were using two lasers with different wavelengths. The schematic diagram of the experimental setup is shown in figure 5.2. A picture of the experimental setup is shown in figure 5.3. A 633 nm He-Ne laser (SP-158), which could be modulated up to 2 kHz, was used for the light source of the voice channel. A 850 nm AlGaAs laser diode (LCW-10), which had a maximum power output of 4 mW CW, was employed for the light source of the video channel. The video channel was transmitted by the major axis of a single-polarization fibre. The audio signal was carried by the light in the minor axis of the polarization-maintaining fibre. The two laser beams were polarized orthogonally by polarizers and were then combined by a plate beamsplitter (as in figure 5.4). The combined beam was coupled to the fibre and was allowed to propagate through the fibre, which had a length of about half a meter. The output light beam from the fibre was splitted into two parts by a prism beamsplitter. The two channels were demultiplexed by two polarizers with polarization angles setting at orthogonal positions (as in figure 5.5). The detected signals were passed through bandpass filters with the bands for the voice frequency and the video frequency to recover the voice signal and video signal.

The experimental power budget is shown in table 5.1. The total insertion loss in the voice channel and the video channel were 23 dB and 32 dB respectively. A common commercial optical communication link at 850 nm has a power budget of about 20 dB. It is cleared that most of the power was lost at the coupling process, which was done by focusing the light beam into the fibre. The power lost were 9 dB and 11 dB in the audio channel and video channel respectively. Worse than the voice channel, the 850 nm laser, light source of video channel, had to be focused into a light beam, since the numerical aperture of a laser diode was much larger than that of a gas laser. The loss in focusing the light was 9 dB.

In the audio channel without the presence of the video channel,

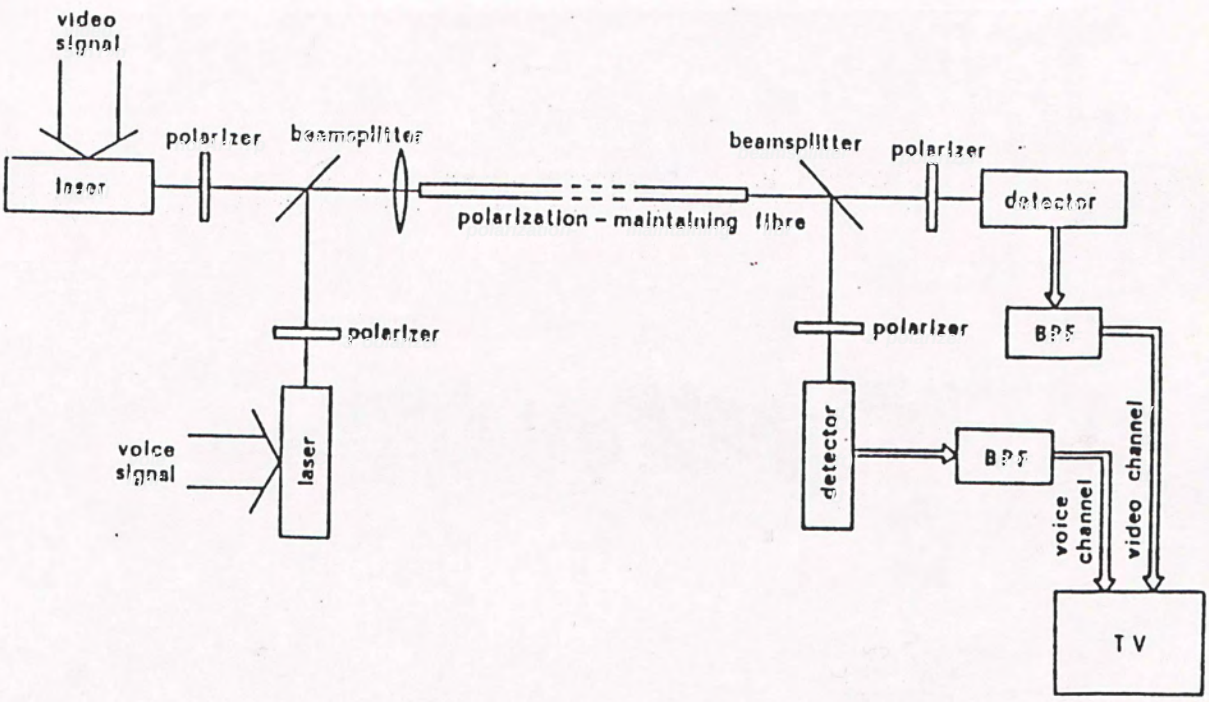

Fig. 5.2 Schematic set-up of polarization-division-multiplexing method.

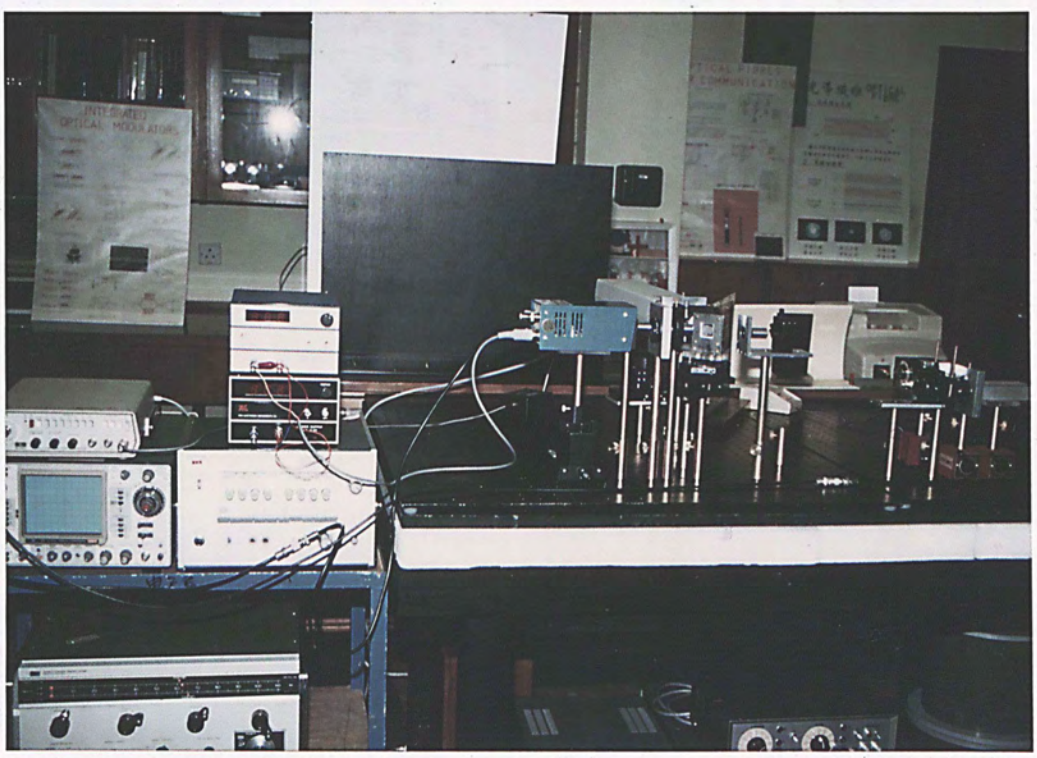

Fig. 5.3 Photograph of experimental setup.

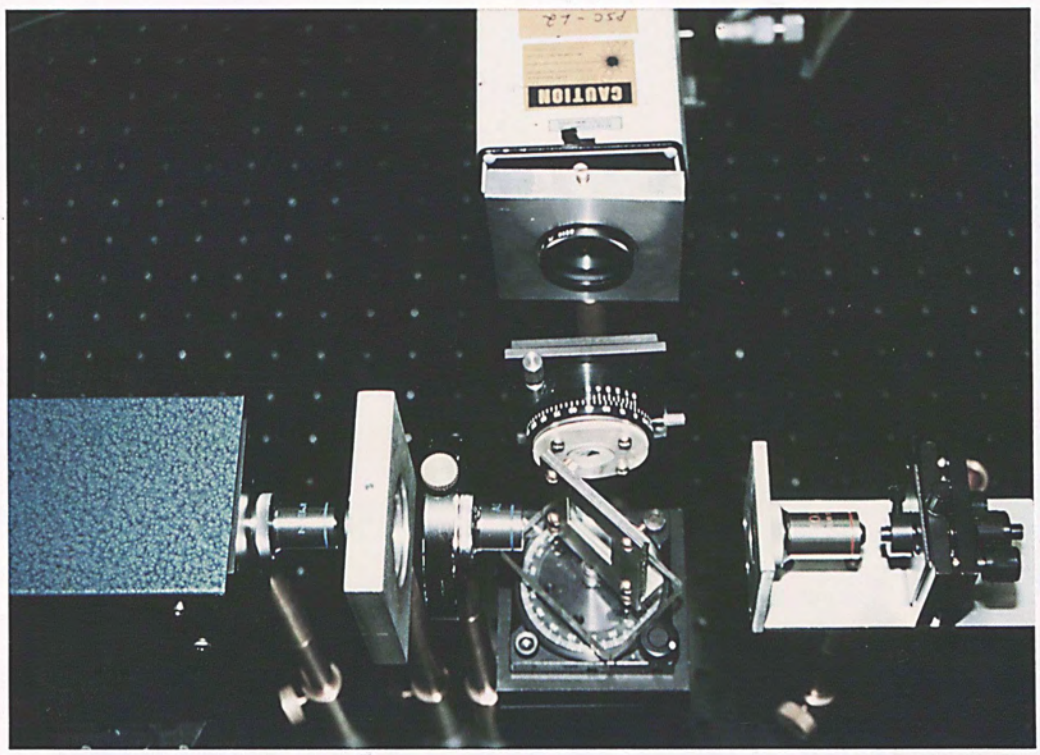

Fig. 5.4 Polarization multiplexing of two channels.

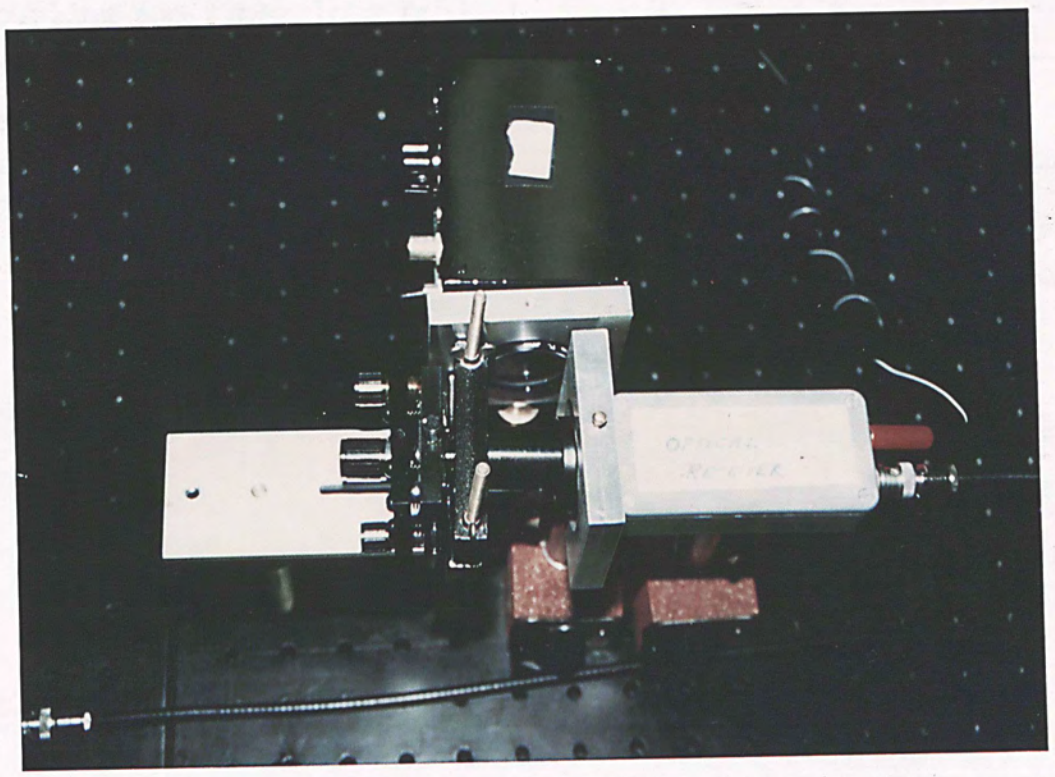

Fig. 5.5 Demultiplexing of two channels which is polarization multiplexed.

items	voice channel	video channel
input power (dBμ)	28	36
focusing lens (dB) *	--------	- 9
halfwave plate (dB) **	- 2	--------
polarizers (dB)	- 6	- 6
beamsplitters (dB)	- 6	- 6
coupling and fiber loss (dB)	- 9	- 11
detected power (dBμ)	5	4

* Since the numerical aperture of a laser diode was large, focusing lenses were needed to focus the output light from the laser diode into a beam.

** The halfwave plate was used to rotate the polarization angle of one of the light beam such that the two light beams were polarized orthogonally.

Table 5.1 Experimental Power Budget

the signal-to-noise ratio was 9.5 dB. It gave the same signal-to-noise ratio at the present of the video channel. The distortion of the signal was 30 %. Actually, the distortion was caused by the present of a large amplitude 100 Hz noise from the power supply of the gas laser. The cross-talk from the video channel was -20 dB.

The signal-to-noise ratio was 18 dB in the video channel without the present of the voice channel. When an audio signal was transmitting in the voice channel, the signal-to-noise ratio was reduced to 12 dB. The distortion of the signal was 50 %. The high distortion was caused by low in received power. The cross-talk from the audio channel was -19.8 dB.

A PANDA fibre had been used instead of the bow-tie fibre. The results were the same. Photographs of a bow-tie fibre and a PANDA fibre are shown in figure 5.6.

The transmitted video signal was generated by a pattern generator. Different patterns had been tried. The pictures of the different video signals and displayed patterns before transmitted and after transmitted are shown in figure 5.7 to figure 5.15. Figure 5.7 and figure 5.8 show the displayed colour bar before transmission and after transmission respectively. The video signals are displayed in oscilloscope as in figure 5.9. The lower one is the input video signal. The upper one is the output video signal. The displayed grey scale before transmission and after transmission are shown in figure 5.10 and figure 5.11 respectively. Figure 5.12 shows the video signals displayed in oscilloscope. The lower one is the input video signal and the upper one is the output signal. Figure 5.13 and figure 5.14 show the displayed black/white pattern before transmission and after transmission respectively. The video signals are displayed in oscilloscope as in figure 5.15.

(a)

(b)

Fig. 5.6 Photographs of the cross-sections of (a) a bow-tie fibre, and (b) a PANDA fibre.

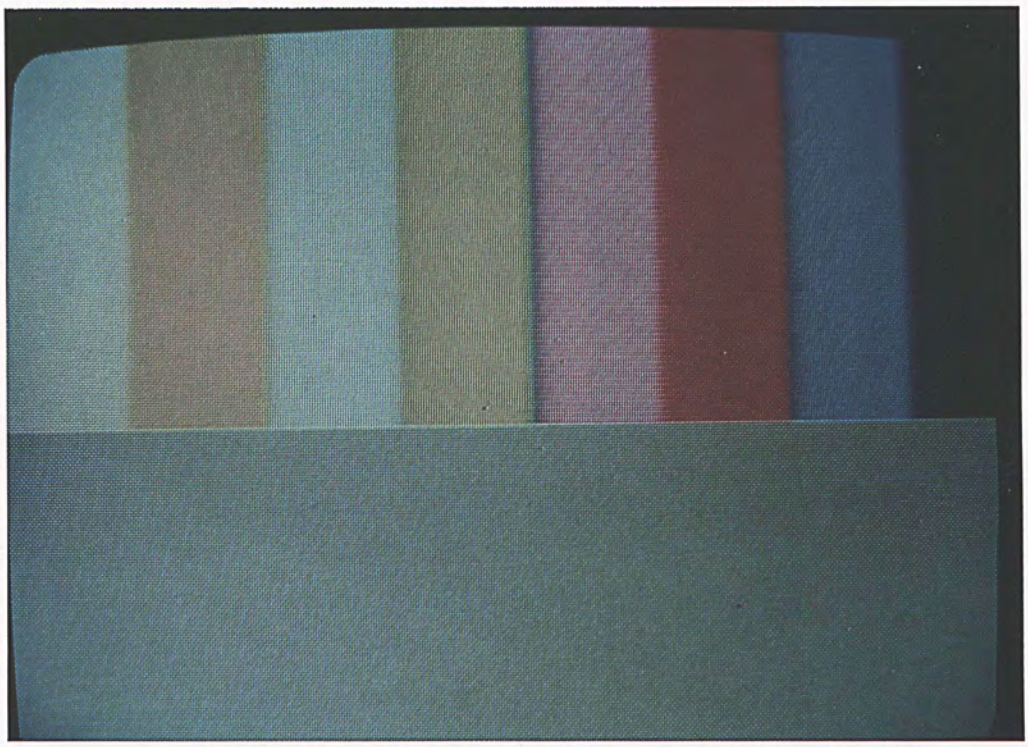

Fig. 5.7 The displayed colour bar before transmission.

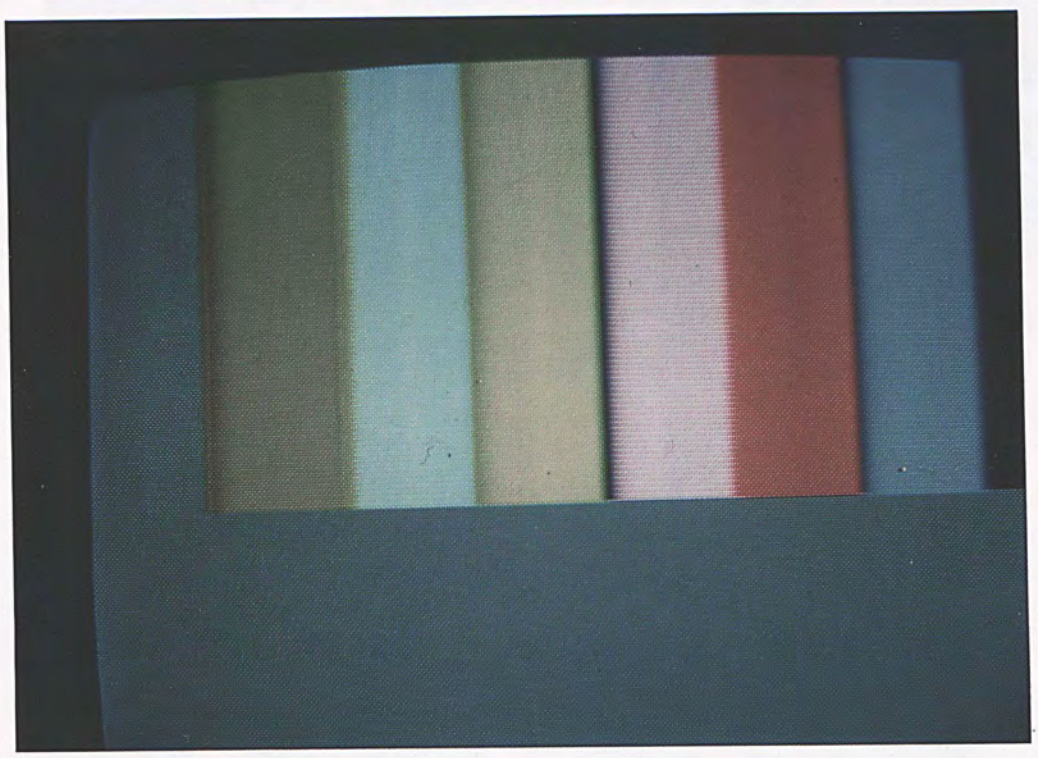

Fig. 5.8 The displayed colour bar after transmission.

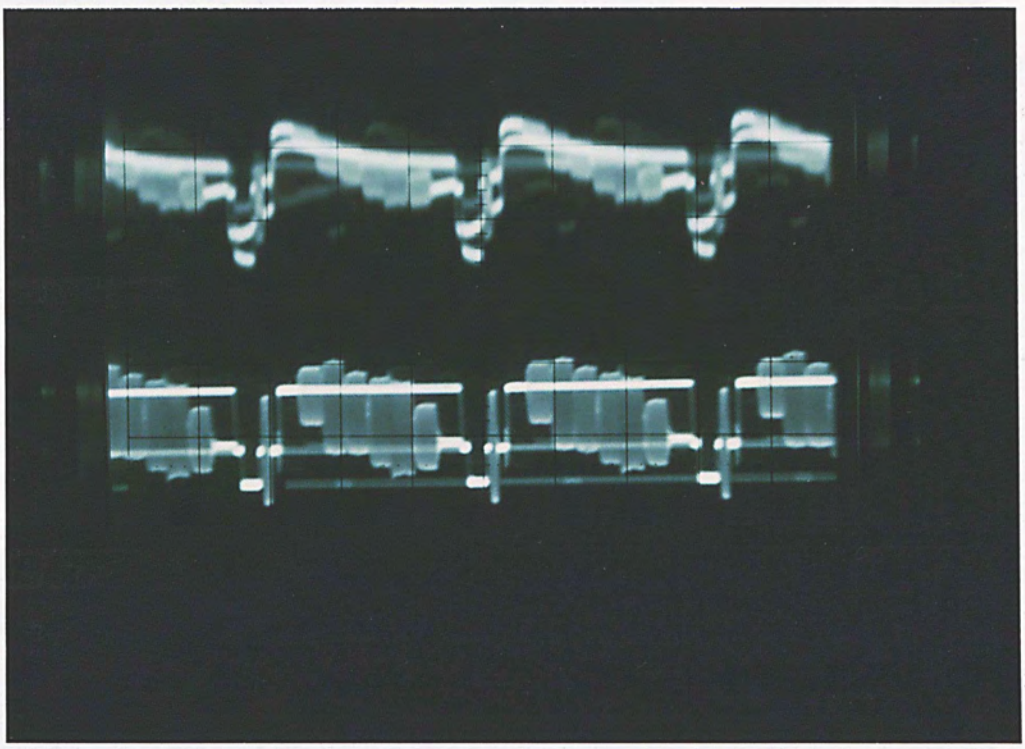

Fig. 5.9 The video signals of colour bar displayed in the oscilloscope. The lower one is the input signal and the upper one is the output signal.

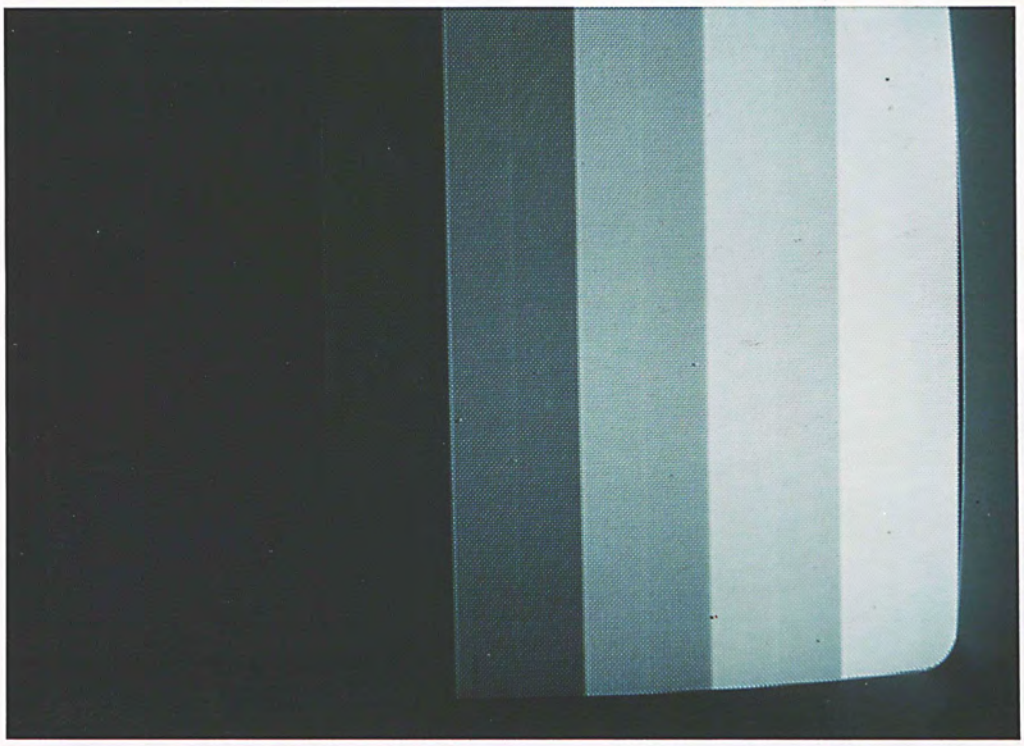

Fig. 5.10 The displayed grey scale before transmission.

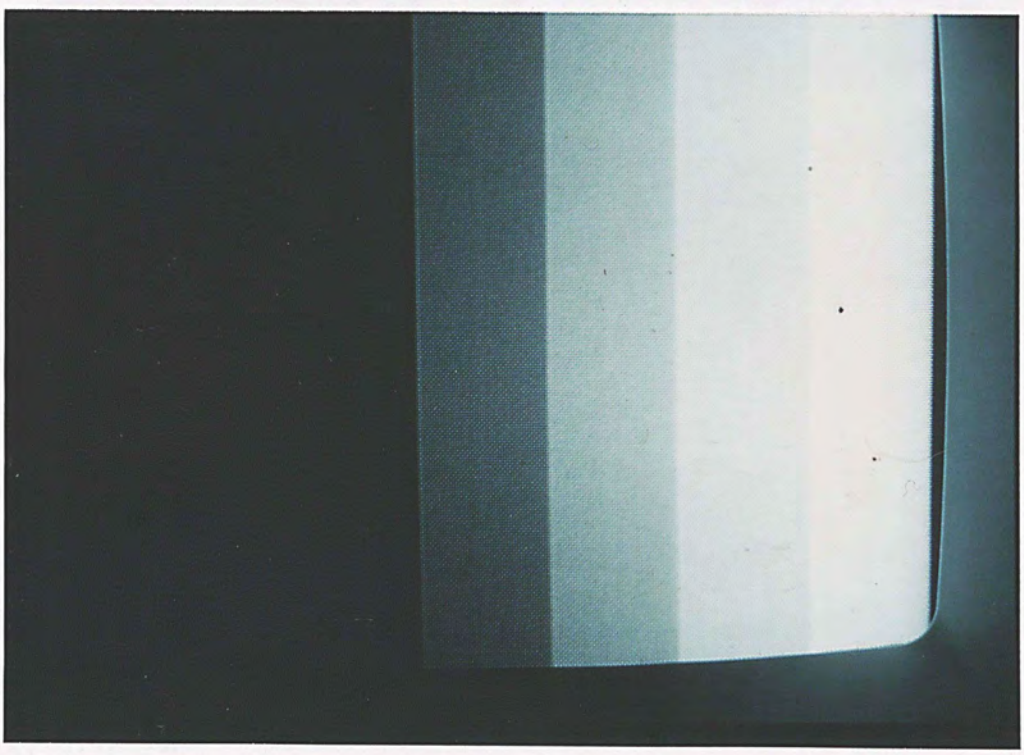

Fig. 5.11 The displayed grey scale after transmission.

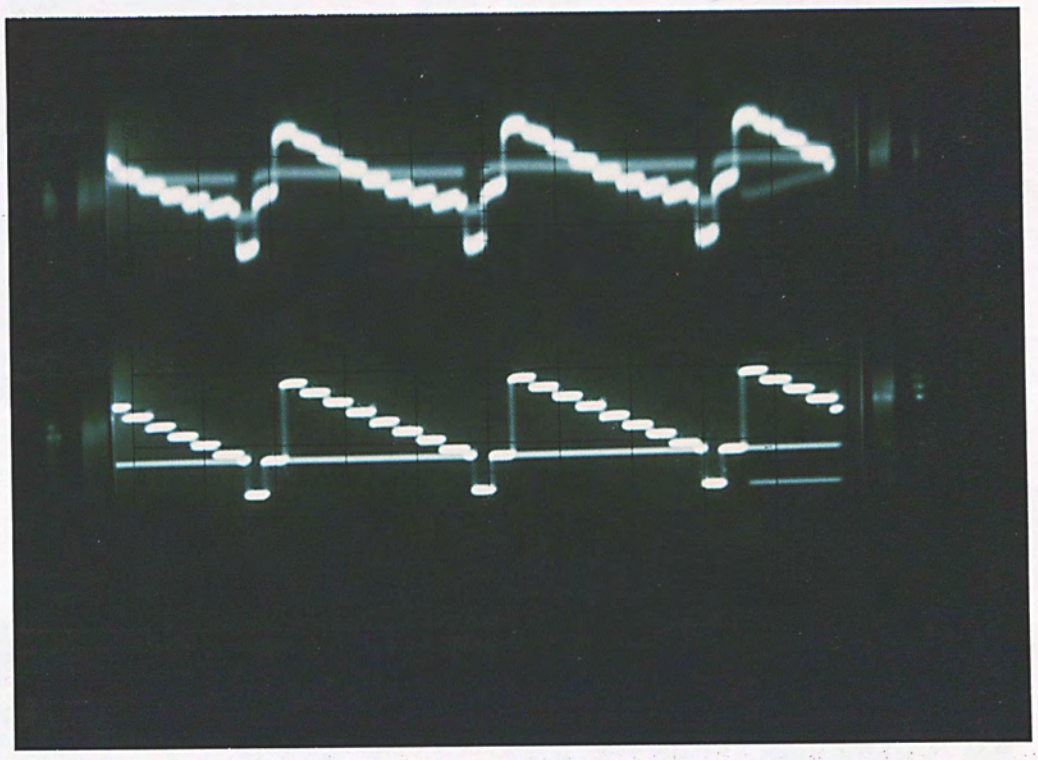

Fig. 5.12 The video signals of grey scale displayed in the oscilloscope. The lower one is the input signal and the upper one is the output signal.

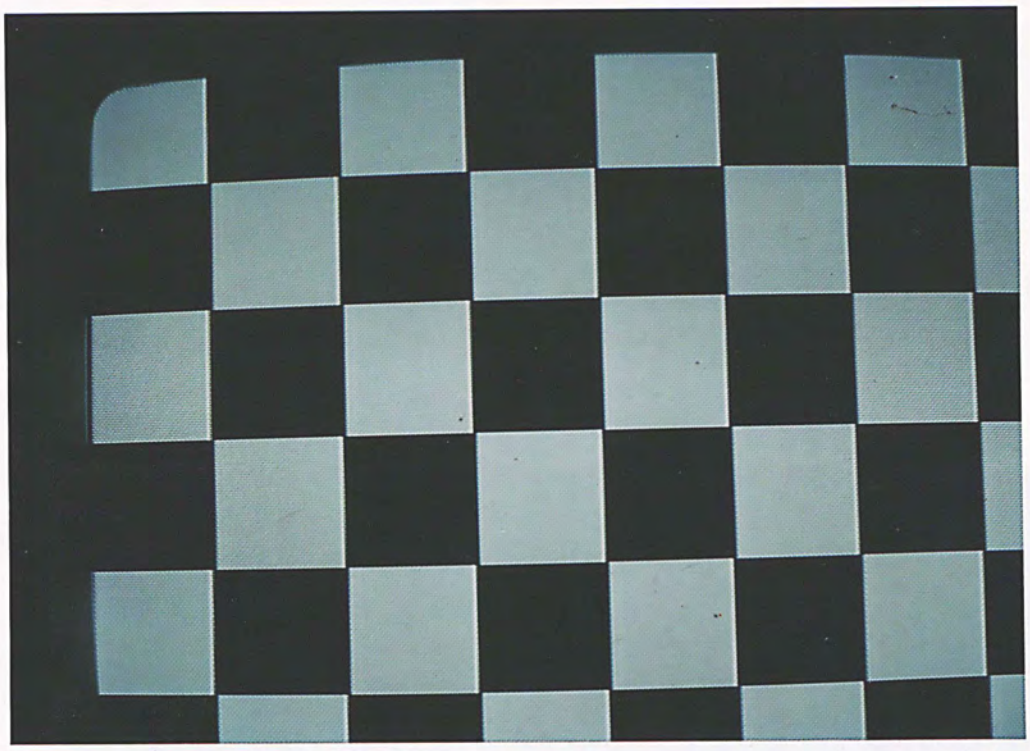

Fig. 5.13 The displayed black/white pattern before transmission.

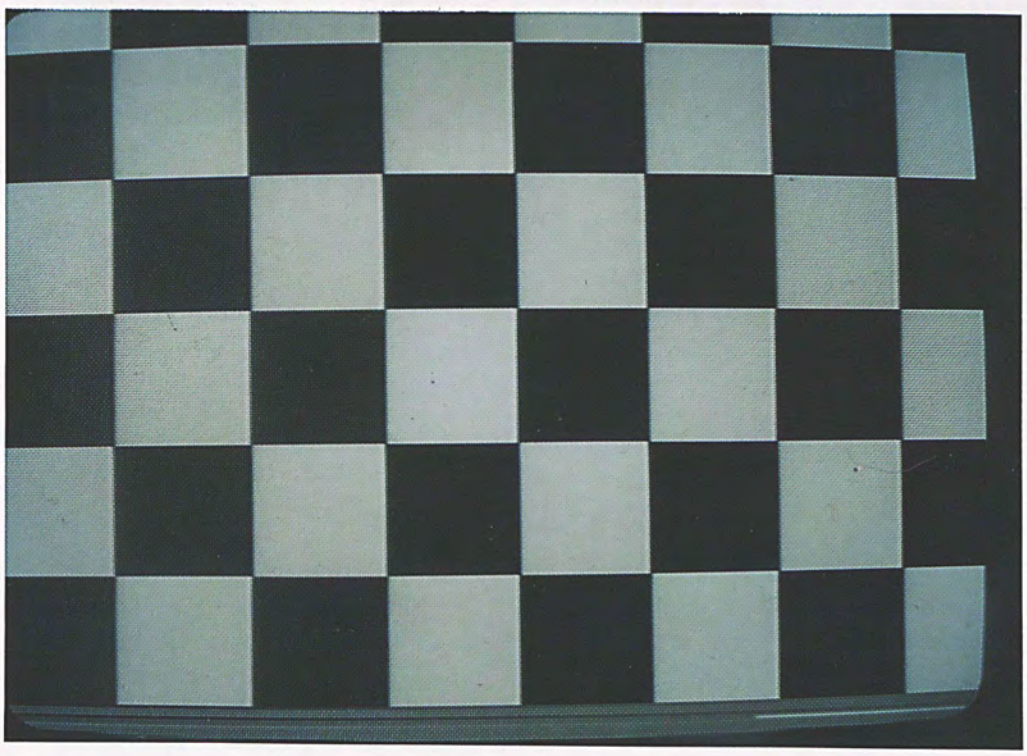

Fig. 5.14 The displayed black/white pattern after transmission.

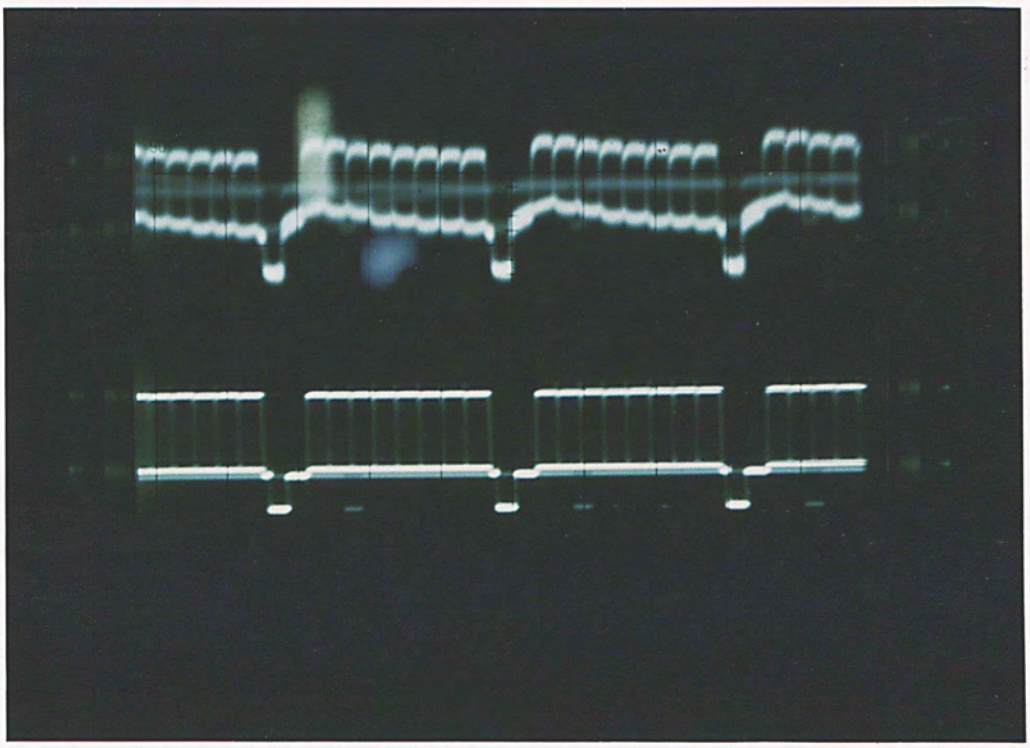

Fig. 5.15 The video signals of black/white pattern displayed in the oscilloscope. The lower one is the input signal and the upper one is the output signal.

5.4 Conclusion

A two channel transmission using polarization-division multiplexing technique has been demonstrated. The encouraging result shows the possibility to double the channel capacity of transmission in the future by using the polarization-division-multiplexing technique. Reduction of coupling loss will make the setup becoming more practical. Effort must also be given to increase the signal to noise ratio and reduce the distortion.

Reference

5.1 A.G. Chynoweth: "Technology - The Irresistible Force", IREE Monitor, pp. 13-16, June/July 1986.

5.2 M.M. Broer and L.G. Cohen: "Heavy Metal Halide Glass Fiber Lightwave Systems", J. Lightwave Tech., vol.LT-4, no.10, pp.1509-1545, October 1986.

5.3 J.E. Midwinter, "Current Status of Optical Communications Technology", J. Lightwave Tech., vol.LT-3, no.5, pp.927-930, October 1985.

5.4 A. Gnauck, et. al.: "4 Gbit/s Transmission over 103 km of Optical Fibre using a Novel Electronic Multiplexer/Demultiplexer", J. Lightwave Tech., vol.LT-3, pp.1032-1035, 1985.

5.5 N.A. Olsson, J. Hegarty, R.A. Logan, L.F. Johnson, K.L. Walker and L.G. Cohen: "Transmission with 1.37 Tbit-km/s Capacity Using Ten Wavelength Division Multiplexed Lasers at 1.5 um", Tech. Dig. Optical Fiber Communications, San Diego, pap. WB6, 1985.

5.6 A.R. Hunwicks and P.A. Rosher: "Duplex-diplex optical transmission in the 1300 nm and 1500 nm fibre windows: and installed system", Elect. Lett., 7 May 1987, vol.23, no.10, pp.542-544.

5.7 J. Noda, K. Okamoto and Y. Sasaki: "Polarization-Maintaining Fibers and their Applications", J. Lightwave Tech., vol.LT-4, no.8, pp.1071-1089, August 1986.

5.8 T. Okoshi: "Recent Advances in Coherent Fiber Communication Systems", J. Lightwave Tech., vol.LT-5, no.1, pp.44-52, January 1987.

5.9 I.P. Kaminow: "Polarization in Optical Fibers", IEEE J. Quantum Electron., vol.QE-17, no.1, pp.15-22, January 1981.

5.10 Q. Li and S. Jian: "An Experiment on Optical Fiber Communication by means of the Polarization Division Multiplexing", Proc. Sino-British Joint Meeting on Optical Fiber Communication, Beijing, pp.47-49, 9-11 May 1986.

5.11 Y. Sasaki, K. Tajima and I. Yokohama: "Bidirectional Optical Transmission Using Polarised Light Waves", Elect. Lett., 18 June 1987, vol.23, no.13, pp.692-694.

5.12 W.C. Poon and P.S. Chung: "An Optical Fibre Communication System using Polarization-division-multiplexing", Proc. International Conf. on Communication Technology, 9-11 Nov 1987, China, pp.512-515.

CHAPTER 6
INTEGRATED OPTICAL COMMUNICATION AND SENSING SYSTEM

6.1 Introduction

Optical fibres are becoming more and more popular in using for long haul communication and integrated services digital networks (ISDN). Many of the copper cables in communication networks are replaced by optical cables. The market of communications, which is a fast growing business, is mainly divided by satellites and optical fibres. Satellites have their own advantages in broadcasting, while optical fibres have their own advantages in long haul communications and ISDN.

Optical fibres are made of silica. This material is very rigid. The diameter of an optical fibre is thinner than a line. Hereto, they are very easy to be broken. To protect an optical fibre, a plastic jacket is generally used. The sheath of an optical fibre cable is a few layers of plastic armours and metal armours. Within the armours of an optical fibre cable, it is a strand of fibres with plastic jackets and steel wires. The steel wires are used for increasing the mechanical strength of the optical fibre cable. High density fibre cable has been reported [6.1] for increasing the transmission capacity in an optical fibre cable.

Under-grounded optical fibre cables are sometimes enclosed by plastic pipes. The pipes are filled with fluid. Remote alarms, which detect the present of invader by monitoring the fluid pressure, are installed to prevent any mechanical damage on the optical fibre cables. It is more difficult to set up an alarm system on a bare optical fibre cable. The above method cannot be applied on it. In this chapter, a method [6.2] is proposed for setting up a remote alarm system on an optical fibre communication system by integrating a fibre optic sensor into the communication system.

6.2 Theory of the Integrated System

When an optical fibre is subjected to an external force, the longitudinal length, the diameter and the refractive index of the fibre will be changed. Thus, the wave propagation characteristics and the state of polarization of the light beam travelling in the fibre will be changed. The changes in the output optical intensity and the state of polarization are related to the external force applied on it. It can be detected by the method described in chapter 4.

The proposed method detects the external force acting on the optical fibre by splitting a small portion of the light beam at the receiving side of a communications link. By using the method described in chapter 4, the external force applied on the optical fibre can be examined.

Since the external force applying on the optical fibre is a static force, the alarm signal is only in a d.c. level. A voice signal consists of a.c. components only. The ears of a human are insensible to the d.c. component and the phase shift of the a.c. components in a sound. A low-pass filter is used to block the audio signal, while a band-pass filter is used to block the alarm signal. With the helps of the band-pass filter and the low-pass filter, the audio signal and the sensing signal can be demultiplexed and recovered.

6.3 Experimental Result

In the experiment, the external force applied onto the optical fibre was tension. Figure 6.1 shows the schematic diagram of the proposed setup of an optical communication system integrated with tension over-loaded protection alarm system. A picture of the setup is shown in figure 6.2. The signal transmitted in the communication link was an audio signal. The voice signal was generated by a signal generator and obtained from radio. A 633 nm He-Ne laser (SP-158), which could be modulated up to 2 kHz, was used as the light source of the transmitter. The modulated laser was polarized and then coupled into a short length of a single-mode fibre. A small portion of the output light beam from the optical fibre was splitted out by a beam splitter. The small portion of light was detected by an photodetector. The electrical output from the photodetector was passed through a low-pass filter and then examined. This value indicated the tension applied on the optical fibre. Another portion of the output light beam was detected by another photodetector. The electrical output from the detector was passed through a band-pass filter. And then the signal was recovered.

The distortion and the signal-to-noise ratio of the audio signal channel are shown in figure 6.3 and 6.4 respectively. It is found that the prototype system was only acceptable in the range from 200 Hz to 2 kHz. At low frequency, the attenuation was set to very high to stop the d.c. signal and the 100 Hz from the power source of the laser. This reduced the signal-to-noise ratio down to zero and increased the distortion up to 90 %. Due to the frequency response of the laser modulator is only up to 2 kHz and the frequency response of the He-Ne laser is non-linear, the signal above this frequency will be attenuated. The distortion above 2 kHz was more than 30 %. The signal-to-noise ratio above 2 kHz was less than 10 dB. The distortion in the operation range of the prototype system, which was from 200 Hz to 2 kHz, was less than 15 %. The signal-to-noise ratio at this range was more than 20 dB. When a nice voice of a female Disc Jocker from the radio was transmitted by the communication channel of the system, the sound, which was recovered at the

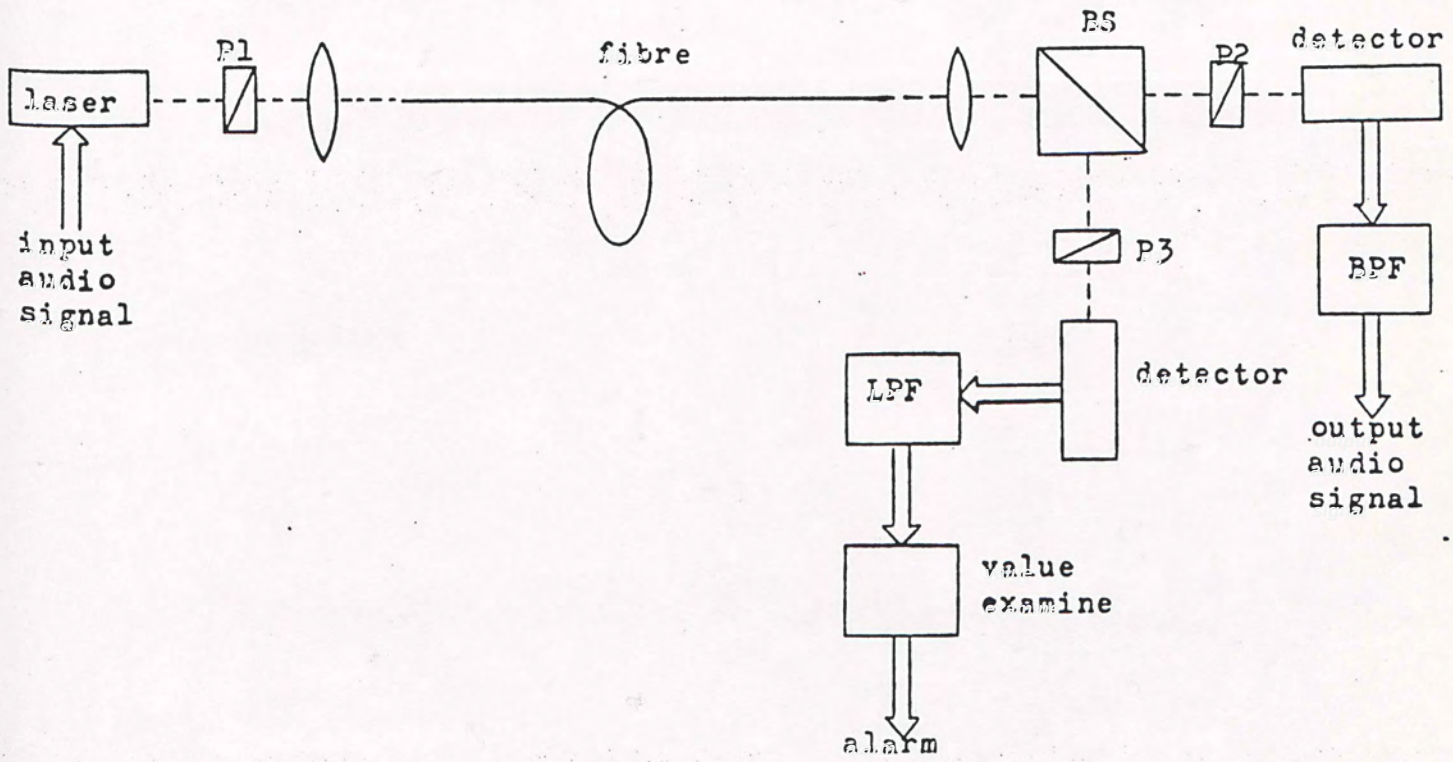

Fig. 6.1 Schematic diagram of an optical communication system integrated with tension over-loaded protection alarm system.

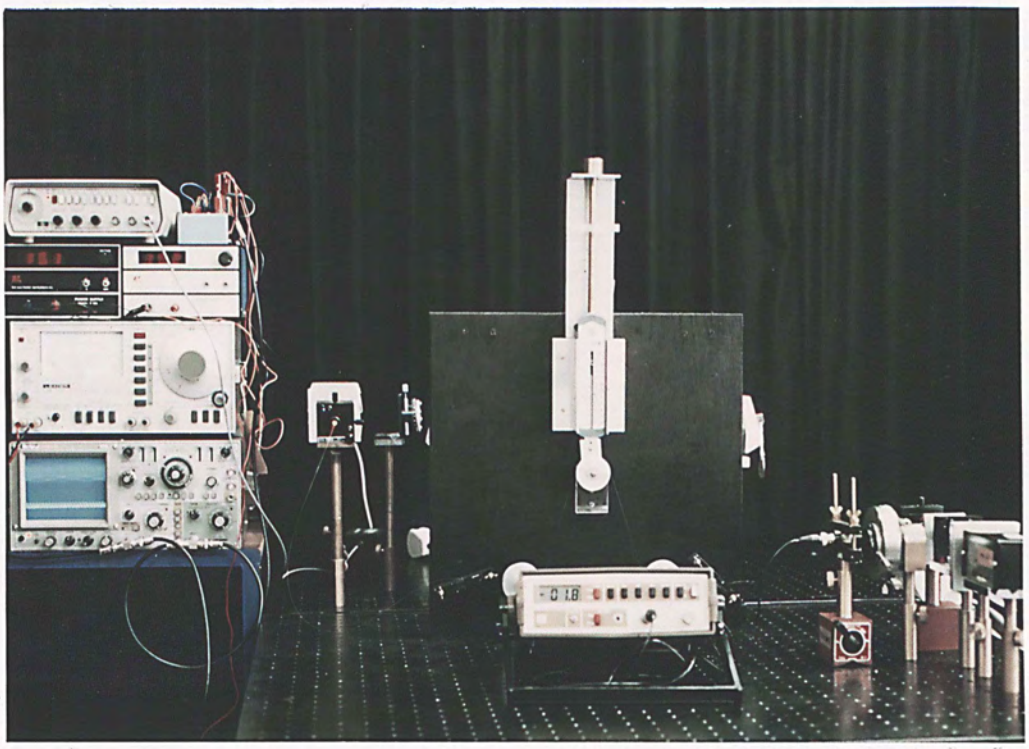

Fig. 6.2 Photograph of experimental setup of an optical communication system integrated with tension over-loaded protection alarm system.

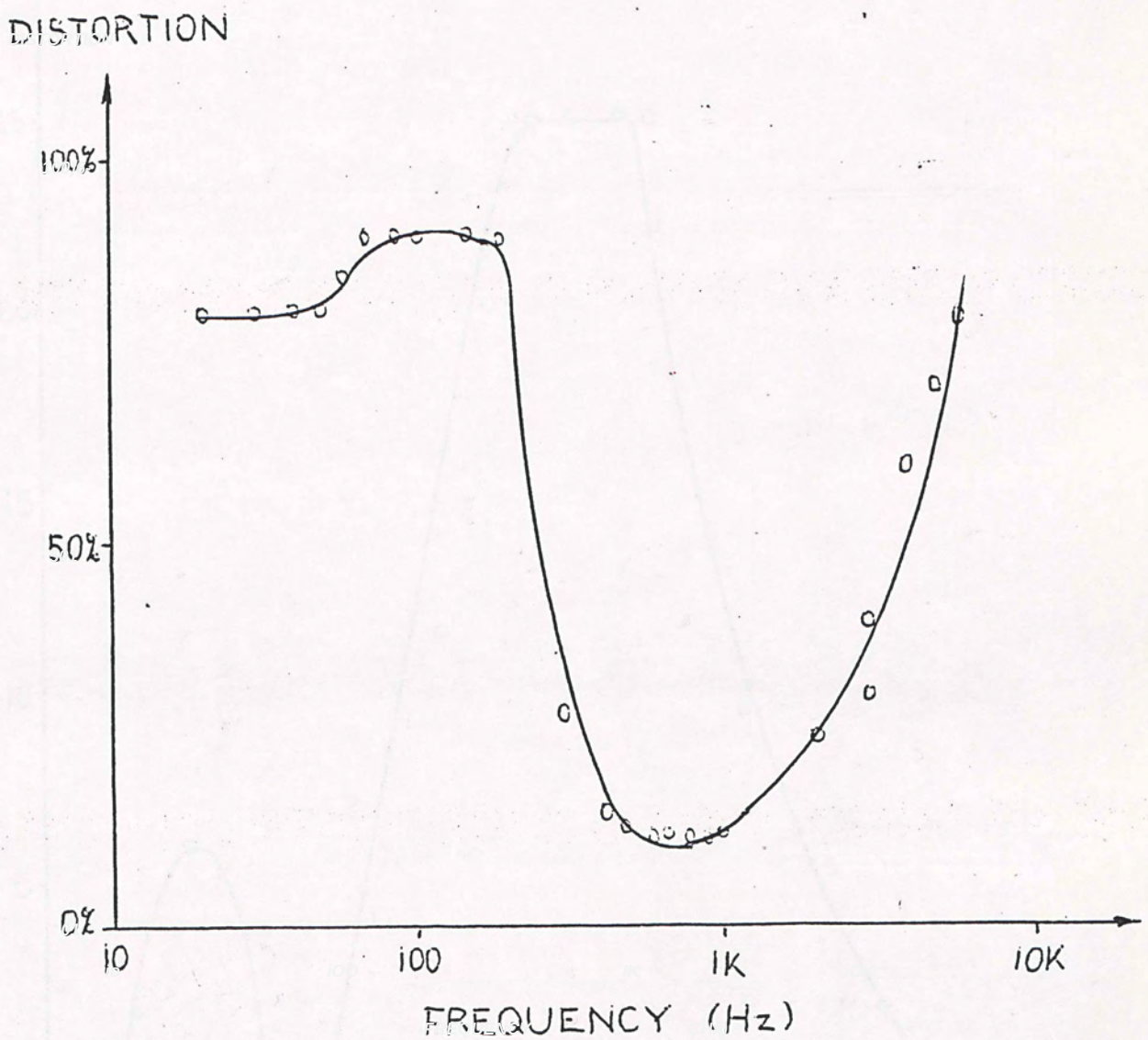

Fig. 6.3 Distortion of the received signal at different frequencies.

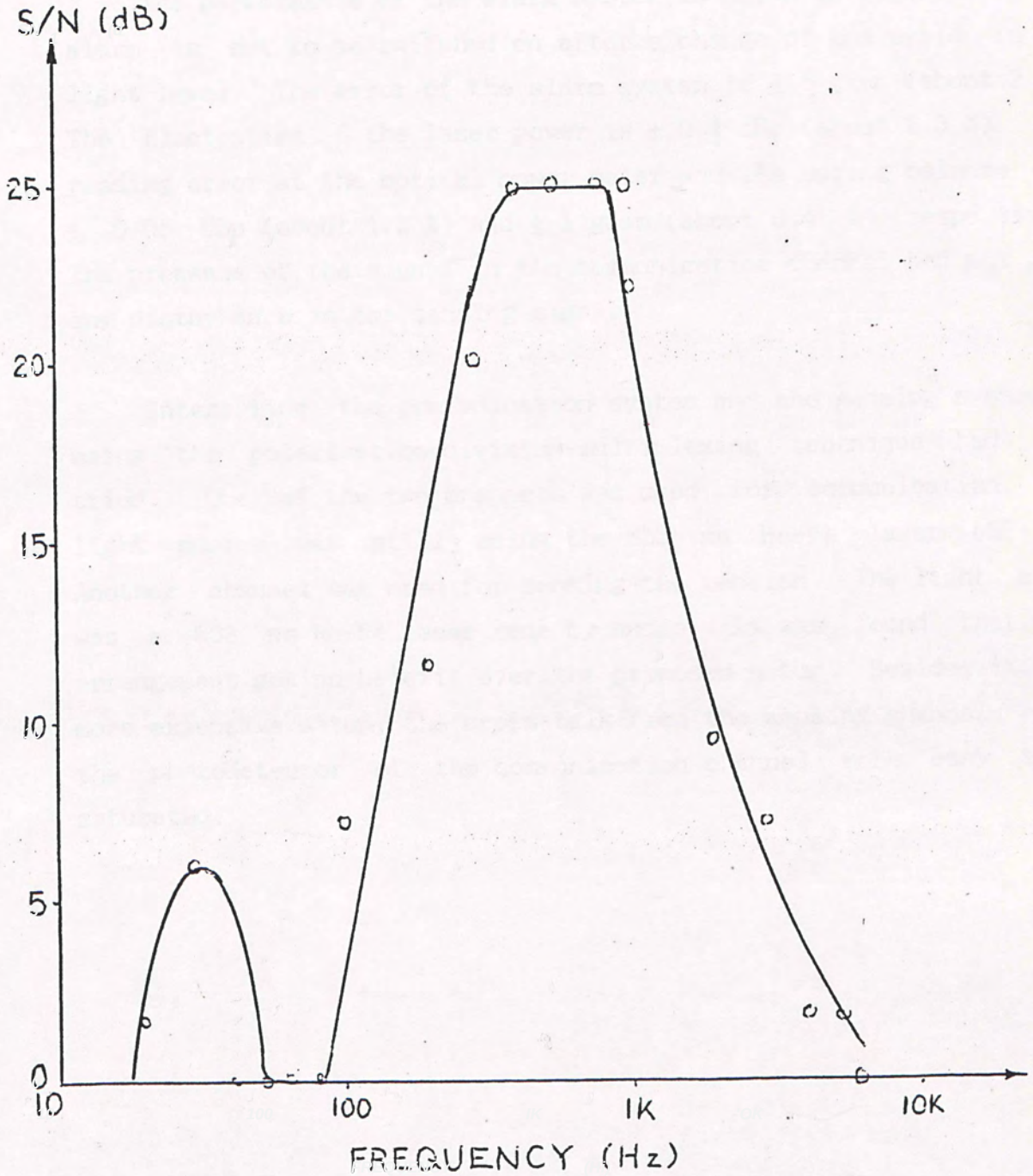

Fig. 6.4 Signal-to-noise ratio of the received audio signal at different frequencies.

receiver, consisted of low frequency hummings. The high frequency components of the sound was distorted by a large value. The band-pass filter in the voice channel was in the order of three.

The performance of the alarm system is shown in figure 6.5. The alarm is set to be switched on after a change of one cycle in the light level. The error of the alarm system is ± 5 gram (about 2 %). The fluctuation of the laser power is ± 0.1 dBμ (about 2.3 %). The reading error at the optical power meter and the spring balance were ± 0.05 dBμ (about 1.2 %) and ± 1 gram (about 0.4 %) respectively. The presence of the signal in the communication channel had not given any disturbance in the sensing signal.

Integrating the communication system and the sensing system by using the polarization-division-multiplexing technique had been tried. One of the two channels was used for communication. The light source was still using the 633 nm He-Ne laser (SP-158). Another channel was used for sensing the tension. The light source was a 633 nm He-Ne laser made by Hudge. It was found that this arrangement got no benefit over the proposed setup. Besides it was a more expensive setup, the cross-talk from the sensing channel caused the photodetector of the communication channel more easy to be saturated.

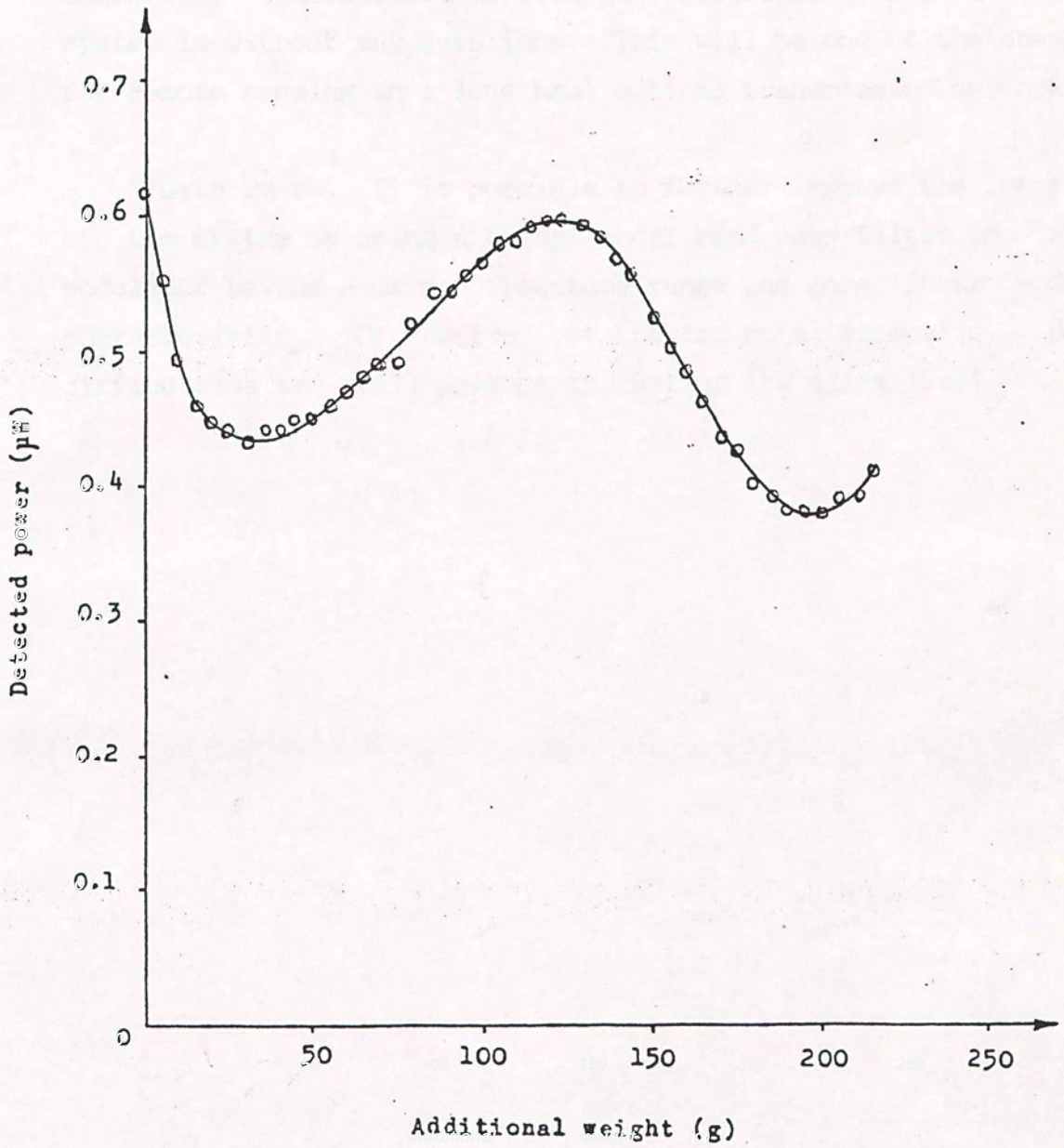

Fig. 6.5 Performance of the tension alarm system.

6.4 Conclusion

An integrated system including communication and sensing had been demonstrated. Although the distortion was higher than a commercial communication system, the realization of this integrated system is without any questions. This will be one of the cheap ways for remote sensing in a long haul optical transmission network.

Furthermore, it is possible to further improve the performance of the system by using a higher order band-pass filter and a laser modulator having a larger frequency range and more linear modulation characteristic. Of course, it costs more expensive. However, difficulties are still present in setting the alarm level.

Reference

6.1 Y. Katsuyama, S. Hatano, K. Hogari and T. Kokubun: "Higher-density single-mode optical fibre cables than 1 fibre/mm2, containing hundreds of fibres", Elect. Lett., 7 May 1987, vol.23, no.10, pp.481-482.

6.2 P.S. Chung, W.C. Poon, C.K. Wong and K.O. Chik: "Fibre Devices for optical sensing systems", Proc. IEEE Asian Electronics Conference, Hong Kong, 1-4 Sep 1987, pp.547-551.

CHAPTER 7
CONCLUSION

For the world market optical fibre sensors in the year 2000 (after Electronicast) was forecasted [7.1] to be projected to nearly US$5 billion. Mainly it is funded by military and government (about 84%), and about 16% is funded by industrial and medical consumer. It was forecasted that North American manufacturers would take a greater share than might be estimated simply by scaling the relative sizes of the respective economies.

Some of optical fibre sensors are no longer restricted in laboratory works, they are either in field testing or being commercial products. Due to the advantages of optical fibre sensors on sensitivity, intrinsically safe, intrinsic freedom from Electromagnetic Interference, forecasting low-cost, etc., much and much more research works are concerned on optical fibre sensors and on eliminating the noise, increasing the sensitivity to measurands and reducing the production cost.

A major attraction of optical fibre technology was perceived to be the market leverage generated by both long-haul telecommunications and local area networks (LANs). Cables containing photon flow in glass fibres are superseding cables containing electron flow in copper pairs or coaxials. Applications are to undersea communication systems, to domestic intercity systems, to metropolitan area trunking systems, to feeder links in the subscriber loop, and to on-premises or local links such as data bus in computers or switching machines.

In the chapter 2, 3 and 4, different sensing techniques by optical fibre have been proposed and demonstrated. They include intensity sensing and modal sensing techniques. The potential of optical sensors to be cheap and accurate sensors by using the two optical sensing techniques have been demonstrated in these few chapters. In chapter 2, the theoretical analysis on the characteristics of a fibre bundle has been developed and compared with the practical setup for measuring displacement. A further

application on measuring weight has been demonstrated in chapter 3. Simply in the setups causes the cheap in cost. Difficulties in preventing leakage of solution and reduction of frictions are the disadvantages. A modal sensing technique is proposed in the chapter 4. This proves the possibility of employing phase modulation without reference arm. It reduces the complicity and cost of a phase sensor. However, the sensitivity is lower than the phase sensor using reference arm.

In chapter 5 a polarization-division-multiplexing technique is proposed. It shows the method to double the information capacity of a transmission link. Although the performance is not so satisfactory, the possibility and the potential were shown. Integrating a communication system and a sensing system is proposed in chapter 6. It shows the way to remote monitoring the stress applied on the fibre cable in an optical communication link. Encouraging result was obtained in the experiment.

The proposed optical sensing techniques and optical communication techniques will probably push a forward step on the fibre optic technology.

As a new sensing technique - modal sensing technique - is proposed, there must be many other applications besides the proposed tension sensor. It is suggested to apply the technique on measuring distance, weight, voltage, etc. Furthermore, it is possible to integrate this technique into a substrate. Consequently, mass production and low production cost can be achieved.

Polarization-division-multiplex is a very new technique. However, efforts of research is still needed for solving the problems in cross-talk.

Reference

7.1 Peter McGeehin: "Optical sensors - developing the technology and the market", Electronics & Power, July 1986, pp.535-538.

APPENDIX A

To start the analysis on the performance of the optical lever, all the rays leaving the source fibre at the same angle are assumed to be meridional and uniformly distributed within the source fibre. The reflecting surface is assumed to be placed perpendicular to the axis of the fibre bundle. The fibre end is assumed to be perfectly, so it is perpendicular to the axis of the fibre. Figure 2.3 shows the geometry of the illuminance of the reflected light on the entrance plane of the return fibre. The luminous intensity of the source fibre is I_o. The luminous flux from the source fibre is assumed to be illuminated at n different angles with equal dividend from θ_{min} to θ_{max}. The interval between adjacent angles is

$$\delta\theta = (\theta_{max} - \theta_{min})/(n - 1) \qquad [A.1]$$

The uniform illuminance from exit plane of the source fibre at each angle is I_o/n. The luminous flux within the light ring of each illumination angle considered at the receiving surface is

$$I = \begin{cases} L\, I_o/n\, \pi\, x_o^2 & \text{for } k \geq 3 \\ L\, I_o/n\, \pi\, [x_o^2 - (x_o - d \tan\theta)^2] & \text{for } k \leq 3 \end{cases} \qquad [A.2]$$

The area of the light ring considered is given by

$$A_L = \begin{cases} \pi\, [(2\, d \tan\theta + x_o)^2 - (2\, d \tan\theta - x_o)^2] & \text{for } k \geq 3 \\ \pi\, [(x_o + 2\, d \tan\theta)^2 - x_o^2] & \text{for } k \leq 3 \end{cases} \qquad [A.3]$$

The illuminance of the reflected light on the entrance plane of the return fibre can be approximated from the geometry shown in figure 4.3 by dividing equation A.2 by equation A.3. It is given by

$$f_I(k) = \begin{cases} C\, I_o/n\, [(5 - k)/(4\, k + 4)] & \text{for } k \leq 3, \\ C\, I_o\, /\, [n\, (4\, k - 4)] & \text{for } k \geq 3, \end{cases} \qquad [A.4]$$

where k is a normalized parameter which is given as the outer radius of the reflected light ring (q) normalized by the fibre core radius (x_o), C is an arbitrary constant counting for the deficiency of the reflecting surface and the fibre end surfaces. Figure 2.4 shows the plane of the fibre ends and the intersect of the reflected light ring with the fibre. As shown in the figure, the two fibres, at which the radius of core is x_o and the cladding thickness is C_1, are placed side by side. The distance between the two fibre axes is

$$b = 2\, x_o + 2\, C_1 \qquad [A.5]$$

The outer boundary q of the light cone on the fibre end surface is given by

$$q = 2\, d\, \tan\theta + x_o \qquad [A.6]$$

where d is the distance between the reflecting surface and the fibre end surface, θ is the angle of the luminous intensity considered. By Cosine Law, the parameters can be related by

$$x_o^2 = q^2 + b^2 - 2\, q\, b\, \cos\Phi \qquad [A.7]$$

Substituting two normalized parameter k and k′ into equation A.7, it can be written as

$$\Phi = \cos^{-1}[(k^2 + k'^2 - 1)/(2\, k\, k')] \qquad [A.8]$$

where k′ is the normalized distance between the fibre axes and is given by $k' = b/x_o$, and k is the normalized radius of the outer boundary of the light ring and is given by $k = q/x_o$. The area of the sector STPS is given by

$$A_1 = 0.5\ \Phi\ q^2 = 0.5\ \Phi\ k^2\ x_o^2 \qquad [A.9]$$

The area of the sector TRVT is given by

$$A_2 = 0.5\ \emptyset\ x_o^2 \qquad [A.10]$$

$$\sin \emptyset = k \sin \Phi \qquad [A.11]$$

$$\emptyset = \begin{cases} \sin^{-1}[k \sin \Phi] & \text{for } k^2 \leq k'^2 + 1 \\ \pi - \sin^{-1}[k \sin \Phi] & \text{for } k^2 \geq k'^2 + 1 \end{cases} \qquad [A.12]$$

The area of the triangle STRS is given by

$$A_3 = 0.5\ q\ b \sin \Phi = 0.5\ x_o^2\ k\ k'\ \sin \Phi \qquad [A.13]$$

The shaded area in the figure, which indicates the area enclosed by the light cone, is given by

$$A = 2\ (A_1 + A_2 - A_3) \qquad [A.14]$$

Substituting equations A.9, A.10, A.12 and A.13 into equation A.14, the following relationship can be obtained

$$A = x_o^2\ \{\Phi\ k^2 + \sin^{-1}[k \sin \Phi] - k\ k'\ \sin \Phi\} \qquad [A.15]$$

In a general case, the function of the subtended area by the light cone with respect to different range of k is given by

$$f_A(k) = \begin{cases} 0; & \text{for } k \le k'-1, \\ x_o^2 \{\Phi\, k^2 + \sin^{-1}[k \sin \Phi] - k\, k' \sin \Phi\}; & \text{for } k'-1 < k \le (k'^2+1)^{1/2}, \\ x_o^2 \{\Phi\, k^2 + \pi - \sin^{-1}[k \sin \Phi] - k\, k' \sin \Phi\}; & \text{for } (k'^2+1)^{1/2} < k \le k'+1, \\ x_o^2 \{\pi - \Phi\, k^2 - \sin^{-1}[k \sin \Phi] + k\, k' \sin \Phi\}; & \text{for } k'+1 < k \le (k'^2+1)^{1/2}+2 \\ x_o^2 \{\sin^{-1}[k \sin \Phi] + k\, k' \sin \Phi - \Phi\, k^2\}; & \text{for } (k'^2+1)^{1/2}+2 < k < k'+3 \\ 0; & \text{for } k'+3 \le k. \end{cases} \qquad [A.16]$$

The luminous flux collected by the return fibre from an angle of illuminance θ at the source fibre is given by

$$f_r(k) = f_I(k)\, f_A(k) \qquad [A.17]$$

The total luminous flux collected by the return fibre from the source fibre is given by

$$F_r(k) = \lim_{n \to \infty} \sum_{\theta_{min}}^{\theta_{max}} f_r(k) \qquad [A.18]$$

APPENDIX B

The numerical aperture of the source fibre is assumed to be filled completely by the optical source. Figure 2.4 shows the geometry of the receiving point P' (b,0) and the luminous intensity chord. The maximum spread angle of the luminous intensity chord with illumination angle of θ is given by

$$\phi = 2 \cos^{-1}[(4 d^2 \tan^2\theta + b^2 - x_o^2)/(4 d b \tan\theta)] \quad [B.1]$$

where d is the vertical displacement between the fibre end surface and the reflecting surface, b is the horizontal displacement between the axis of the source fibre and the receiving point, and x_o is the radius of the core of the source fibre. The coordinates of the image point P of the receiving point on the reflecting surface is (b,2d). The shaded area of the luminous intensity chord in figure 2.4 is given by

$$A = (1\, d\theta)(2 d \tan\theta)(\phi) \quad [B.2]$$

By the cosine law of illuminance, the illuminance at the point P due to a point source of luminous intensity I_o is given by

$$I_p = I_o \cos\theta / l^2 \quad [B.3]$$

where l is the distance between the receiving point and the illuminating point. The illuminance at the point P due to the shaded area is given by

$$I_p = C (I_o/l) \phi (2 d \tan\theta) \cos\theta \, d\theta$$

$$= C I_o \phi \sin\theta \cos\theta \, d\theta \quad [B.4]$$

where C is an arbitrary constant counting for the deficiency of the reflecting surface and the fibre end surface. The illuminance at the point P due to the whole source fibre is given by

$$I_p = \int_{\theta_{min}}^{\theta_{max}} \{2\ C\ I_o \cos^{-1}[(4\ d^2 \tan^2\theta + b^2 - x_o^2)/(4\ d\ b \tan\theta)] \sin\theta \cos\theta\}\ d\theta \qquad [B.5]$$

where $$\theta_{min} = \tan^{-1}[(b - x_o)/(2\ d)] \qquad [B.6]$$

$$\theta_{max} = \begin{cases} \sin^{-1}(NA) & \text{for } NA/\sqrt{(1-NA^2)} \leq (b+x_o)/(2d) \\ \tan^{-1}[(b+x_o)/(2d)] & \text{for } NA/\sqrt{(1-NA^2)} > (b+x_o)/(2d) \end{cases} \qquad [B.7]$$

The luminous flux collected by the return fibre from the source fibre is given by

$$I_r = \int_{b_{min}}^{b_{max}} I_p\ \emptyset\ b\ db \qquad [B.8]$$

Appendix C

Firstly, the hydraulic system is considered at no-load condition. For staying at an equilibrium stage, the following equation must be satisfied:

$$(W_1 - F)/A_1 + \rho g d_1 = W_2/A_2 + \rho g d_2 \qquad [C.1]$$

where W_1 and W_2 are the weights of the pistons of the primary cylinder and the secondary cylinder in kilogramme respectively. ρ is the density, in kilogramme per meter cube, of the solution used in the hydraulic system. g is the acceleration due to gravity in meter per second square. A_1 and A_2 are the internal cross-sectional area of the primary cylinder and the secondary cylinder in meter cube respectively. F is the initial compression in newton on the spring. d_1 and d_2 are the displacement of the piston surfaces of the primary cylinder and the secondary cylinder in meter to a reference plane. When a measured object of weight W is placed on the supporter at the primary side, the equation for equilibrium is given as

$$(W + W_1 - F - k\,\delta d_1)/A_1 + \rho g (d_1 - \delta d_1) = W_2/A_2 + \rho g (d_2 + \delta d_2) \qquad [C.2]$$

where k is the spring constant in kilogramme per meter. δd_1 and δd_2 are the level change in meter at the pistons of the primary cylinder and the secondary cylinder respectively. Subtracting equation C.1 from equation C.2, the equation becomes

$$(W - k\,\delta d_1)/A_1 - \rho g \delta d_1 = \rho g \delta d_2 \qquad [C.3]$$

$$W = \rho g (\delta d_1 + \delta d_2) A_1 + k \delta d_1 \qquad [C.4]$$

The viscosity is zero. Assuming the volume of the solution used in the hydraulic system is constant [3.1,3.2]. Hence, the algebraic summation of volume change in the primary cylinder and the secondary cylinder is zero. It can be equated as

$$A_1 \, sd_1 = A_2 \, sd_2 \qquad [C.5]$$

Substituting equation C.5 into equation C.4, the weight of the measured object is given by

$$W = [\rho \, g \, (A_1 + A_2) + k \, A_2/A_1] \, sd_2 \qquad [C.6]$$

Putting $sd_2 = y - y_0$, where y_0 is the initial position of the sensing head and y is the position of the sensing head when an object is being measured. Finally, the weight of the measured object is expressed as

$$W = [\rho \, g \, (A_1 + A_2) + k \, A_2/A_1] \, (y - y_0) \qquad [C.7]$$

As ρ, g, k, A_1 and A_2 are constants, the weight of the measured object is proportional to the distance between the sensing head and the reflecting surface. The equation C.7 can be written as

$$W = m \, y + c \qquad [C.8]$$

where $m = \rho \, g \, (A_1 + A_2) + k \, A_2/A_1$ [C.9]

$$c = - [\rho \, g \, (A_1 + A_2) + k \, A_2/A_1] \, y_0 \qquad [C.10]$$

Appendix D

Assuming the cladding and core has the same polarization axis (if not, it can be resolve into the same axis), the resultant E-field at a certain point will be given by:

$$E_o \sin(\omega t - \beta_c z) + E_{cl1} \sin(\omega t - \beta_{cl1} z) + E_{cl2} \sin(\omega t - \beta_{cl2} z) + \ldots . \quad [D.1]$$

where E_c is the amplitude of the E-field in core;
E_{cl1} is the amplitude of the 1st mode of the E-field in cladding;
E_{cl2} " " " " " 2nd " " " " " "
.
.
.
E_{cln} " " " " " nth " " " " " "
β_c is the phase change of the E-field in core;
β_{cl1} is the phase change of the 1st mode of the E-field in cladding;
β_{cl2} " " " " " " 2nd " " " " " "
.
.
.
β_{cln} " " " " " " nth " " " " " "

The square of the resultant E-field at the point is given by:

$$E_R^2 = E_c^2 \sin^2(\omega t - \beta_c z) + \sum_{n=1}^{N} E_{cln}^2 \sin^2(\omega t - \beta_{cln} z)$$
$$+ 2 E_c \sin(\omega t - \beta_c z) \sum_{n=1}^{N} E_{cln} \sin(\omega t - \beta_{cln} z)$$
$$+ 2 \sum_{n=1}^{N} \sum_{\substack{m=1 \\ m \neq n}}^{N} E_{cln} E_{clm} \sin(\omega t - \beta_{cln} z) \sin(\omega t - \beta_{clm} z) \quad [D.2]$$

where N is the maximum number of mode in cladding.

The intensity at that point is given by:

$$I = (1/nT) \int_0^{nT} E_R^2 \, d(\omega t) \qquad [D.3]$$

$$I = (1/2)\,(E_c^2 + \sum_{n=1}^{N} E_{cln}^2) + \sum_{n=1}^{N} E_c\, E_{cln} \cos[(\beta_{cln} - \beta_c)z] + \sum_{n=1}^{N} \sum_{\substack{m=1 \\ m \neq n}}^{N} E_{cln}\, E_{clm} \cos[(\beta_{clm} - \beta_{cln})z] \qquad [D.3]$$

Since $d\beta/dT$ is negligible comparing with dz/dT, hence

$$dI/dT = (\partial I/\partial z)(dz/dT) \qquad [D.4]$$

$$dI/dT = \{ \sum_{n=1}^{N} E_c\, E_{cln}\, (\beta_c - \beta_{cln}) \sin[(\beta_{cln} - \beta_c)z] + \sum_{n=1}^{N} \sum_{\substack{m=1 \\ m \neq n}}^{N} E_{cln}\, E_{clm}\, (\beta_{cln} - \beta_{clm}) \sin[(\beta_{clm} - \beta_{cln})z] \}(dz/dT) \qquad [D.5]$$

dI/dT is the sensitivity of the tension measuring characteristic.

Appendix E

In the HB fibres, there are two kinds of fibres: two-polarization fibres and single-polarization fibres. Two-polarization fibres are conventionally called PM fibres. Single-polarization fibres have been successfully demonstrated with bow-tie fibres [E.1], flat depressed-cladding fibres [E.2], and PANDA fibres [E.3], utilizing the large difference of the bending losses between the orthogonal modes. Table E.1 shows the various kinds of polarization-maintaining (PM) fibres classified from the viewpoint of linear polarization-maintenance according to the definition made systematically by Okoshi et al. [E.4]. In the table, PM, HB, LB, SP, TP, GE and SE are representing the words "Polarization Maintaining", "High-Birefringent", "Low-Birefringent", "Single-Polarization mode", "Two-Polarization mode", "Geometrical Effect" and "Stress Effect" respectively.

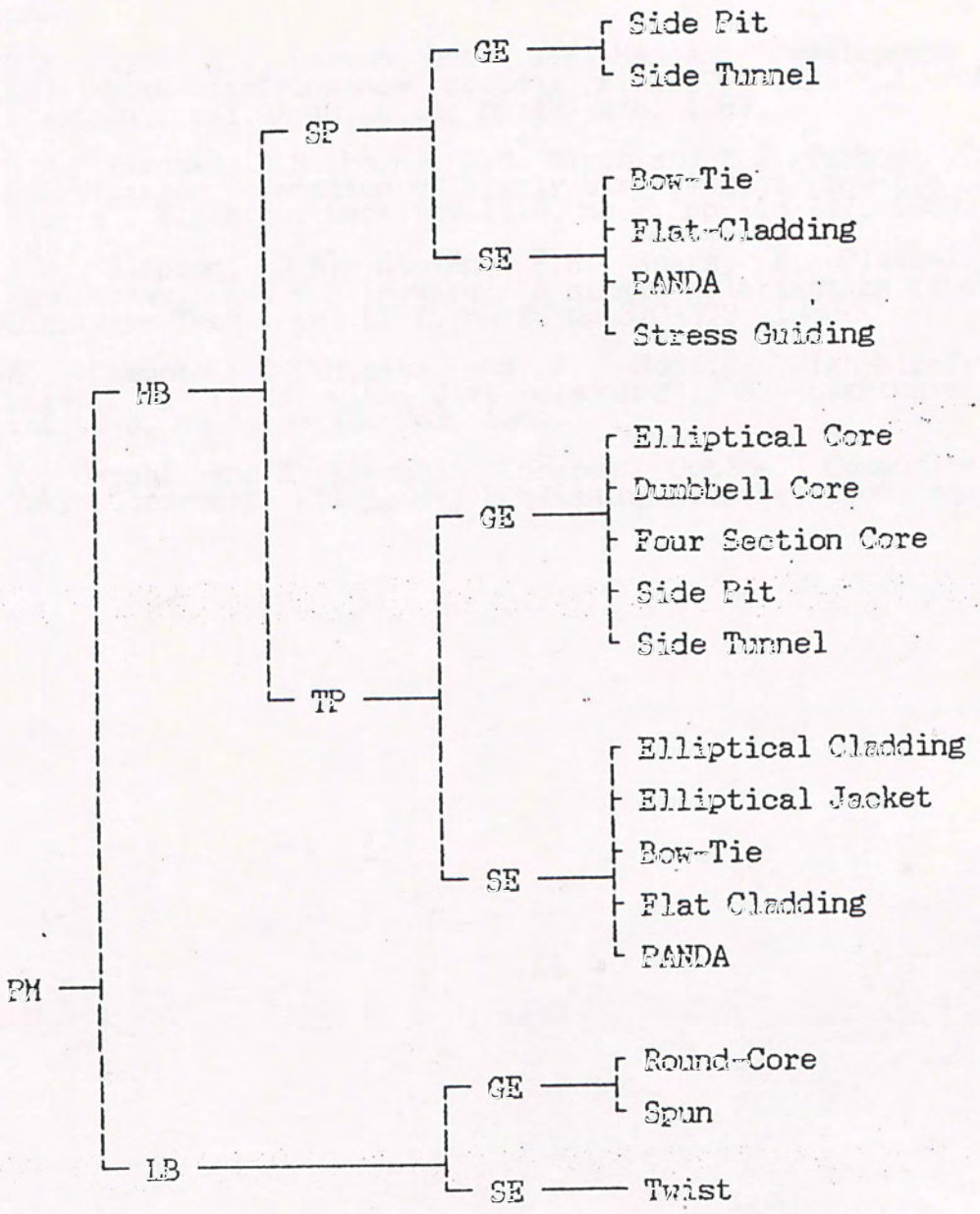

Table E.1 kinds of Polarization-maintaining fibres classified from linear-polarization maintenance view point.

Reference

E.1 D N. Payne, A.J. Barlow, and J.J.R. Hansen: "Development of low- and high-birefringence optical fibers", IEEE J. Quantum Electron., vol.QE-18, no.4, pp.477-488, 1982.

E.2 M.P. Varnham, D.N. Payne, R.D. Birch and E.J. Tarbox: "Single-polarization operation of highly birefringent bow-tie optical fibers", Electron. Lett., vol.19, no.7, pp.246-247, 1983.

E.3 J.R. Simpson, R.H. Stolen, F.M. Sears, W. Pleibel, J.B. MacChesney, and R.E. Howard: "A single-polarization fiber", J. Lightwave Tech., vol.LT-1, no.2, pp.370-373, 1983.

E.4 K. Okamoto, T. Hosaka and J. Noda: "High-birefringence polarizing fiber with flat cladding", J. Lightwave Tech., vol.LT-3, no.4, pp.758-762, 1985.

E.5 T. Okoshi and K. Kikuchi: "Coherent Optical Communications", Tokyo-Dordrecht: KTK-Reidel Publishing Company, 1988, ch.9.